

6-25-2010

Documenting multiple metasomatic events within the Finero phlogopite peridotite using chlorine isotopes, Ivrea zone, Italy

Melissa Halick

Follow this and additional works at: https://digitalrepository.unm.edu/eps_etds

Recommended Citation

Halick, Melissa. "Documenting multiple metasomatic events within the Finero phlogopite peridotite using chlorine isotopes, Ivrea zone, Italy." (2010). https://digitalrepository.unm.edu/eps_etds/33

This Thesis is brought to you for free and open access by the Electronic Theses and Dissertations at UNM Digital Repository. It has been accepted for inclusion in Earth and Planetary Sciences ETDs by an authorized administrator of UNM Digital Repository. For more information, please contact disc@unm.edu.

Melissa A. Halick

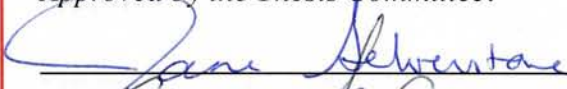
Candidate

Earth and Planetary Sciences

Department

This thesis is approved, and it is acceptable in quality
and form for publication:

Approved by the Thesis Committee:

 _____, Chairperson

 _____

 _____

**DOCUMENTING MULTIPLE METASOMATIC EVENTS
WITHIN THE FINERO PHLOGOPITE
PERIDOTITE USING CHLORINE ISOTOPES,
IVREA ZONE, ITALY**

BY

MELISSA A. HALICK

**BACHELOR OF SCIENCE
B.S. GEOLOGY
UNIVERSITY OF TEXAS AT AUSTIN
2005**

THESIS

Submitted in Partial Fulfillment of the
Requirements for the Degree of

**Master of Science
Earth and Planetary Sciences**

The University of New Mexico
Albuquerque, New Mexico

May, 2010

©2010, Melissa A. Halick

Dedicated to family, for their unconditional love and support through all my years in academia; I couldn't have succeeded without you. Also, to my Grandpa and Mimi, I will miss you always.

ACKNOWLEDGEMENTS

I would like to acknowledge Jane Selverstone and Zach Sharp, for giving me the opportunity to grow as a scientist and for their constant encouragement. Many thanks to Jaime Barnes, for her dedication in teaching me sample preparation and teaching me how to use the unruly mass spectrometer. Thanks to Mousumi Roy for serving on my committee and providing feedback. I would also like to acknowledge Nina Lanza, Travis Naibert, and Jack Grow, for their kindness, patience, love, and guidance. Additional thanks to Viorel Atudorei, for help in the stable isotope lab. Funding for this research was provided by the Wengerd Travel funds donated to the Earth and Planetary Sciences Department at the Univ. of New Mexico, the Gorham Research Assistant award, E&PS Dept., Univ. of New Mexico, Graduate and Professional Student Association (GPSA) research grant, Univ. of New Mexico, Geological Society of America research grant (2008) and NSF grant #EAR-0911669 to J. Selverstone and Z.D. Sharp.

**DOCUMENTING MULTIPLE METASOMATIC EVENTS
WITHIN THE FINERO PHLOGOPITE
PERIDOTITE USING CHLORINE ISOTOPES,
IVREA ZONE, ITALY**

BY

MELISSA A. HALICK

ABSTRACT OF THESIS

Submitted in Partial Fulfillment of the
Requirements for the Degree of

**Master of Science
Earth and Planetary Sciences**

The University of New Mexico
Albuquerque, New Mexico

May, 2010

**DOCUMENTING MULTIPLE METASOMATIC EVENTS
WITHIN THE FINERO PHLOGOPITE
PERIDOTITE USING CHLORINE ISOTOPES,
IVREA ZONE, ITALY**

by

Melissa A. Halick

B.S., Geology, University of Texas at Austin, 2005

M.S., Earth and Planetary Sciences, University of New Mexico, 2010

ABSTRACT

Depleted mantle peridotites from the Finero body in the Ivrea Zone were infiltrated by metasomatizing melts/fluids prior to their incorporation into the lower continental crust. Metasomatism resulted in pervasive development of phlogopite and amphibole throughout much of the body, as well as the formation of phlogopite-rich segregations. Previous trace element and isotopic data have been interpreted by different authors to reflect metasomatism induced by slab-derived, rift-related (continental), or plume-related melts/fluids. Several of these geochemical studies conclude that the rocks experienced two discrete metasomatic events. Here we combine chlorine and hydrogen stable isotopic data with field and petrologic data to better constrain the number of alteration events, the source(s) of the metasomatizing fluid/melt, and the migration mechanism(s) of the fluid/melt.

Four types of samples were collected from two localities: (1) foliated phlogopite + amphibole peridotite, (2) crosscutting phlogopite + amphibole segregations, (3) a single crosscutting phlogopite + orthopyroxene segregation, and (4) cumulate amphibole peridotites. Group 1 peridotites range in textures from massive, showing few deformation features, to samples with well-developed olivine + orthopyroxene \pm phlogopite \pm amphibole shape-preferred orientation and evidence for subgrain rotation recrystallization of olivine and orthopyroxene. Thermodynamic modeling using Perple_X indicates that Group 1 samples equilibrated at temperatures of $\sim 800\text{-}900^\circ\text{C}$, which is consistent with deformation microstructures seen in samples collected for this study.

Microprobe data from Group 1 samples show large variations within and between samples. Three distinct populations of amphiboles are defined on the basis of Na, K, Al, and Cr concentrations. Group 1 samples show a weak correlation in Cl vs. Na concentrations in amphibole, with an R^2 value of 0.414. Large variations in chlorine and hydrogen isotopic values occur both within and between groups, and do not obviously correlate with major cation or whole-rock concentrations: Group 1: $\delta^{37}\text{Cl} = -1.3$ to $+3.3\text{‰}$ (whole rock, $n=8$), $\delta\text{D} = -48$ to -36‰ (phlogopite, $n=2$); Group 2: $\delta^{37}\text{Cl} = -2.1$ and -1.7‰ (WR, $n=2$), $\delta\text{D} = -49$ and -40‰ (phlogopite, $n=2$); Group 3, one sample: $\delta^{37}\text{Cl} = -0.1\text{‰}$ (WR, $n=1$), $\delta\text{D} = -80\text{‰}$ (phlogopite, $n=1$); Group 4: $\delta^{37}\text{Cl} = +0.8$ to $+1.9$ (WR, $n=3$), δD not yet available. There is no correlation between $\delta^{37}\text{Cl}$ values and sample location, chlorine concentration, major element composition, or phlogopite and amphibole abundances.

The isotopic and compositional heterogeneity within and between groups could reflect interaction between peridotite and (a) multiple fluids from different sources, or (b) a single fluid that evolved chemically. However, hypothesis (b) would require large chlorine and hydrogen isotopic fractionations to have occurred under mantle conditions, a conclusion that is inconsistent with experimental and theoretical studies. The lack of correlation between the isotope and petrologic data is more consistent with multiple pulses of chemically and isotopically distinct fluids, with evidence for meter-scale or smaller equilibration distances. It is unlikely that the large range of $\delta^{37}\text{Cl}$ values could have been produced solely by mantle melting in a rift or plume setting. Instead, the heterogeneity likely reflects relatively small-scale pulses of fluid/melt derived from different slab components and mantle melts in a subduction setting. Some studies argue that large-scale breakdown of serpentine at depths of ~ 200 km in the subducting lithosphere plays the major role in hydrating the mantle wedge and triggering formation of arc magmas. However, the Finero mantle peridotite shows that repeated smaller scale episodes of hydration from shallower, isotopically distinct slab sources can also cause significant modification of the mantle wedge. Similarly heterogeneous rocks in the upper levels of modern mantle wedges may contribute to the arc signature of melts either by interaction with magmas that pass through them or by downward entrainment into the zone of partial melting.

TABLE OF CONTENTS

LIST OF TABLES	xi
LIST OF FIGURES	xii
PREFACE	xiii
INTRODUCTION	1
GEOLOGICAL SETTING	4
Ivrea-Verbano Zone	4
Finero Complex	7
Previous Interpretations	9
FIELD AND SAMPLE DESCRIPTIONS	12
Phlogopite-Amphibole Peridotite: Mantle Tectonite.....	12
Group 1	13
Group 2	14
Group 3	15
Amphibole Peridotite: Ultramafic Cumulate	15
Group 4	15
ANALYTICAL METHODS	17
Whole-Rock Chemistry.....	17
Perple_X Modeling.....	17
Mineral Chemistry	18
Anion Analysis.....	19
Cl Isotopic Analysis and Cl Extraction.....	19

Hydrogen Isotopic Analysis	21
RESULTS	22
Whole-Rock Geochemistry and Cl Concentrations	22
Modeled Pressure and Temperature Constraints	22
Mineral Chemistry (Groups 1 and 4)	24
Stable Isotopic Analysis: Chlorine and Hydrogen	33
DISCUSSION	36
Tectonic Setting of Metasomatism	36
Subduction Fluids: Multiple Episodes and Possible Sources	38
CONCLUSIONS	41
REFERENCES	43
APPENDICES	52
Perplex Modeling	52
Microprobe Sections	68

LIST OF TABLES

Table 1a. XRF Analyses of Phlogopite + Amphibole Peridotite (Group 1)	26
Table 1b. XRF Analyses of Amphibole Cumulate Peridotite (Group 4).....	27
Table 2a. Representative Phlogopite Analyses (Group 1).	28
Table 2b. Representative Amphibole Analyses (Groups 1 and 4)	29
Table 3. Compilation of Isotopic and Chemical Data.....	34

LIST OF FIGURES

Figure 1. Geodynamic Setting.....	2
Figure 2. Geologic Map and Location of Sample Sites	6
Figure 3. Outcrop Photographs of Different Rock Groups	13
Figure 4. Photomicrographs of Groups 1 and 4	16
Figure 5. P-T Perple_X Equilibration Diagram	23
Figure 6. Major Element X-ray Maps	24
Figure 7a. Mineral Chemistry: K ₂ O vs. Al ₂ O ₃ and Na ₂ O vs. Cr ₂ O ₃ Plots	30
Figure 7b. Mineral Chemistry: Na ₂ O vs. Al ₂ O ₃ and Na vs. Al Plots.....	31
Figure 7c. Mineral Chemistry: Na ₂ O vs. Cl and K ₂ O vs. Cl Plots.....	32
Figure 8. $\delta^{37}\text{Cl}$ ‰ vs. Na ₂ O, K ₂ O, and Cl Plots.....	35
Figure 9. $\delta^{37}\text{Cl}$ ‰ vs. δD ‰ plot.	41

PREFACE

The following manuscript discusses the use of chlorine isotopes to document separate metasomatic events within the Finero peridotite body, located in the Italian Alps. This study addresses the geodynamic setting in which metasomatism occurred and speculates on the origins of the metasomatic fluids. All samples used in this study were collected by Dr. Selverstone and myself in the summer of 2008. Drs. Selverstone and Sharp were advisors for this study.

The author of this thesis was responsible for sample preparation, including billet preparation for thin sections and whole rock powders for bulk chemistry. The author acquired all of the bulk chemical data, most of the microprobe analyses, and all of the chlorine isotopic analyses. The author was also responsible for petrography, pseudosection modeling, and sample preparation for hydrogen isotopic analysis. Microprobe data were acquired in collaboration with Dr. Selverstone, bulk geochemical analyses under the supervision of Dr. Ali, and chlorine isotopic analyses under the supervision of Drs. Barnes and Sharp. Hydrogen isotopic analyses were provided by Dr. V. Atudorei. Interpretations of the data were made in collaboration with Drs. Selverstone and Sharp.

Results of this study were presented at the American Geophysical Union (AGU) in Fall 2009 by Dr. Selverstone. This thesis will be converted into a coauthored manuscript (Halick, Selverstone, Sharp, and Barnes) that will be submitted to a peer-reviewed journal.

INTRODUCTION

The phlogopite peridotites of the Finero Complex in the Italian Western Alps show clear evidence for mantle metasomatism prior to their incorporation in the continental crust (Exely et al., 1982; Coltorti et al., 1984; Farrario and Garuti, 1990; Shervais and Mukasa, 1991; Hartmann and Wedepohl, 1993; Zanetti et al., 1999; Garuti et al., 2001; Grieco et al., 2001; Grieco et al., 2004; Zaccarini et al., 2004; Matsumoto et al., 2005; Raffone et al., 2006; Morishita et al., 2008). Two different hypotheses dominate the literature regarding the cause of mantle metasomatism at this locality: (1) metasomatism resulted from mantle upwelling, either in response to continental rifting or mantle plume activity (e.g., Zaccarini et al. 2004), or (2) metasomatism resulted from subduction fluids infiltrating the mantle wedge above an ancient subduction system (e.g., Zanetti et al. 1999) (Figure 1).

In general, extension-dominated settings result in asthenospheric upwelling and partial melting of fertile or depleted lithospheric mantle, producing elemental enrichments and chemical re-equilibration of the overlying mantle (e.g., Bailey, 1982; Hawkesworth et al., 1984). In this setting, as well as a mantle plume-type setting, metasomatism due to partial melting contributes to the enrichment of incompatible elements (e.g., REE, K, Na, Rb, Pb, U, Th, Nb and Ta). In convergent settings, mantle metasomatism is mostly due to hydrous, slab-derived fluids/melts infiltrating the mantle wedge. This type of metasomatism also causes elemental enrichments, however large ion lithophile elements (LILE) and high field strength elements (HFSE) are strongly decoupled. This geochemical decoupling is a unique geochemical signature that is linked

to devolatilizing, hydrous fluids derived from a subducting lithospheric slab (e.g., Hawkesworth et al., 1993).

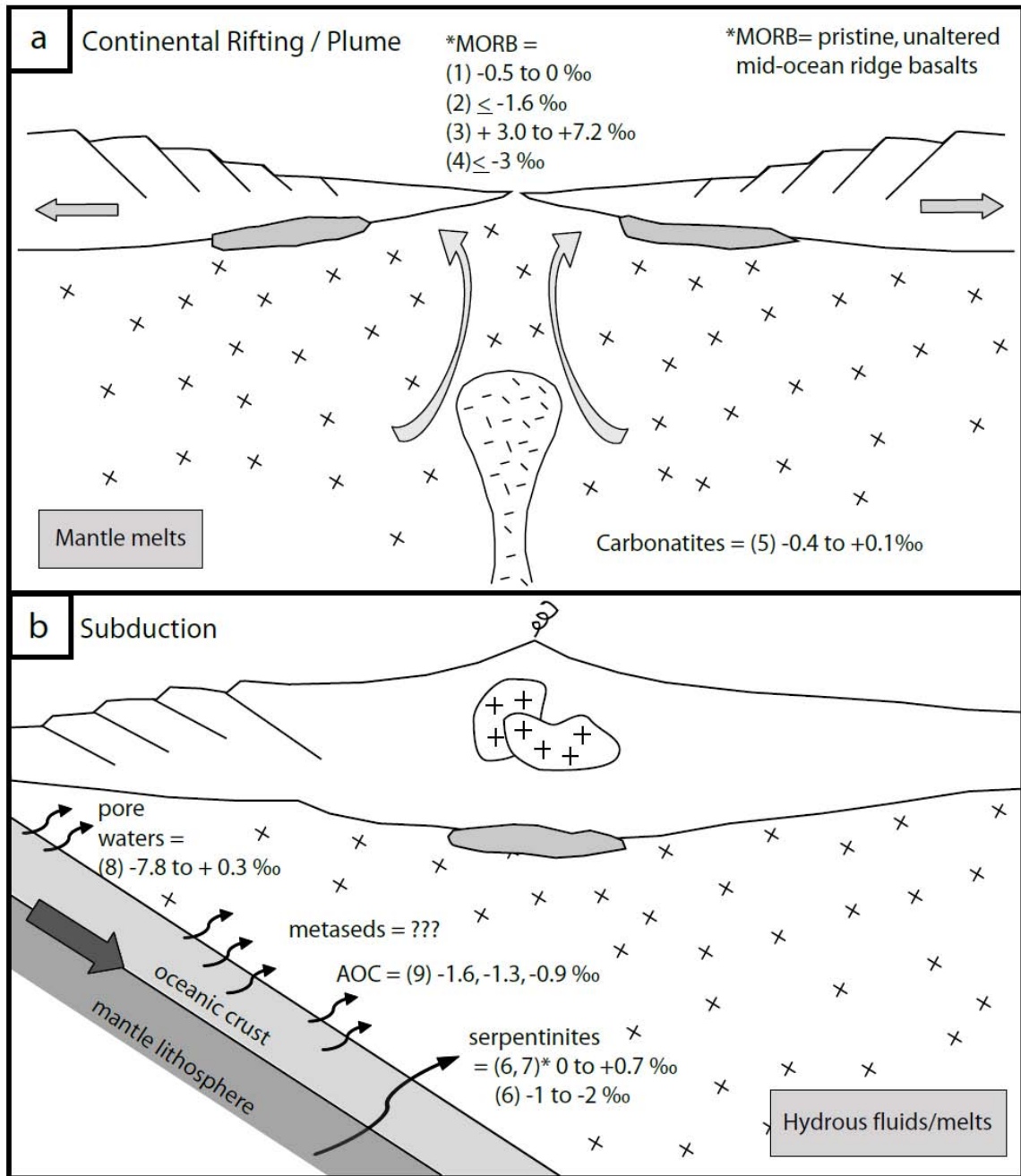


Figure 1. Cartoon sketch showing two geodynamic hypotheses for the Finero phlogopite + amphibole peridotite. (a) Continental extension/mantle plume setting with previously documented $\delta^{37}\text{Cl}$ values. Metasomatism is caused by mantle-derived melts above an upwelling zone. Infiltrating melts will have mantle $\delta^{37}\text{Cl}$ values similar to those of the host peridotites, producing little to no outcrop-scale isotopic variability. (b) Subduction setting with previously documented $\delta^{37}\text{Cl}$ values for possible subduction

fluid/melt sources. Subduction fluids released from different components of the subducting slab may be isotopically distinct. Infiltration of discrete fluid packages into the mantle wedge produces isotopic heterogeneities over outcrop or regional scale. Isotopic values compiled from (1) Sharp et al., 2007; (2) Bonifacie et al., 2008a; (3) Magenheimer, 1995; (4) Layne et al., 2009; (5) Eggenkamp and Koster van Groos, 1997; (6) Barnes and Sharp, 2006; (7) Bonifacie et al., 2008b; (8) compiled in Barnes and Sharp, 2008; (9) Bonafacie et al., 2007. Asterisk in the lower diagram denotes that the majority of oceanic serpentinites fall within the $\delta^{37}\text{Cl}$ range of 0 to +0.7 ‰.

In this study, we use a relatively new geochemical technique, chlorine isotope geochemistry, combined with other geochemical data to distinguish between these two tectonic settings, both of which have been proposed for metasomatism at Finero. Chlorine is not a major rock-forming element and is strongly incompatible and hydrophilic, preferentially partitioning into a hydrous fluid phase (Note: we use “fluid” to refer to either a supercritical hydrous fluid or a hydrous silicate melt). In silicates, chlorine substitutes for the hydroxyl site in hydrous minerals, such as micas, amphiboles, and serpentines (Volfinger et al., 1985). In addition, chlorine isotopic fractionation is theorized to be negligible at high temperatures for silicate minerals (Schauble et al., 2003). Thus, if little to no fractionation occurs under lithospheric mantle conditions, chlorine isotope ratios should reflect the fluid sources involved in mantle metasomatism and the pathways along which fluid moved through the lithospheric mantle.

Chlorine has two stable isotopes, ^{37}Cl and ^{35}Cl , that are reported using the standard per mil notation versus SMOC (Standard Mean Ocean Chloride), where $\delta^{37}\text{Cl} = [((^{37}\text{Cl}/^{35}\text{Cl})_{\text{sample}}/(^{37}\text{Cl}/^{35}\text{Cl})_{\text{SMOC}})-1]$. Consensus over the average $\delta^{37}\text{Cl}$ value of the mantle is still under discussion. Sharp et al. (2007) state that upper mantle $\delta^{37}\text{Cl}$ values are approximately 0‰ (Sharp et al., 2007), whereas Bonifacie et al. (2008a) and Layne et

al. (2009) argue for isotopically lighter values of $\leq -1.6\text{‰}$ and $< -3\text{‰}$, respectively, and Magenheimer (1995) argues for isotopically heavy $\delta^{37}\text{Cl}$ values of $+4.7\text{‰}$. Regardless of the previously reported $\delta^{37}\text{Cl}$ values, our expectation is that melts sourced from the mantle should be isotopically uniform if metasomatism at Finero resulted from infiltration of mantle melts. This hypothesis assumes that chlorine isotope fractionation is negligible at high temperatures. If this assumption is correct, then $\delta^{37}\text{Cl}$ values throughout the phlogopite peridotite should be relatively homogeneous (Figure 1). Alternatively, if metasomatism was a result of infiltrating fluids/melts derived from different parts of the subducting slab, then the reasonable expectation is that isotopic heterogeneities should be preserved under mantle conditions.

Therefore, bulk rock $\delta^{37}\text{Cl}$ values from Finero peridotites should reflect the isotopic nature of metasomatizing fluids and the tectonic setting in which metasomatism occurred. Here, we attempt to resolve the geodynamic setting of mantle metasomatism and document outcrop-scale chemical heterogeneities (if any) based on chlorine and hydrogen isotope ratios and mineral geochemistry of phlogopite and amphibole. In addition, we address possible fluid sources of the altering agent(s) and relate geochemical differences to field occurrences to constrain whether fluid migration at Finero was pervasive or limited.

GEOLOGICAL SETTING

Ivrea-Verbano Zone

The Ivrea-Verbano Zone (IVZ) is located in the southern Alps in northwestern Italy and represents a relatively intact, steeply dipping section of the Adriatic lower crust

with tectonically emplaced slices of the underlying lithospheric mantle (Quick et al., 1995). Three large, well-documented mantle peridotites of the IVZ are exposed near the villages of Finero, Balmuccia, and Baldissero, where all peridotite bodies are exposed near the Insubric Line, a major tectonic fault zone that generally separates the European plate from rocks with Adriatic continental affinity (Figure 2). These mantle tectonites are geochemically and isotopically distinct from one another, exhibiting different degrees of melt depletion, crustal assimilation and metasomatism (Hartmann and Wedepohl, 1993). The Balmuccia and Baldissero mantle bodies show little melt depletion or re-enrichment (Hartmann and Wedepohl, 1993), whereas the Finero mantle peridotite was depleted by approximately 18% melt (MORB) extraction and subsequently re-enriched via mantle metasomatism. The presence of phlogopite and amphibole in the Finero mantle peridotite requires at least one H₂O-rich metasomatic episode prior to lower-crustal emplacement.

Early work in this area interpreted the exposed lower crustal rocks, ultramafic cumulates, and mantle peridotites as a pre-Alpine crust-lithospheric mantle transition, or a relict petrologic Moho (e.g., Mehnert, 1975). This view dominated the literature for decades until recent field studies (Quick et al., 1995; Quick et al., 2003) showed that, at least at Balmuccia, the exposed mantle peridotite is tectonically interfingering with deep-crustal metasedimentary rocks and mafic rocks. The present-day configuration and large-scale geologic structures are attributed to rapid exhumation during the Alpine orogeny (see Peressini et al., 2007, for a full review of geochronologic data from the IVZ).

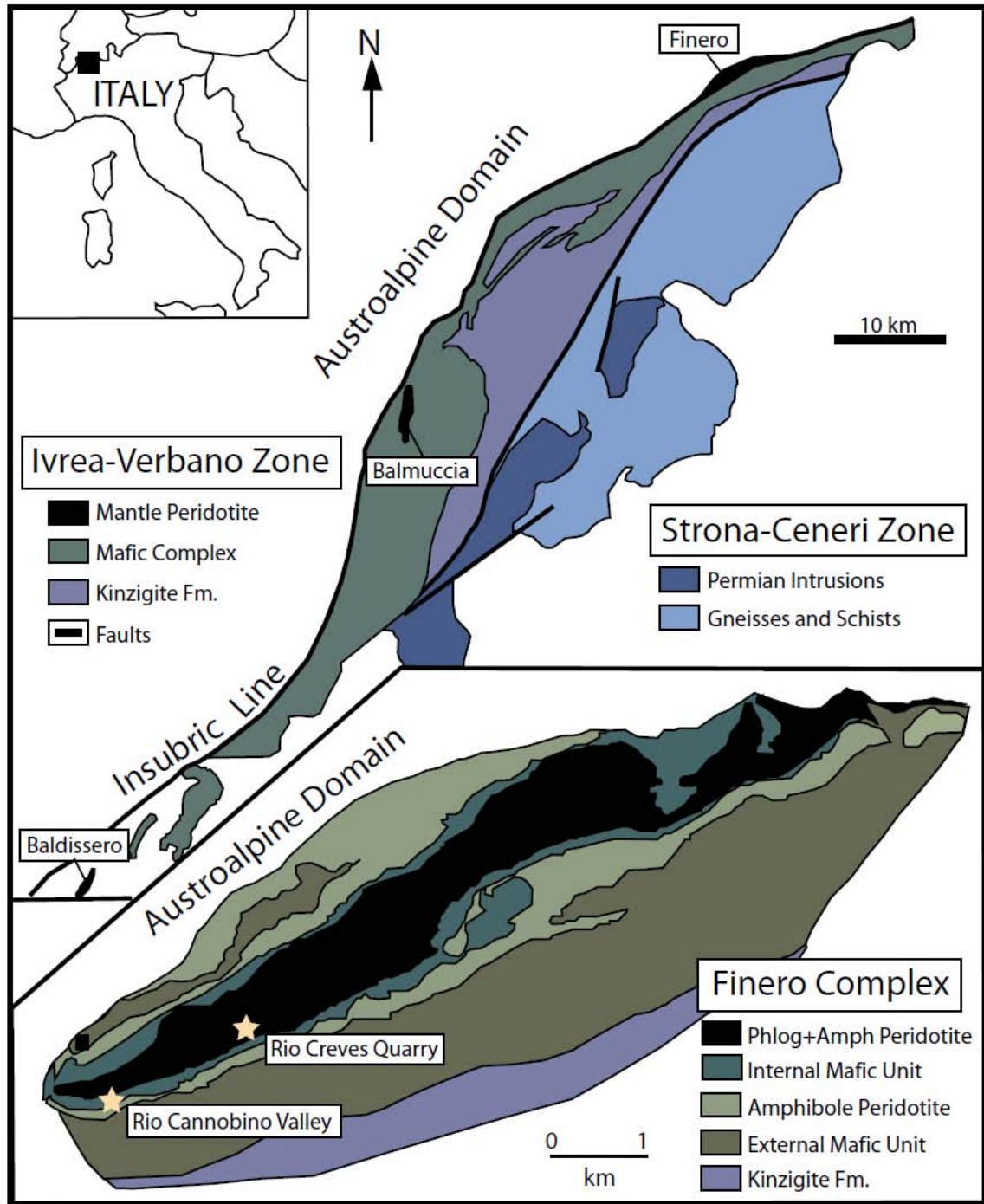


Figure 2. Simplified geological map of the Ivrea-Verbano Zone and Finero Complex modified from Zanetti et al. (1999). Upper inset is a regional geologic map (based on Zingg, 1983) that shows the location of the Ivrea-Verbano Zone. Lower inset is a detailed map of the Finero mafic-ultramafic complex originally from Steck and Tieche (1976). Sample locations (Rio Cannobino Valley and Rio Creves quarry) are marked by stars.

Finero Complex

The Finero Complex is an antiformal structure consisting of four main lithologic units: Upper/External Metagabbro, Amphibole Peridotite, Lower/Internal Metagabbro, and Phlogopite Peridotite (Lensch, 1968; Hunziker, 1974; Cawthorn, 1975; Coltorti and Siena, 1984; Siena and Coltorti, 1989; Voshage et al., 1987; Hartmann and Wedepohl, 1993). These units, excluding the Phlogopite Peridotite, represent a series of voluminous mafic magmas that intruded a thick metasedimentary package, the Kinzigite Formation, while resident in the lower crust. The metasedimentary package records amphibolite-granulite conditions and consists of schist, marble, and mafic schist/gneiss. The younger Mafic Complex intruded the Kinzigite Formation in discrete pulses over an extended period during the Permian (Lu et al. 1997) and consists of metagabbro, garnet-rich diorite, pyroxenite, hornblendite, cumulate amphibole gabbro, and cumulate ultramafic rocks (i.e., amphibole peridotite). The phlogopite peridotite was tectonically emplaced into the lower crust after intense metasomatism and is not genetically linked to the cumulate amphibole peridotite (Voshage et al., 1987; Hartmann and Wedepohl, 1993; Lu et al., 1997). Quick et al. (1995) and others argue that the phlogopite peridotite was emplaced prior to mafic plutonism. However, magmatic or crosscutting contacts are not exposed at the Finero locality and the timing of emplacement relative to intrusion of the Mafic Complex still remains unresolved.

The phlogopite peridotite body is dominated by spinel, phlogopite- and amphibole-bearing harzburgite (locally lherzolite or dunite), with highly variable phlogopite and amphibole abundances. It differs from the other peridotite bodies in the IVZ in being more depleted (~18% MORB extraction) and yet highly enriched in

incompatible elements (e.g., Hartmann and Wedepohl, 1993; Exley et al., 1982). The peridotite is pervasively enriched in K, Na, Cl, F, Ba, B, Li, Rb, Sr and LREEs and depleted in high field strength elements (HFSE) (Hunziker and Zingg, 1982; Hartmann and Wedepohl, 1993; Lu et al., 1997; Raffone et al., 2006), with local enrichment of Zr, U, Th, P, and HFSE, particularly in apatite-bearing and chromite-bearing layers (Ferrario and Garuti, 1990; Zanetti et al., 1999; Zaccarini et al., 2004; Matsumoto et al., 2005; Raffone et al., 2006; Morishita et al., 2008).

Previous studies of REE distributions in amphiboles from the phlogopite peridotite show two distinct patterns: one that is enriched in LREEs and one that shows a chondritic REE distribution (Hartmann and Wedepohl, 1993). These variations, along with differences in measured $^{87}\text{Sr}/^{86}\text{Sr}$ ratios ($^{87}\text{Sr}/^{86}\text{Sr} \sim 0.7030$ and 0.7070) have been attributed to two separate pulses of H_2O -rich metasomatizing fluid (Hartmann and Wedepohl, 1993). Zanetti et al. (1999) and Morishita et al. (2008) document variable mineral compositions and suggest that the heterogeneous distribution of phlogopite and amphibole throughout the massif reflects multiple fluid infiltration events.

Despite a large number of geochronologic studies, the timing of metasomatism at Finero remains poorly constrained, thus the tectonic setting in which metasomatism occurred is also poorly understood. U-Pb crystallization ages of zircon in metasomatic chromitites in the phlogopite peridotite range from 204 to 208 Ma (Von Quadt et al., 1993; Grieco et al., 2001). Phlogopite-bearing syenite dikes that crosscut the phlogopite peridotite massif yield zircon dates of 225 ± 13 (Stähle et al., 1990). The authors of these studies argue that the ages are consistent with formation of mantle melts during passive uplift of subcontinental lithospheric mantle during the early Triassic.

Rb-Sr and K-Ar dates on phlogopite and/or amphibole are likely to represent cooling ages rather than crystallization ages. However, some of these dates are older than the inferred crystallization ages determined from zircon. Hartmann and Wedepohl (1993) obtained Rb-Sr dates of 226 to 163 Ma on four amphibole-phlogopite pairs, in contrast to K-Ar dates of 208 ± 9 Ma determined by Hunziker (1974) on phlogopite. Vosage et al. (1987) presented a whole-rock Rb-Sr date of 293 ± 13 Ma for the phlogopite peridotite. It is unclear whether any of these ages are meaningful, and the timing of mantle metasomatism is thus still open to debate.

Previous Interpretations

The tectonic setting of the Finero peridotites at the time of mantle metasomatism has been a question of debate. Various authors have argued that the geochemistry of the phlogopite peridotites constrains the metasomatizing agent to be either (1) mantle melts generated above a subcontinental mantle plume or in response to continental rifting (e.g., Zaccarini et al. 2004; Garuti et al., 2001), or (2) metasomatism resulted from subduction fluids infiltrating the mantle wedge above an ancient subduction system (e.g., Zanetti et al. 1999). These interpretations imply completely different tectonic settings (extensional vs. compressional). In addition, previous studies have documented chemical heterogeneities in the phlogopite + amphibole peridotite and suggest that metasomatism resulted from fluid multiple events (Hartmann and Wedepohl, 1993). A brief review of the literature surrounding these two interpretations is described below.

1) Exley et al. (1982) suggested that the metasomatizing agent responsible for phlogopite formation was an alkali-rich fluid of mantle origin. Subsequent studies link

the geochemistry of the apatite- and chromitite-bearing lithologies to carbonatitic and alkaline metasomatism, consistent with magmatic processes during continental rifting or mantle plume activity (Shervais and Mukasa 1991; Garuti *et al.*, 2001; Zaccarini *et al.* 2004). In addition, Stähle *et al.* (1990) documented the presence of syenite dikes within the peridotite massif that retain high Th, Nb and U contents. Based on these HFSE enrichments, these authors ruled out the interpretation that dike formation was a result of subduction-derived fluids. Sr and Nd isotopic ratios of the syenite dikes also have been interpreted to reflect melts derived from a mantle source. (Stähle *et al.*, 1990). Zaccarini *et al.* (2004) go into further detail, suggesting that the metasomatizing agent evolved with decreasing temperature, thereby enriching the melt in highly incompatible elements such as Zr, U, Th, Cl, F, P, and CO₂ and forming chromitites on the periphery of the mantle peridotite. They state that metasomatic production of the phlogopite peridotite is consistent with mantle diapirism at the base of continental crust and was most likely associated with continental rifting. Accessory minerals rich in Zr, U, and Th, such as zirconolite, have been linked to the phlogopite + amphibole assemblage and are interpreted to have crystallized from silica-undersaturated, hydrous melts that were rich in alkalis, LILE and HFSE (Ferrario and Garuti, 1990; Grieco *et al.*, 2001, 2004; Zaccarini *et al.*, 2004). Such fluids would be consistent with mantle derived melts and therefore likely represent a continental plume or rift-type setting (Ferrario and Garuti, 1990; Grieco *et al.*, 2001, 2004; Zaccarini *et al.*, 2004). However, all of these studies focus on rare and localized features and accessory minerals of the phlogopite peridotite and may not apply to the entire phlogopite + amphibole peridotite massif.

2) Other studies focus on subduction fluids/melts as the main metasomatizing agents (Hartmann and Wedepohl, 1993; Lu et al., 1997; Zanetti et al., 1999; Matsumoto et al., 2005; Raffone et al., 2006; Morishita et al., 2008). Detailed geochemical and isotopic studies show that the phlogopite + amphibole peridotite retains a crustal signature based on Nd and Sr isotopic compositions and is not related to crustal anatexis or crustal interactions during tectonic emplacement (e.g., Lu et al., 1997). These authors agree that „contamination“ occurred while the host body was resident in the mantle and that the crustal imprint must thus be a result of subduction-related fluids. Hartmann and Wedepohl (1993) document depletion in Nb, Ti, U, Th, and other high-valence elements and strong enrichment of incompatible elements such as LREEs, Na, K, Cl, F, a signature that is consistent with subduction zone fluids (excluding the apatite layers, chromitite-rich pods, and zircon-rich syenite dikes). Zanetti et al. (1999) also document whole rock Sr ratios of 0.7055 to 0.7093 and negative ϵ_{Nd} values, as well as δD (amphibole & phlogopite: δD -29 to -44) and $\delta^{18}\text{O}$ values (amphibole: avg. +6.2‰; phlogopite: avg. +6.2‰) that are consistent with a crustal signature. Furthermore, various authors argue that apatite-bearing layers/regions have a different geochemical signature compared to the apatite-free phlogopite + amphibole peridotites and can be explained by evolution of immiscible, H_2O - CO_2 subduction melts/fluids (Zanetti et al., 1999; Matsumoto et al., 2005; Morishita et al., 2008). An alternative hypothesis is that apatite-bearing and apatite-free peridotites reflect two separate metasomatic events: one that is mantle derived and one that is slab derived (Raffone et al., 2006). This study focuses primarily on apatite-free, hydrous peridotites, with only a single sample containing significant apatite (FIN-22B).

FIELD AND SAMPLE DESCRIPTIONS

Phlogopite peridotites were collected along the banks of the Cannobino River and in an abandoned quarry along the hillslope northwest of the Creves River. Samples of the cumulate amphibole peridotite of the Mafic Complex were collected along the bank of the Cannobino River south of the village of Finero. Detailed transects along fresh outcrops were sampled to document isotopic and geochemical heterogeneities across the phlogopite and amphibole peridotite bodies.

Phlogopite-Amphibole Peridotite: Mantle Tectonite

This peridotite is referred to as the phlogopite peridotite in the literature, although amphibole locally occurs in higher abundances than phlogopite. This peridotite is foliated with amphibole- and phlogopite-rich bands similar in orientation to the main peridotite foliation. Some randomly oriented phlogopite-rich segregations crosscut the dominant peridotite foliation and thus are interpreted to be younger than phlogopite-amphibole assemblages in the host peridotite. In this study, samples from the mantle peridotite are classified into three groups based on mineralogy and field occurrence: (1) phlogopite-amphibole peridotite (mainly harzburgite); (2) crosscutting phlogopite + amphibole segregations; and (3) a single phlogopite + orthopyroxene segregation (cross-cutting relationship unknown) (Figure 3).

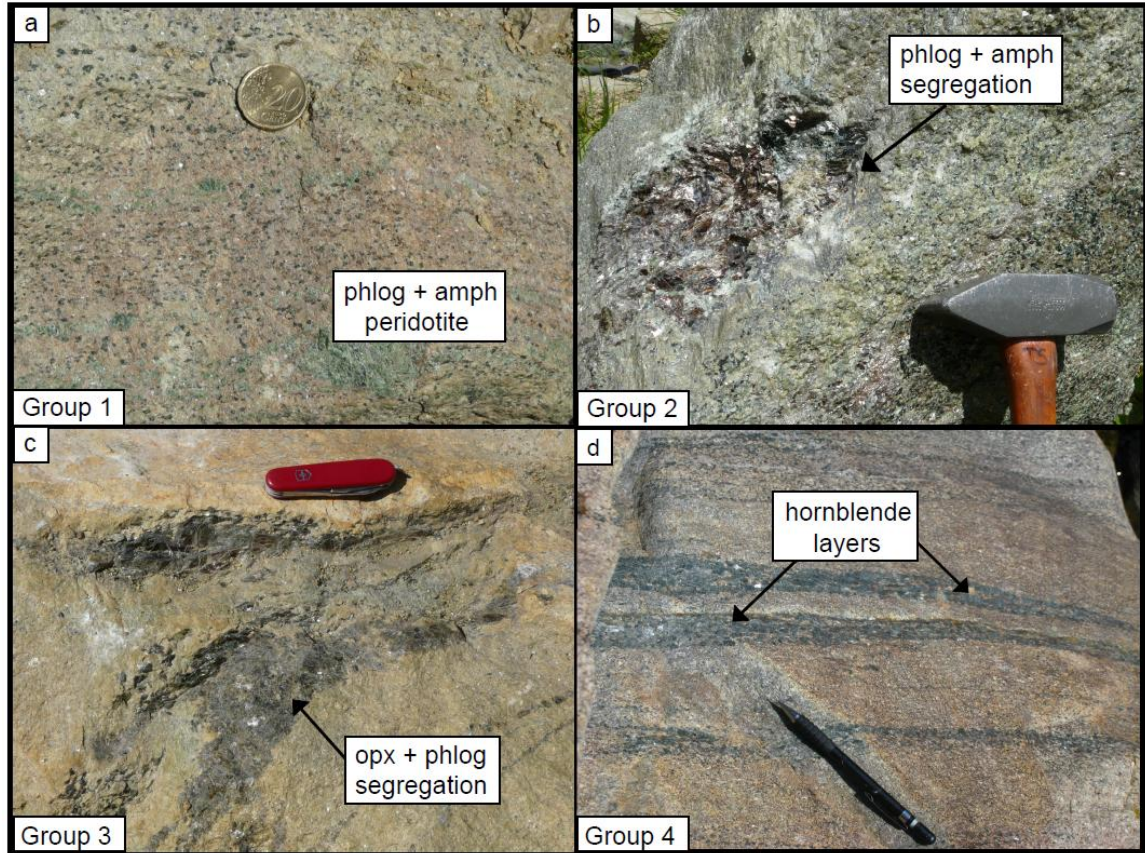


Figure 3. Photographs of outcrop appearance of the four rock types collected. (a) Group 1: foliated phlogopite + amphibole peridotite. (b) Group 2: phlogopite + amphibole segregation cross-cutting peridotite foliation. (c) Group 3: phlogopite + orthopyroxene segregation cross-cutting peridotite foliation. (d) Group 4: cumulate amphibole peridotite showing concordant hornblende layers (magmatic origin).

Group 1:

Representative samples of this group are foliated phlogopite + amphibole harzburgites (locally lherzolites and dunites), which we interpret to represent the oldest metasomatic event(s) of the three groups (Figure 3a). Petrographically, this group is distinct from the cumulate peridotite as it contains dark brown spinel and Cr-bearing edenitic to magnesiohastingsitic amphibole (bright green), and lacks cumulate textures. Phlogopite and amphibole are present in varying abundances, both ranging from <1% to ~15%. Amphibole and phlogopite appear both as isolated grains and in fine-scale

intergrowths that indicate co-crystallization with one another (Figure 4). Grains are typically euhedral and are heterogeneously distributed between olivine and pyroxene grains; layers of interconnected phlogopite grains are rare. Both olivine and orthopyroxene show a prominent shape-preferred orientation (SPO) in most samples and are characterized by deformation lamellae, with some samples showing evidence for subgrain rotation recrystallization. These features are consistent with deformation under high-temperature conditions, most likely while resident in the mantle and before emplacement into the lower crust (e.g., Hirth et al., 2002; Jung and Karato, 2001). Phlogopite is strongly aligned in the olivine foliation, and is locally kinked. There is no evidence to suggest that phlogopite growth postdates development of the olivine-pyroxene foliation, and we thus infer that growth and alignment of the hydrous minerals also occurred in the mantle. No reaction textures are preserved, suggesting that equilibration between the mantle peridotite and metasomatizing fluid was attained.

Group 2

Rare, localized amphibole + phlogopite segregations/pods were observed at both localities but were only sampled on the hillside of the Rio Creves. These segregations are 5-10 cm in length and appeared as clearly defined, isolated pods containing only books of phlogopite and massive green, Cr-rich amphibole (Figure 3b). These segregations crosscut the peridotite foliation of Group 1, signifying a younger metasomatic event. Phlogopite flakes were extracted with a knife from two separate segregations. Owing to the small amount of sample material that was collected, only isotopic data are available for these samples.

Group 3

In addition, a rare orthopyroxene + phlogopite segregation, was sampled (Figure 3c). This segregation was collected from a float block in the Rio Creves quarry and the cross-cutting relationship to the peridotite foliation is ambiguous for this sample. This segregation was the only one of its kind that we observed. The sample was collected as described for Group 2 samples and all sample material was used for isotopic analysis.

Amphibole Peridotite: Ultramafic Cumulate

Group 4

Amphibole \pm spinel (olive-green in thin section) peridotite is present at the base of a layered cumulate body in the Mafic Complex. Group 4 amphiboles are dominantly pargasitic and are chemically and texturally unrelated to amphiboles from the other previously described rock groups. Rock types within the peridotite body range from dunite with 2% interstitial amphibole to lherzolite with up to 35% amphibole (Figure 3d). Although highly variable, amphibole modal abundances generally increase towards the internal mafic unit. Cumulate textures are well preserved, with olivine as the major cumulate phase. Enstatite and amphibole generally occur as intercumulus phases, with amphibole typically rimming opaque minerals (Figure 4). Phlogopite was not observed, although Coltorti and Siena (1984) reported the presence of phlogopite rimming amphibole. Coarse-grained, concordant pyroxenite and amphibole-rich layers or sills are prevalent and range in size from a few millimeters to tens of centimeters in width.

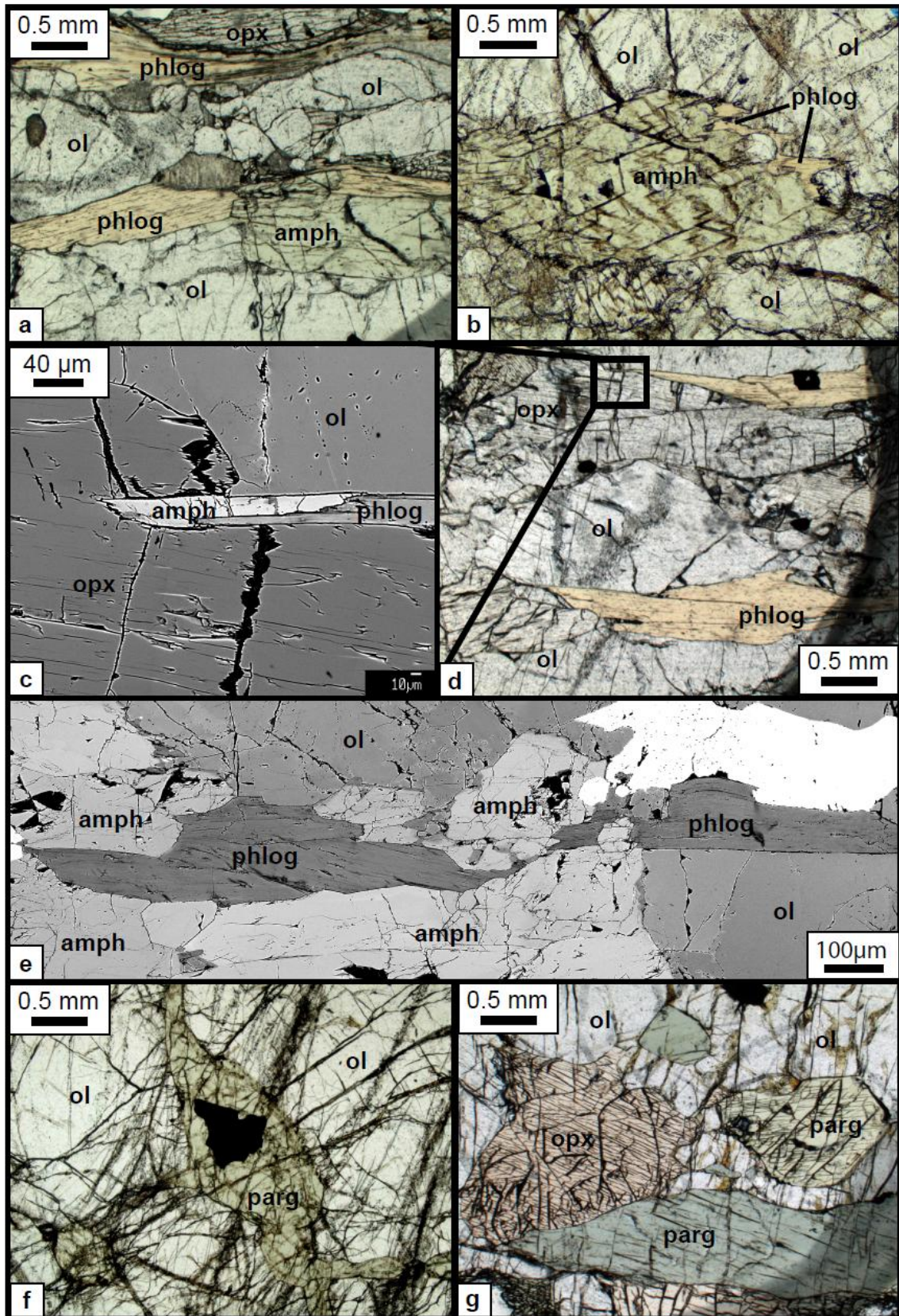


Figure 4. (a, b) Photomicrographs of foliated, phlogopite + amphibole peridotite (Group 1). Amphibole is associated with and/or intergrown with phlogopite, indicating co-crystallization. (c, d) Backscattered electron (BSE) image and photomicrograph showing amphibole intergrown with phlogopite. (e) Merged BSE image showing textural equilibration of phlogopite and amphibole. (f, g,) Photomicrographs of (Group 4) cumulate amphibole peridotite. Pargasite typically occurs as a cumulate phase surrounding opaque minerals.

ANALYTICAL METHODS

Whole-Rock Chemistry

The whole-rock compositions of samples from Group 1 and 4 were determined by X-ray fluorescence spectrometry using a Rigaku ZSX Primus II wavelength dispersive X-ray spectrometer. All rock samples were powdered and pressed using 9 g of sample and 1 g of powdered boric acid as a binder. Major and trace elements were analyzed semi-quantitatively using the EZscan method and the Rigaku internal reference library. Replicate analyses of standard reference materials BVHO-1 as secondary standards yielded values within ± 10 relative percent of the reported values for most elements. A quantitative routine was set up for chlorine using nine standard reference materials with reported values ranging between 71 and 1200 ppm Cl; standard SDC-1 (32 ppm Cl) was utilized as a secondary standard.

Perple_X Modeling

Pressure-temperature pseudosections were calculated to help constrain the conditions of metasomatism for Group 1 samples using the thermodynamic software Perple_X_07 (Connolly, 2009). Bulk compositional data for the samples are discussed below. To model Cr-rich, hydrous peridotites, we used the solution file solut_08.dat in

conjunction with the cr_hp02ver.dat data file (Klemme et al., 2009). Stable assemblages were calculated over the range 10-24 kbar and 800-1200°C, with no saturated phase components. Thermodynamic components selected were SiO₂, Al₂O₃, Cr₂O₃, MgO, FeO, CaO, Na₂O, K₂O, and H₂O, assuming different weight amounts of H₂O depending on the modal abundances of hydrous minerals. Solution models used were O(HP), Cpx(HP), Opx(HP), CrSp, Bio(HP), Gt(HP), and Pl(h) (Dienier et al., 2007; Holland and Powell, 1996; Holland and Powell, 1998; Newton et al., 1980; Powell and Holland, 1999). The range of amphibole stability was approximated by using endmember pargasite for the final calculations. Because the amount of H₂O at the time of metasomatism is unknown, we used a minimum and maximum quantity of water to constrain the range of conditions needed for equilibration of phlogopite and amphibole. The minimum water content for each sample was taken to be the H₂O content below which sanidine ± feldspathoid appeared in place of phlogopite in the calculated mineral assemblages. Maximum water contents were distinguished by the presence of free H₂O as a phase in the model output. The determined maximum water contents used for this study are likely the more realistic approach for modeling P-T conditions during fluid infiltration and metasomatism.

Mineral Chemistry

Quantitative analysis on multiple samples from the phlogopite peridotite, amphibole peridotite and the internal mafic unit was performed using the JEOL JXA-8200 electron microprobe located in the Earth and Planetary Sciences Department at the University of New Mexico. Points of interest for quantitative analysis included intergrown phlogopite and amphibole, solitary phlogopite, and solitary amphibole.

Analytical conditions were 10 nA and 15 kV, for count times ranging from 15 to 50 seconds. A wide range of well-characterized natural and synthetic minerals were used as standards.

X-ray compositional maps of major elements (Ca, Na, K, Mg, and Fe) in phlogopite and amphibole were obtained to look for evidence of chemical zoning. Analytical conditions for major-element maps were 300 nA, 15 kV and 30-60 msec dwell times. Pixel size was 1 μm and the maps ranged in size from 150 to 650 pixels on a side. High-intensity Cl and Cr maps (1 μA , 15 kV and 100-500 msec dwell times) were obtained in the same areas as the major-element maps in order to correlate trace-element distributions with major element features. Cl and Cr were targeted because they represent fluid-mobile and -immobile elements, respectively, and any zoning in these elements would help to constrain the degree of fluid evolution during metasomatism.

Anion Analysis

The three phlogopite segregations were sampled by scraping mica sheets out of *in situ* pods in the field. The amount of material recovered was insufficient for XRF analysis. Therefore, samples were prepared using the Cl extraction procedure described below and collected solutions were analyzed for Cl^- using a Dionex DX-100 Ion Chromatograph.

Cl Isotopic Analysis and Cl Extraction

All samples were prepared for measuring structurally bound chlorine in hydrous minerals; water-soluble chlorine was not considered. Weathered portions of all samples

were removed and fresh rock samples were crushed to centimeter-millimeter size and sonicated in 3 separate batches for 15 minutes each with 18M Ω deionized water. This ensures that any contamination of chlorine during sample collection and initial preparation is negligible. Cleansed rock fragments were then powdered and bulk chlorine was extracted from powdered rock via pyrohydrolysis (Magenheim et al., 1994) following the method described in Barnes and Sharp (2006). Bulk chlorine was collected in a hydrous solution and ultimately transformed into methyl chloride (CH₃Cl) as described in Eggenkamp (1994) and Eggenkamp et al. (1995). This process is based on the assumption that all structurally bound chlorine is released during devolatilization when heated to sufficient temperatures (>1100°C). Previous studies have shown that extracted chlorine yields are close to the predicted whole-rock values (e.g., Bonifacie et al., 2007; Barnes and Sharp, 2006). However, peridotite powders were difficult to fuse and there was concern that the structurally bound chlorine from the hydrous phases (phlogopite + amphibole) did not undergo complete devolatilization. Thus, powdered, ultrapure lithium tetraborate (Li₂B₄O₇) was used as a flux to lower the melting temperature of the system and ensure that all chlorine was released.

After pyrohydrolysis, the solution is reacted with 4 mL of 1 M KNO₃ to raise the ionic strength of the solution and 2 mL of Na₂HPO₄-citric acid buffer is used to fix the pH at 2.2 (e.g., Eggenkamp 1994; Barnes and Sharp, 2006). The solution is gently heated to 80°C, releasing any dissolved CO₂ from solution. 1 mL of 0.4 M AgNO₃ is added to the solution, which causes Cl⁻ to precipitate as AgCl. The complete reaction of Cl⁻ to AgCl occurs in approximately 12 hours in darkness to prevent photo-oxidation. Solutions are then filtered through a silica fiber filter, where AgCl precipitate is collected and dried.

The AgCl precipitate and silica filter are inserted into a clean Pyrex tube and pumped to vacuum. While maintaining vacuum, methyl iodide (CH_3I) is injected into the Pyrex tube in excess (40 μL) and is frozen in the reaction tube using liquid nitrogen. The Pyrex tube is then sealed under vacuum and heated to 80°C in the dark for 48 hours to ensure that all AgCl precipitate is transformed into CH_3Cl .

CH_3Cl is measured on a Finnigan MAT Delta XL Plus mass spectrometer following the method of Barnes and Sharp (2006). Excess $\text{CH}_3\text{I}_{(\text{g})}$ and $\text{CH}_3\text{Cl}_{(\text{g})}$ are separated using a gas chromatograph column (Barnes and Sharp, 2006) before gas enters and is analyzed by the mass spectrometer. Samples were measured using either dual inlet or continuous flow methods. Ongoing lab precision is $\pm 0.4\text{‰}$ using continuous flow and $\pm 0.1\text{‰}$ using dual inlet. All samples are referenced to the SMOC standard (Standard Mean Ocean Chloride) and written in per mil notation.

Hydrogen Isotope Analysis

Hydrogen isotopic analyses were obtained for phlogopite segregations and separates. In order to have hydrogen isotopic values coincide with bulk chlorine isotopic values (amphibole + phlogopite), analysis of bulk hydrogen using whole-rock powders was attempted, but due to the small amount of hydrogen in each sample, the data were inconsistent and are not used in this study. Instead, we used phlogopite separates, which were sonicated with 18 M Ω DI water for three, five-minute intervals. Separates were then heated to temperatures greater than 100°C to remove any contamination. All samples were then placed in silver foil capsules and dropped into a furnace. Gases were separated

using a GC column and hydrogen ratios were measured using a Finnigan MAT Delta^{PLUS}. This procedure closely follows the method detailed in Sharp et al. (2001).

RESULTS

Whole-Rock Geochemistry and Chlorine Concentrations

XRF analyses of samples from groups 1 and 4 are shown in Table 1a and 1b. These data were primarily used to calculate pseudosections to constrain the P-T conditions of metasomatism of Group 1 samples. Whole-rock chlorine concentrations were used to determine how much sample was needed for chlorine isotopic analysis. Chlorine concentrations from Group 1 samples range from 50 to 679 ppm and chlorine concentrations from Group 4 samples range from 81 to 90 ppm. Higher chlorine concentrations in Group 1 samples correspond to greater modal abundances of amphibole and phlogopite. Phlogopite segregations from Group 2 have chlorine concentrations of 558 and 893 ppm and the phlogopite separate from Group 3 yielded a concentration of 750 ppm (anion analysis).

Modeled Pressure and Temperature Constraints

Preliminary modeled pseudosections were matched up with the actual mineral assemblage present for each corresponding sample, and the region of equilibration in P-T space is where the modeled mineral assemblage matches the actual mineral assemblage present in thin section. These equilibrium conditions correspond to the left side (low T side) of the lines indicated in Figure 5 (see appendix for all modeled samples). Equilibration conditions are constrained by two samples, FIN-25B and FIN-21D. Sample

FIN-21D places the tightest constraints on temperatures estimates to ~800-900°C. This temperature estimate is based on the pargasite-out reaction line shown in Figure 5. Sample FIN-25B helps constrain the pressures to ~1.2-1.4 GPa. This pressure estimate is based on the presence of chromium spinel stability field. Because all samples were collected in close proximity to one another, it is reasonable to assume that all samples reached similar equilibration conditions. Thus, these preliminary equilibration pressures and temperatures common to all samples is constrained to 800-900°C and ~1.2-1.4 GPa, consistent with the spinel lherzolite stability field (Figure 5). These pressures and temperatures are in agreement with previous studies that conclude that metasomatism and equilibration occurred under upper mantle conditions (Ernst, 1978; Hartmann and Wedepohl, 1993; Ferraris et al., 2004). Microstructures (deformation lamellae and SPO) observed in olivine and orthopyroxene are also consistent with this temperature range (e.g., Passchier and Trouw, 2005).

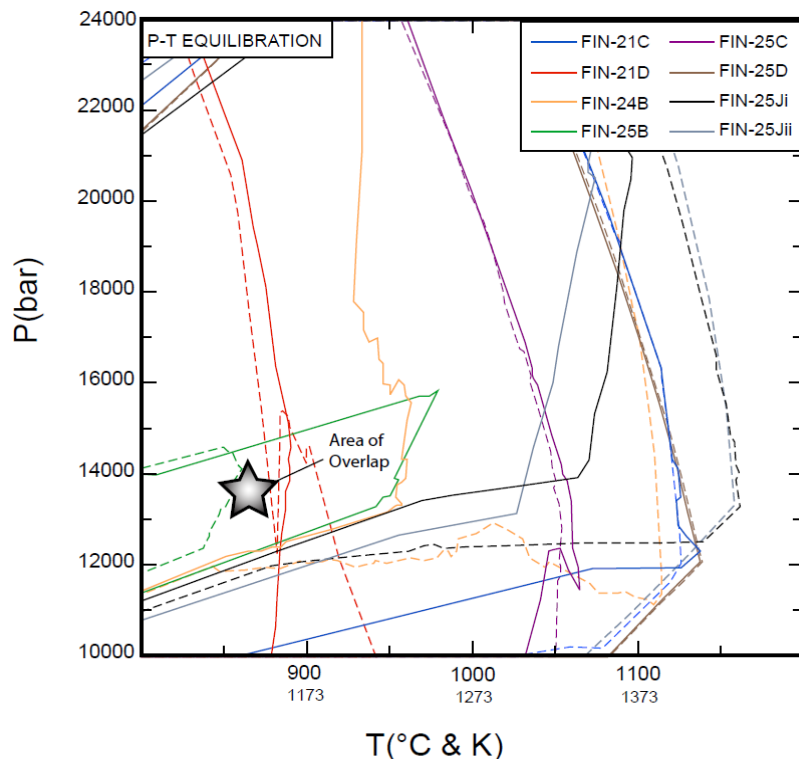


Figure 5. Preliminary P-T equilibration diagram generated with *Perple_X*. Solid lines show stable assemblages using minimum H₂O contents calculated for each sample. Dashed lines show stable assemblages using maximum H₂O contents appropriate for each sample. The left side of the lines represent the modeled assemblage that correlates with the assemblage observed in thin section. Two samples, FIN-25B and FIN-21D, tightly constrain the pressures and temperatures of equilibration. Area of overlap for all bulk compositions is ~800-900°C and ~1.2-1.4 GPa

Mineral Chemistry (Groups 1 and 4)

Microprobe analyses reveal significant variations in phlogopite and amphibole compositions within and between samples from the phlogopite peridotite massif (Table 2a and 2b). Phlogopite shows detectable differences in Al, Na, and K in samples collected within a few meters (or less) of one another in the same outcrop (Figure 6 and 7). X-ray maps (Figure 6) show no major element zoning; however, there are Na-rich and Na-poor bands parallel to mica cleavage planes (Figure 6). These bands have been previously interpreted to result from a miscibility gap between aspidolite and phlogopite, the Na and K endmembers (Costa et al., 2001; Banno et al., 2005). Group 1 amphiboles also show relatively large variations in Al_2O_3 , Na_2O , and K_2O contents between samples (Figure 7a, 7b, 7c). Distinct differences are easily seen in Na_2O vs. Al_2O_3 and K_2O vs.

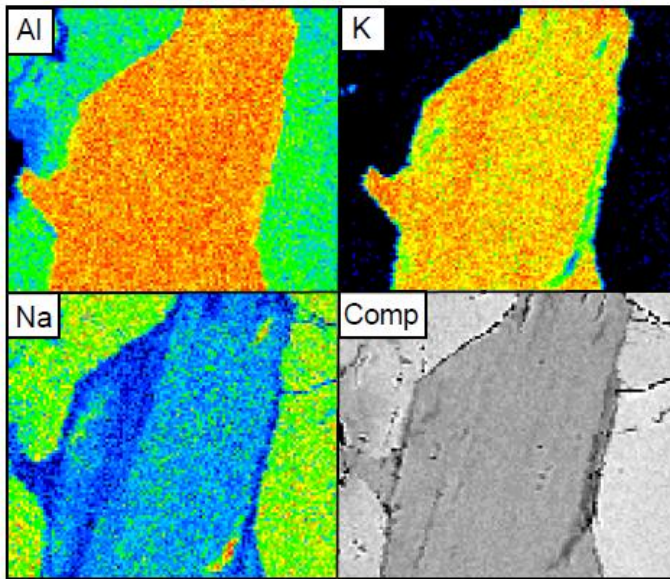


Figure 6. Major element (K, Na, and Al) X-ray maps and BSE image of phlogopite showing Na-rich and Na-poor bands parallel to cleavage mica planes from one Group 1 sample. These features are consistent with a miscibility gap at high temperatures between Na-rich and K-rich endmembers, aspidolite and phlogopite, respectively. Al X-ray map shows no evidence of chemical zoning. Each map is $\sim 100 \mu\text{m}$ on each side.

Cr₂O₃ plots (Figure 7a, 7b, 7c). Na-rich bands in phlogopite may fortuitously explain the large variations in Na and K contents within Group 1, but not the large variability in Na and K contents in amphiboles from the same samples. Chlorine concentrations of phlogopite and amphibole are also variable, but may simply reflect the analytical limitations of analyzing a volatile element. Within Group 1 amphiboles, chlorine concentrations are weakly correlated with Na₂O abundances ($R^2 = 0.414$). Based on Na₂O concentrations, amphibole compositions define three distinct populations within Group 1 (Figure 7).

Table 1a. XRF analyses for Group 1 samples.

Major Oxides	FIN-21C	FIN-21D	FIN-22A	FIN-22B	FIN-22D	FIN-24B	FIN-25B	FIN-25C	FIN-25D	FIN-25G	FIN-25Ji	FIN-25Jii
SiO ₂	43.30	46.30	51.50	41.50	48.90	40.50	40.70	41.90	44.30	46.40	45.00	43.40
TiO ₂	0.04	0.07	0.13	0.05	0.13	0.02	0.33	0.03	0.06	0.11	0.13	0.44
Al ₂ O ₃	1.03	1.50	1.83	1.74	2.47	0.39	8.07	0.81	1.92	3.42	3.44	9.53
MgO	43.50	37.30	20.30	38.60	25.10	46.90	35.60	44.70	40.90	35.60	38.50	29.20
FeO*	9.00	7.36	3.66	8.53	5.04	9.63	7.69	8.83	8.18	7.05	7.79	5.32
MnO	0.16	0.14	0.12	0.19	0.12	0.19	0.11	0.15	0.15	0.13	0.14	0.08
CaO	0.85	5.18	20.80	4.86	16.00	0.11	1.36	1.49	2.03	3.87	1.77	3.80
Na ₂ O	0.10	0.19	0.37	0.67	0.56	0.03	0.40	0.11	0.19	0.25	0.44	0.76
K ₂ O	0.05	0.11	0.04	0.16	0.12	0.02	3.68	0.04	0.36	1.26	0.88	5.03
Cr ₂ O ₃	0.47	0.67	0.75	0.56	0.73	0.60	0.64	0.45	0.48	0.55	0.56	1.13
NiO	0.42	0.33	0.07	0.38	0.13	0.45	0.40	0.44	0.39	0.33	0.38	0.29
SO ₃	0.01	0.00	0.00	0.02	0.01	0.01	0.01	0.01	0.01	0.02	0.01	0.01
P ₂ O ₅	0.02	0.01	0.01	1.66	0.02	0.02	0.01	0.01	0.01	0.01	0.01	0.01
Total	98.94	99.16	99.58	98.92	99.33	98.87	98.99	98.96	98.97	99.00	99.05	98.99
Trace Elements												
F	-	-	-	-	-	-	-	-	-	-	-	1260
Cl*	107	50	165	679	118	296	129	87	91	133	131	246
Co	81	54	0	76	37	91	71	76	74	58	68	55
Sr	18	49	216	558	227	-	44	-	30	47	50	185
Rb	-	-	-	-	-	-	117	-	-	77	31	217
Ba	-	-	-	-	-	-	1334	-	-	666	-	1307
Nb	-	-	-	12	-	-	-	-	-	-	-	-
Zn	62	38	-	67	39	75	53	61	55	41	63	39
Zr	-	78	74	41	53	19	80	66	64	23	58	-
Y	-	-	-	-	13	-	-	-	-	-	-	-
V	-	-	115	-	89	-	-	-	-	-	80	157
Group #	1	1	1	1	1	1	1	1	1	1	1	1

* Bulk Cl concentration obtained via quantitative x-ray fluorescence method
All other analyses obtained using the EZscan x-ray fluorescence method

Table 1b. XRF analyses for Group 4 samples.

Major Oxides	FIN-20A	FIN-20C	FIN-20D	FIN-20E	FIN-20F	FIN-20G	FIN-20H	FIN-20I	FIN-20J
SiO ₂	38.80	39.20	40.90	37.50	47.60	40.70	41.30	38.70	39.10
Al ₂ O ₃	1.53	0.56	6.15	1.40	5.38	6.65	8.14	5.90	1.60
MgO	42.60	43.00	32.90	41.70	26.50	27.20	27.30	28.90	39.20
FeO*	13.59	13.86	11.43	15.30	11.79	14.58	14.22	16.47	16.02
MnO	0.22	0.23	0.20	0.25	0.23	0.24	0.25	0.25	0.27
CaO	0.54	0.36	5.05	0.39	1.89	5.35	5.20	4.29	0.54
Na ₂ O	0.15	0.26	0.90	0.08	0.43	0.99	1.15	0.90	0.10
K ₂ O	0.02	0.01	0.10	0.01	0.32	0.10	0.10	0.10	0.01
Cr ₂ O ₃	0.44	0.12	0.29	0.30	0.19	0.28	0.14	0.33	0.28
TiO ₂	0.03	0.02	0.27	0.03	0.09	0.26	0.18	0.26	0.03
NiO	0.18	0.28	0.17	0.28	0.43	0.23	0.17	0.23	0.35
SO ₃	0.30	0.74	0.16	0.91	3.97	1.69	0.14	1.80	0.61
P ₂ O ₅	0.01	0.01	0.01	0.01	0.00	0.01	0.01	0.01	0.01
Total	98.40	98.65	98.50	98.15	98.82	98.28	98.30	98.14	98.12
Trace Elements									
Cl*	151	114	403	152	140	81	85	110	91
Co	102	100	72	114	102	74	75	86	109
Cu	185	200	41	302	991	175	45	283	171
Sr	28	-	158	29	21	119	131	102	-
Rb	-	-	-	-	-	-	-	-	-
Ba	-	-	-	-	-	-	-	-	-
Nb	-	-	-	-	-	-	-	-	-
Zn	84	88	57	81	73	85	80	106	111
Zr	-	36	36	-	38	17	35	41	17
Y	-	-	-	-	-	-	-	-	-
V	-	-	193	-	-	-	86	-	-
Group #	4	4	4	4	4	4	4	4	4

* Bulk Cl concentration obtained via quantitative x-ray fluorescence method

All other analyses obtained using the EZscan x-ray fluorescence method

Table 2a. Representative phlogopite analyses for Group 1.

ANALYSIS	FIN-22B 1-2	FIN-22B 1-8	FIN-22B 1-12	FIN-22B 1-11	FIN-22B 3-1	FIN-25B 4-1	FIN-25D 3-7	FIN-25D 4-9	FIN-25Ji 4-2	FIN-25Ji 4-4	FIN-25Jii 1-5	FIN-25Jii 2-3
Mass %												
SiO ₂	41.06	41.73	41.18	41.55	39.63	40.03	40.18	40.28	40.81	40.76	41.49	41.15
Al ₂ O ₃	14.05	13.63	13.91	13.68	15.88	16.02	16.19	15.71	15.11	15.48	14.62	14.64
TiO ₂	0.52	0.51	0.50	0.50	0.90	0.89	0.82	0.74	0.75	0.66	0.73	0.71
MgO	26.88	26.91	26.92	26.99	25.23	25.33	25.68	25.42	25.97	26.90	25.82	25.99
FeO	2.48	2.60	2.48	2.53	2.70	2.54	2.42	2.59	2.56	2.63	2.43	2.52
MnO	0.03	0.00	0.01	0.02	0.02	0.00	0.01	0.03	0.02	0.02	0.01	0.02
Cr ₂ O ₃	1.26	1.28	1.33	1.33	1.31	1.14	1.12	1.28	1.44	1.09	1.35	1.39
CaO	0.04	0.02	0.04	0.03	0.03	0.00	0.00	0.00	0.02	0.06	0.00	0.01
Na ₂ O	1.80	1.84	1.73	1.63	0.54	0.51	0.66	0.60	1.21	0.74	0.80	1.12
K ₂ O	7.67	7.91	8.00	8.13	9.09	9.33	9.20	9.24	8.53	7.59	8.93	8.62
F	0.00	0.00	0.01	0.00	0.00	0.00	0.00	0.00	0.01	0.00	0.00	0.00
Cl	0.026	0.048	0.035	0.059	0.048	0.017	0.026	0.019	0.039	0.035	0.057	0.025
Total	95.81	96.47	96.12	96.42	95.38	95.81	96.30	95.90	96.45	95.95	96.23	96.19
Cation Total												
Si	2.857	2.887	2.861	2.879	2.785	2.798	2.791	2.813	2.829	2.818	2.864	2.844
Ti	0.027	0.026	0.026	0.026	0.048	0.047	0.043	0.039	0.039	0.034	0.038	0.037
Al	1.152	1.112	1.139	1.117	1.316	1.320	1.325	1.293	1.235	1.261	1.190	1.193
Mg	2.788	2.776	2.788	2.787	2.644	2.639	2.659	2.646	2.683	2.773	2.657	2.678
Fe	0.144	0.150	0.144	0.147	0.159	0.148	0.141	0.152	0.148	0.152	0.126	0.131
Mn	0.002	0.000	0.001	0.001	0.001	0.000	0.001	0.002	0.001	0.001	0.000	0.001
Cr	0.070	0.070	0.073	0.073	0.073	0.063	0.062	0.071	0.079	0.059	0.074	0.076
Ca	0.003	0.002	0.003	0.002	0.002	0.000	0.000	0.000	0.002	0.004	0.000	0.001
Na	0.243	0.247	0.233	0.220	0.073	0.069	0.088	0.081	0.163	0.099	0.108	0.150
K	0.681	0.698	0.710	0.719	0.815	0.832	0.815	0.823	0.754	0.669	0.786	0.760
F	0.000	0.000	0.002	0.000	0.000	0.000	0.000	0.000	0.002	0.000	0.001	0.001
Cl	0.003	0.006	0.004	0.007	0.006	0.002	0.003	0.002	0.005	0.004	0.007	0.003
Total	7.970	7.974	7.985	7.977	7.923	7.917	7.928	7.921	7.940	7.876	7.850	7.875
Mg/(Mg+Fe)	0.951	0.949	0.951	0.950	0.943	0.947	0.950	0.946	0.948	0.948	0.955	0.953
Group #	1	1	1	1	1	1	1	1	1	1	1	1

Table 2b. Representative amphibole analyses for Groups 1 and 4.

ANALYSIS	FIN-22B 1-4	FIN-22B 1-13	FIN-25D 4-5	FIN-25D 4-8	FIN-25Ji 4-6	FIN-25Ji 4-8	FIN-20H 1-2	FIN-20H 2-2	FIN-20I 1-2	FIN-20I 3-3	FIN-20J 3-3	FIN-20J 3-4
Mass %												
SiO ₂	48.37	48.31	46.92	46.90	47.19	47.53	43.35	43.55	44.41	44.05	43.41	43.63
Al ₂ O ₃	7.41	7.70	10.45	10.50	9.99	10.03	14.33	14.42	13.22	13.58	13.79	13.05
TiO ₂	0.33	0.37	0.44	0.43	0.48	0.46	0.45	0.37	0.65	0.69	0.44	0.43
MgO	20.72	20.83	19.78	19.77	20.41	20.31	17.09	17.24	17.65	17.13	17.91	18.12
FeO	3.22	3.15	3.23	3.20	3.22	3.11	7.20	7.21	7.13	7.26	5.64	5.76
MnO	0.06	0.07	0.05	0.06	0.06	0.06	0.07	0.08	0.10	0.07	0.08	0.09
Cr ₂ O ₃	1.84	1.99	1.95	1.89	2.05	2.10	0.22	0.29	0.50	0.61	0.75	0.74
CaO	10.89	11.22	12.42	12.56	11.88	12.22	12.01	11.79	12.04	12.22	11.85	12.06
Na ₂ O	3.84	3.80	2.18	2.20	3.06	3.11	2.77	2.62	2.47	2.45	2.39	2.52
K ₂ O	0.40	0.33	0.84	0.75	0.62	0.45	0.21	0.19	0.27	0.27	0.16	0.15
F	0.02	0.01	0.00	0.00	0.00	0.01	0.00	0.00	0.00	0.01	0.02	0.02
Cl	0.049	0.053	0.023	0.03	0.028	0.038	0.012	0.025	0.013	0.005	0.011	0.000
Total	97.10	97.80	98.28	98.28	98.97	99.40	97.70	97.77	98.45	98.34	96.43	96.55
Cation Total												
Si	6.877	6.825	6.602	6.597	6.598	6.611	6.223	6.238	6.320	6.257	6.266	6.303
Ti	0.036	0.039	0.046	0.046	0.050	0.048	0.049	0.040	0.069	0.075	0.048	0.047
Al	1.241	1.282	1.733	1.740	1.647	1.644	2.426	2.435	2.217	2.306	2.346	2.222
Mg	4.390	4.386	4.149	4.146	4.253	4.211	3.656	3.680	3.745	3.681	3.853	3.902
Fe	0.383	0.372	0.380	0.377	0.377	0.361	0.864	0.863	0.849	0.851	0.681	0.696
Mn	0.007	0.008	0.006	0.008	0.007	0.007	0.008	0.010	0.012	0.010	0.010	0.011
Cr	0.207	0.223	0.217	0.210	0.227	0.230	0.025	0.033	0.056	0.057	0.085	0.084
Ca	1.659	1.698	1.873	1.892	1.779	1.822	1.847	1.809	1.836	1.870	1.833	1.867
Na	1.058	1.042	0.594	0.599	0.829	0.837	0.770	0.726	0.681	0.702	0.670	0.705
K	0.072	0.059	0.150	0.134	0.110	0.080	0.039	0.035	0.049	0.057	0.029	0.027
F	0.007	0.005	0.000	0.001	0.000	0.003	0.000	0.000	0.000	0.000	0.005	0.004
Cl	0.012	0.013	0.003	0.004	0.007	0.009	0.001	0.003	0.003	0.001	0.001	0.000
Total	15.947	15.951	15.755	15.758	15.885	15.863	15.910	15.875	15.839	15.866	15.833	15.871
Mg/(Mg+Fe)	0.032	0.035	0.025	0.035	0.030	0.031	0.242	0.237	0.180	0.145	0.107	0.112
Group #	1	1	1	1	1	1	4	4	4	4	4	4

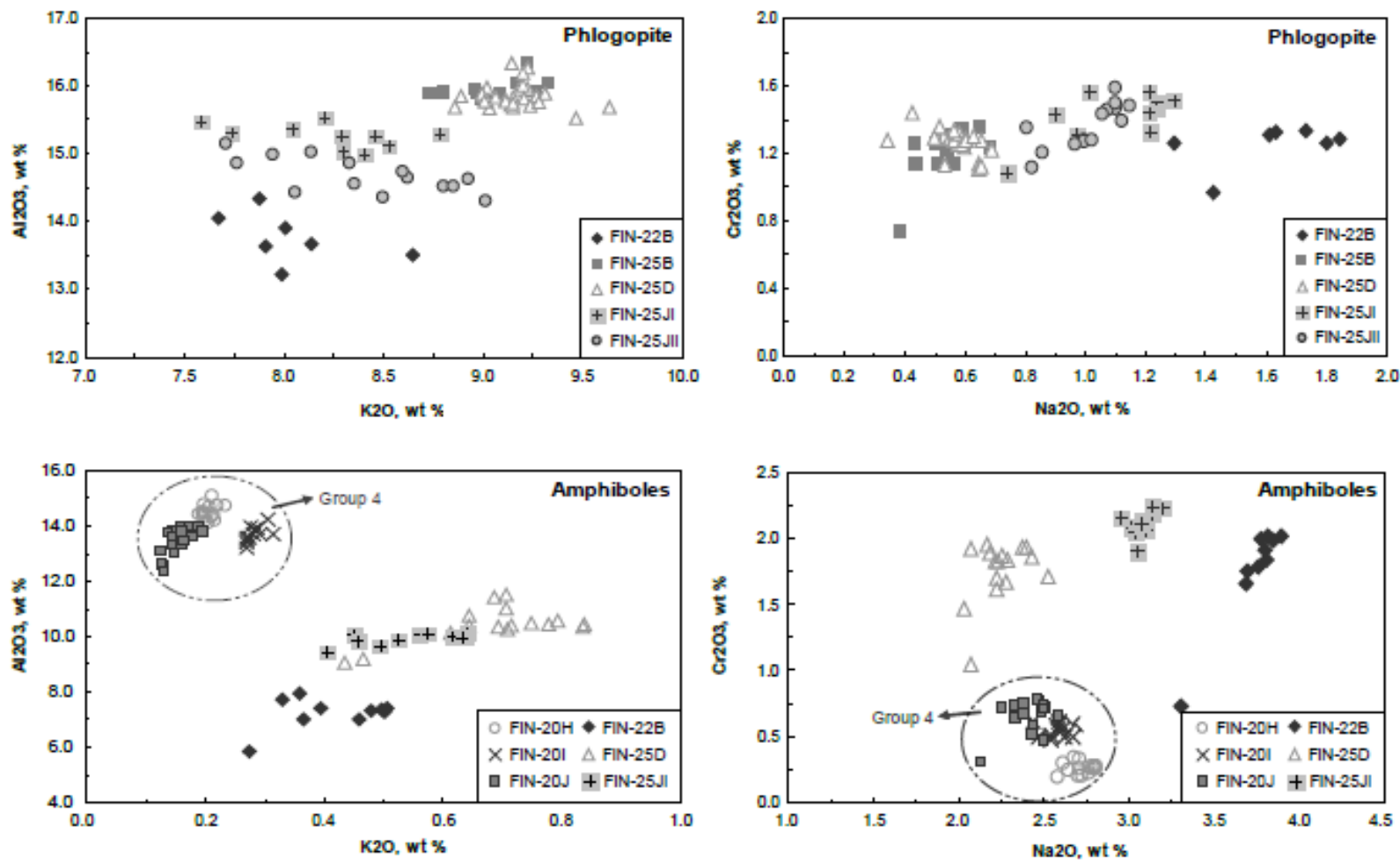


Figure 7a. Major element variation diagrams of phlogopite and amphibole compositions from Group 1 and Group 4. Phlogopite and amphibole: K_2O vs. Al_2O_3 (wt %) and Na_2O vs. Cr_2O_3 (wt %). Note that amphiboles from Group 1 show larger chemical variability than amphiboles from Group 4. Group 4 amphiboles cluster tightly, showing little chemical heterogeneity.

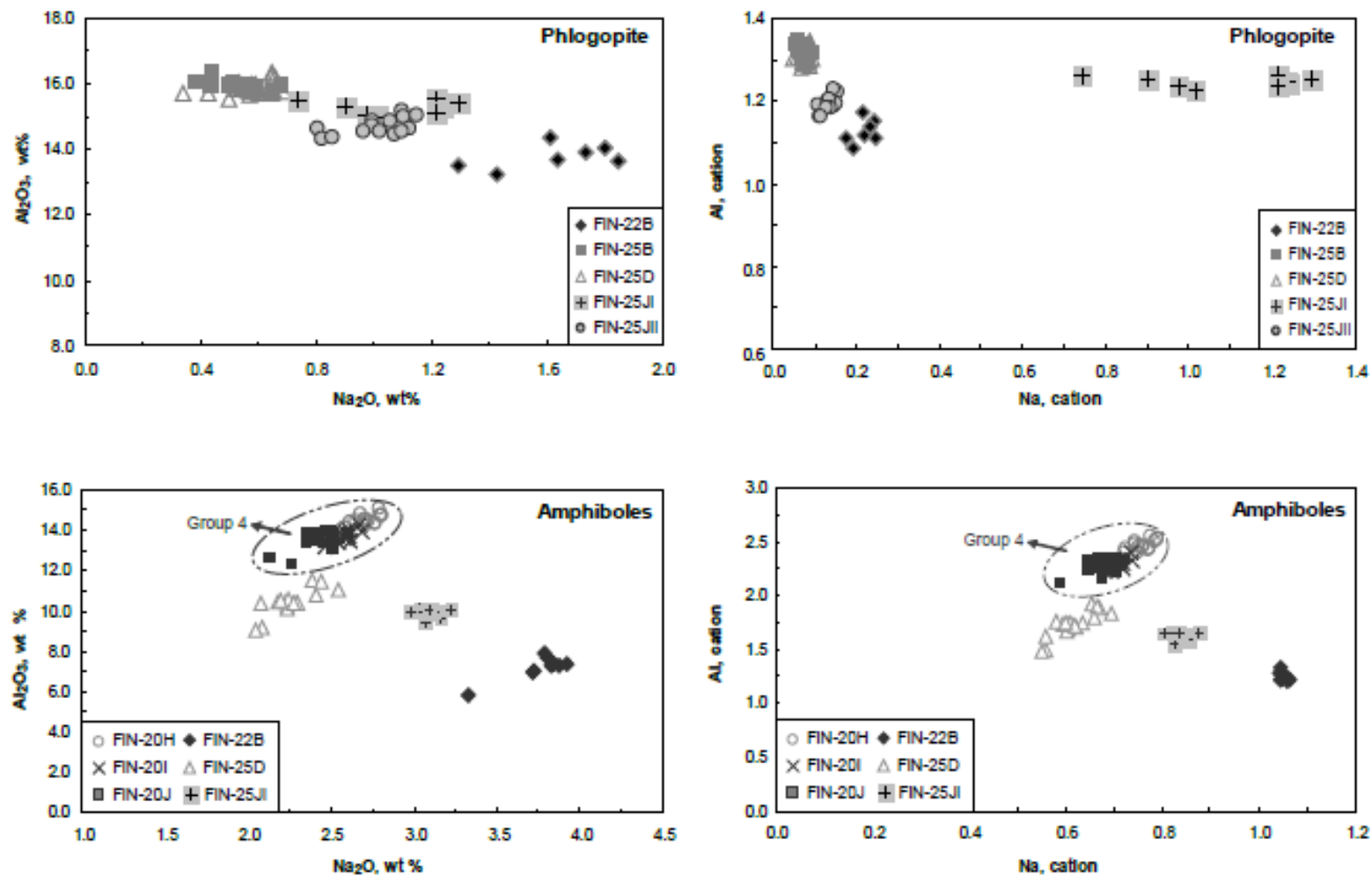


Figure 7b. Phlogopite and amphibole: Na₂O vs. Al₂O₃ (wt. %) and Na vs. Al (cation). Note distinct amphibole populations within Group 1.

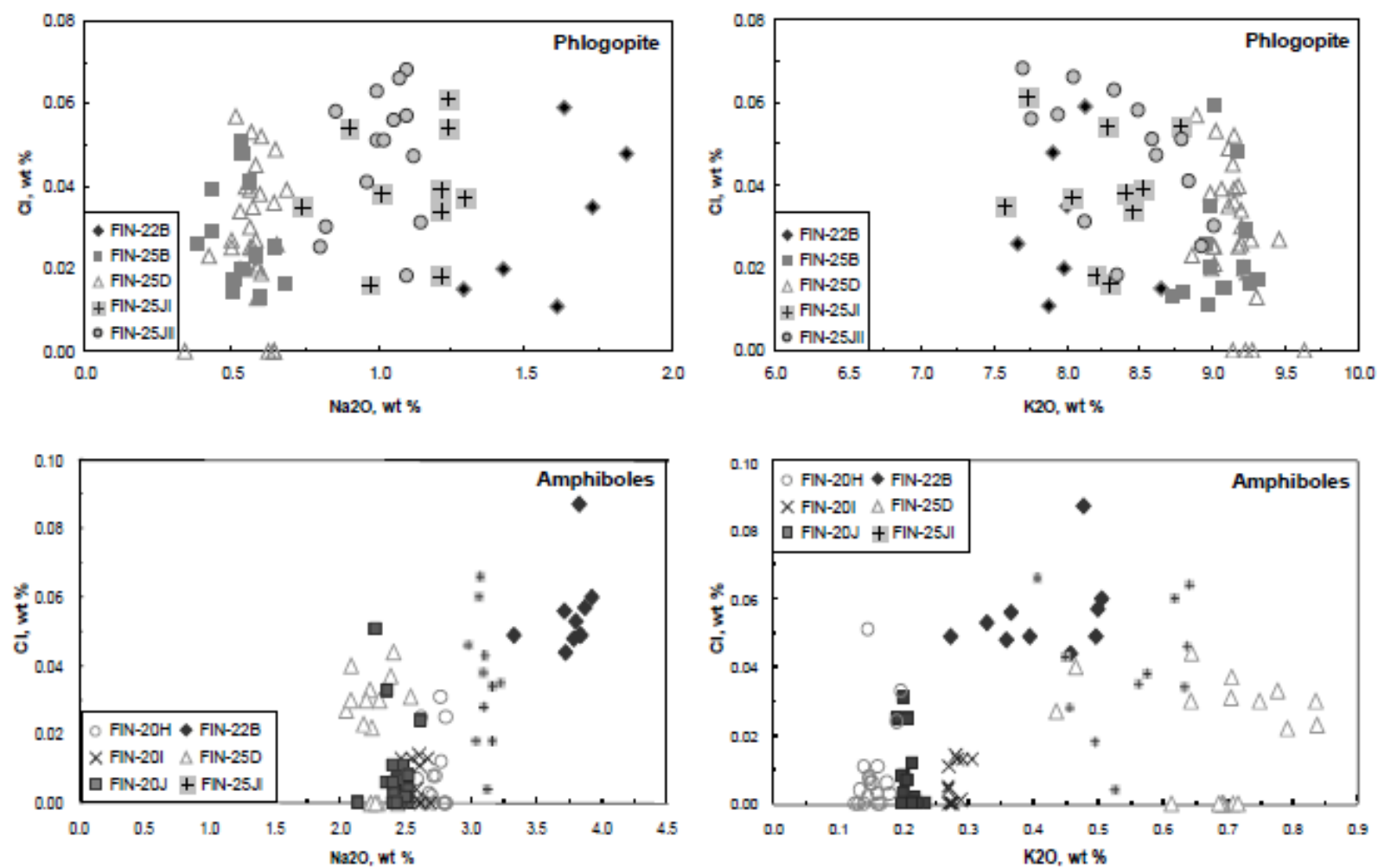


Figure 7c. Phlogopite and amphibole: Na₂O vs. Cl (wt %) and K₂O vs. Cl (wt %). Note that Cl concentrations in phlogopite do not correlate with K or Na, but Cl contents in amphiboles from Group 1 show a slight correlation with higher Na contents.

Amphiboles from the cumulate peridotite (Group 4) are pargasitic and less variable in composition than the amphiboles from Group 1 (Table 2b). The microprobe data are tightly clustered in Al_2O_3 vs. K_2O and Cr_2O_3 vs. Na_2O plots, with little heterogeneity within or between samples (Figure 7a, 7b, 7c). K_2O and Na_2O concentrations range between ~0.1 to 0.3 and ~2.2 to 2.7 wt%, respectively, and are significantly lower compared to Group 1 amphiboles. Chlorine concentrations are also lower compared Group 1 and are more homogeneous within and between samples.

Stable Isotopic Analysis: Chlorine and Hydrogen

Table 3 shows chlorine and hydrogen isotopic data for samples from the different rock groups. Large variations in chlorine and hydrogen isotope composition are found both within and between groups. $\delta^{37}\text{Cl}$ values show a large range from -2.1 to +3.3‰, the largest spread that has been reported for peridotites. Group 1 shows the most variation, with $\delta^{37}\text{Cl}$ values ranging from -0.9 to +3.3 (WR) and δD values ranging from -48 to -36‰ (phlogopite separates). The $\delta^{37}\text{Cl}$ value, +3.3, is one of the heaviest isotopic values ever reported for peridotites and may be questionable, although repeat analyses of SMOC standards during the same analytical session revealed no analytical issues, suggesting that this value is of real significance. There is no systematic relationship between $\delta^{37}\text{Cl}$ values, bulk rock chlorine concentrations or mineral abundances (amphibole and phlogopite) seen in the harzburgites from Group 1 (Table 3). In addition, there are no obvious correlations between $\delta^{37}\text{Cl}$ and sample locations, whole-rock Na and K concentrations, or chlorine concentrations (Figure 8). Group 2 samples have relatively

Table 3.

Sample	Rock Type	Group #	Bulk Cl (ppm)	Avg Cl wt%	Avg Cl wt%	$\delta^{37}\text{Cl}$ ‰ WR	δD ‰ phlog	Phlog abund	Amph abund
FIN-21D	Phlog + Amph Perid.	1	50	-	-	1.4	-	<1%	5%
FIN-22A	Phlog + Amph Perid.	1	165	-	-	-0.4	-	0%	2-3%
FIN-22B	Phlog + Amph + Ap Perid.	1	679	0.031	0.053	0.7; 0.8	-	5-7%	10-15%
FIN-24B	Phlog + Amph Perid.	1	296	-	-	1.1	-36	1%	0%
FIN-25B	Phlog + Amph Perid.	1	129	0.028	-	-0.9	-	15-20 %	1%
FIN-25D	Phlog + Amph Perid.	1	91	0.034	0.012	-0.2	-	5-7 %	2%
FIN-25Ji	Phlog + Amph Perid.	1	131	0.039	0.04	3.3	-42	10-15%	5-7%
FIN-21A	Phlog + Amph segregation	2	893*	-	-	-1.7; -1.4	-40	-	-
FIN-22C	Phlog + Amph segregation	2	558*	-	-	-2.1	-49	-	-
FIN-21F	Phlog + Opx segregation	3	750*	-	-	-0.1	-80	-	-
FIN-20G	Amph. Cumulate Perid.	4	81	-	-	0.8	-	0	35-40%
FIN-20H	Amph. Cumulate Perid.	4	85	-	0.009	1.9	-	0	45-50%
FIN-20J	Amph. Cumulate Perid.	4	90	-	0.009	1.6	-	0	5%

Bulk Cl concentration obtained via quantitative x-ray fluorescence on all other samples

* Cl concentration obtained via ion chromatography

light $\delta^{37}\text{Cl}$ values of -1.4, -1.7 (duplicate), and -2.1‰ and corresponding δD values of -49 and -40‰ (phlogopite separates). Group 3 (orthopyroxene + phlogopite segregation) only has one sample, but it is distinctly different ($\delta^{37}\text{Cl} = -0.1\text{‰}$, $\delta\text{D} = -80\text{‰}$) from the Group 2 segregations. Group 4 (amphibole cumulate peridotite) has isotopically heavy $\delta^{37}\text{Cl}$ values that are relatively uniform compared to Group 1, ranging from +0.8 to +1.9. An earlier stable isotope study of the phlogopite peridotite yielded δD values that vary over the same range as our data from Groups 1 and 2 (Hartmann and Wedepohl, 1993).

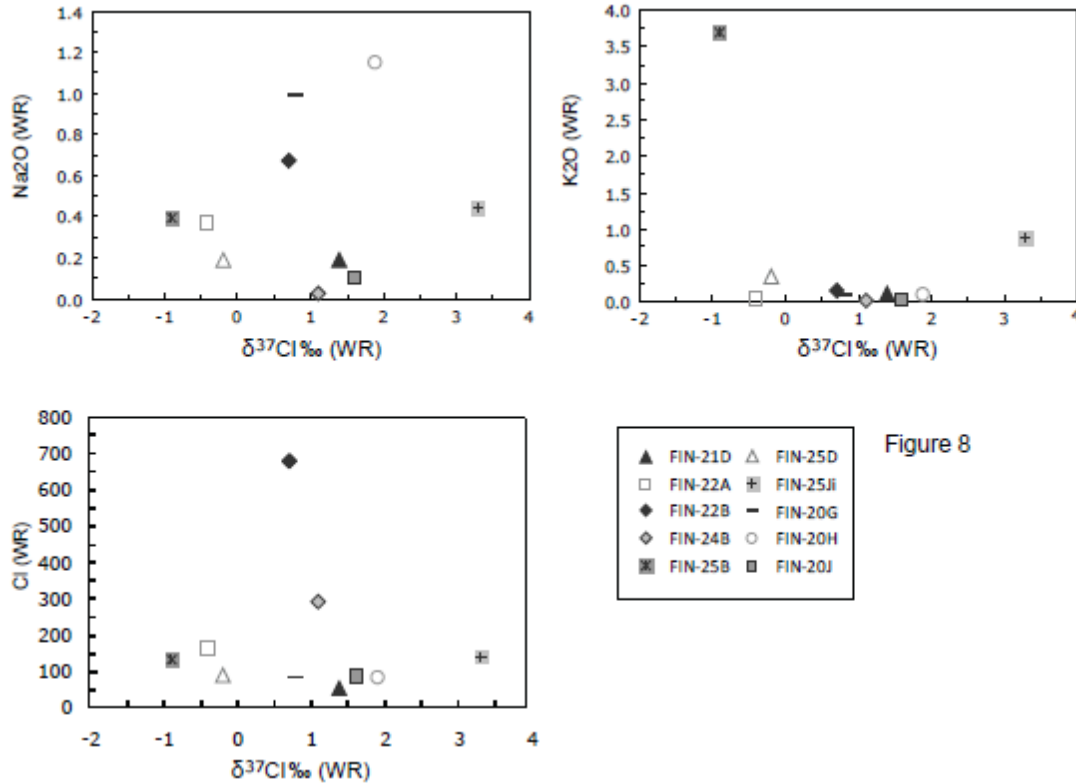


Figure 8. (a) Plot of $\delta^{37}\text{Cl}$ vs. whole rock Na₂O (b) Plot of $\delta^{37}\text{Cl}$ vs. whole rock K₂O (c) $\delta^{37}\text{Cl}$ vs. whole-rock Cl. There is no correlation between the whole rock concentrations of fluid-mobile elements (Na, K, and Cl) and $\delta^{37}\text{Cl}$ values in samples from Groups 1 and 4.

DISCUSSION

Perple_X modeling indicates equilibration of the phlogopite + amphibole assemblages at upper mantle conditions of 800-900°C and 1.2 -1.4 GPa. These modeled conditions are consistent with temperature estimates from two-pyroxene thermometry of 894±94°C (Ernst et al., 1978) and temperature estimates of ~750 °C based from δD water-mineral fractionations from amphibole and biotite (Hartmann and Wedepohl, 1993). Chlorine fractionation under these conditions has been theoretically predicted to be minimal (Schauble et al., 2003). We thus assume that fluid-mineral and mineral-mineral chlorine isotope fractionation was negligible during metasomatism.

Tectonic Setting of Metasomatism

The large range of $\delta^{37}\text{Cl}$ and δD values from Group 1 samples reveal large heterogeneities over small length scales (<1m in some cases) at the two sample localities. These heterogeneities indicate that isotopic and chemical homogenization for chlorine and hydrogen did not occur on meter-length scales and that chemical signatures of various metasomatizing agents were preserved under mantle conditions. These heterogeneities are also seen in major element concentrations, especially Na and K concentrations, in amphibole and phlogopite. Therefore, we interpret the different isotopic signatures and differences in mineral chemistry in samples from Group 1 to reflect multiple metasomatizing agents that were sourced from different rock types. Groups 2 and 3 are interpreted as a result from different fluid episodes based on their very different isotopic ratios (Group 2: $\delta^{37}\text{Cl}$ = -1.7, -1.4, -2.1 and δD = -40 and -49; Group 3: $\delta^{37}\text{Cl}$ = -0.1 and δD = -80) and their crosscutting relationship (Group 2) with

respect to Group 1 samples. In addition, Groups 2 and 3 are segregations rather than evenly distributed phlogopite and amphibole as seen in Group 1, hinting that migration mechanisms were different for the segregation fluids relative to the fluids that produced the pervasive phlogopite and amphibole.

Based on the large variations in chlorine and hydrogen isotope compositions and the predictions for the different tectonic settings (Figure 1), we argue that growth of phlogopite and amphibole from Groups 1 and 2 and phlogopite from Group 3 resulted from at least three infiltrating events with at least three different sources. In addition, the presence of these significant chemical variations over less than tens of meters suggests a tectonic environment where multiple sources can infiltrate the upper mantle on extremely small length scales. We thus conclude that the samples from Group 1 and 2 are most likely to have formed from fluid(s) that were sourced from a subducting slab. This interpretation is consistent with high chlorine concentrations, heavy hydrogen isotopic values compared to the average δD mantle values (~ -80), and the high alkali content needed to produce abundant and evenly distributed hydrous minerals (phlogopite and amphibole) throughout the massif. This interpretation also agrees with previously obtained geochemical data: enrichment in LILEs, depletion of HFSEs, and crustal radiogenic signatures (e.g., Hartmann and Wedepohl, 1992; Zanetti et al., 1999; Raffone et al., 2006). These signatures all suggest that the main metasomatic agents were hydrous fluids and/or melts, consistent with subduction-zone metasomatism (Hunziker and Zingg, 1982; Cumming et al., 1987; Hartmann and Wedepohl, 1992; Zanetti et al., 1999; Raffone et al., 2006).

Based on our model, chlorine and hydrogen isotopes from the cumulate peridotites (Group 4) are predicted to have isotopically homogenous chlorine ratios, reflecting crystallization from a single mantle melt. Chlorine isotopic values from Group 4 do in fact show little isotopic variability and suggest that the pargasitic amphibole crystallized from one mantle-derived melt. In addition, mineral geochemistry shows small variations compared to Group 1, which is also in agreement with equilibration with *one* melt source.

Subduction Fluids: Multiple Episodes and Possible Sources

Determining the composition of fluids released during subduction has been the topic of many previous studies (e.g., Scambelluri and Philippot, 2001). However, understanding how fluids leave the devolatilizing slab remains poorly understood. Some studies suggest a continuous dewatering process from progressive mineral breakdown in the slab between 60-120 km (e.g., Bebout and Barton, 1993), whereas others suggest discrete, episodic pulses corresponding to discontinuous dehydration reactions, especially at greater depths (e.g., Philippot, 1993; Fröh-Green et al., 2001). Scambelluri and Philippot (2001) suggest that large volumes of hydrous fluid are derived from devolatilization of serpentinites, which are estimated to store up to 13 weight percent H₂O to ≥ 200 km depth. Because dehydration of the subducting slab contributes large amounts of hydrous fluid into the upper mantle, devolatilization is an important source for recycling chlorine into the mantle (e.g., Philippot, 1998; Sharp and Barnes, 2004). Once devolatilization occurs, fluids may enter the overlying mantle wedge via pervasive and/or channelized flow. In either case, once hydrous fluids are released, interaction with mantle

rocks with which the fluids are chemically out of equilibrium induces hydration of the mantle. The chemistry of the resulting metasomatic minerals partially reflects the chemistry of the altering agent and provides information regarding possible fluid sources. Because chlorine readily fractionates into the fluid phase (e.g., Kullerud et al., 2001) and because of its low abundance in the mantle, chlorine isotopes can be used to track fluid sources in different parts of a subduction setting.

The Finero peridotite preserves several isotopic signatures, which we interpret to represent discrete pulses of fluids that were derived from several geochemically distinct sources derived from a down-going slab. Preservation of isotopic heterogeneities on relatively small length scales (less than a few meters in most cases) is interpreted to be a result of channelized fluids from distinct infiltration events. This interpretation contrasts with previous studies that argue for one single pervasive metasomatic event, with chemical evolution of the fluid producing the chemical heterogeneity observed in the mantle peridotite (e.g., Zanetti et al., 1999).

The source(s) of the metasomatizing fluid cannot be identified because the isotopic compositions are not unique. Previous studies show that chlorine isotopic values for serpentinites, depending on tectonic setting, range from -1.8‰ to $+0.5\text{‰}$ (Barnes and Sharp, 2006; Bonifacie et al., 2008b). Marine pore fluids are also isotopically light (-7.8‰ to $+0.3\text{‰}$; e.g., Ransom et al., 1995; see compilation in Barnes et al., 2008), as is altered oceanic crust (-1.6‰ to -0.9‰ ; Bonifacie et al., 2007). The range in chlorine isotopic compositions of high-pressure, low-temperature metasedimentary rocks have yet to be determined. The large range in $\delta^{37}\text{Cl}$ values determined from Group 1 samples in this study likely requires input from several fluid sources with possible mixing of the

different chlorine isotopic signatures. In all cases, the fluids must have been enriched in K, Na, and Cl and were most likely subduction related.

Amphibole + phlogopite segregations from Group 2 are distinctly isotopically light in terms of chlorine isotopic values ($\delta^{37}\text{Cl} = -1.4\text{‰}$ & -1.7‰ , -2.1‰) and have high δD values (-40‰ and -49‰), indicating that metasomatism was possibly a result of a serpentinite-derived fluid phase or seafloor alteration of basalts. If devolatilizing serpentinite was the original source for isotopically light values (amphibole + phlogopite) at Finero, soluble elements such as K and Na must have been leached out of the oceanic crustal package as fluids passed through the upper portion of the subducting plate.

One data point from Group 3 (orthopyroxene + phlogopite segregation) has a $\delta^{37}\text{Cl}$ value near zero and δD of -80‰ , most likely representing a pure mantle signature (Figure 9). This occurrence is significantly different from Group 1 and 2 and most likely represents a different metasomatic event. Despite the lack of consensus over the average $\delta^{37}\text{Cl}$ value of the mantle, the δD value clearly indicates that phlogopite + orthopyroxene segregations are a result of mantle-derived melts. Raffone et al. (2006) also documented a pristine mantle signature in apatite-bearing peridotites and suggested that Finero consists of at least two metasomatic events with different components: one that is alkali or carbonatitic and one that is subduction related.

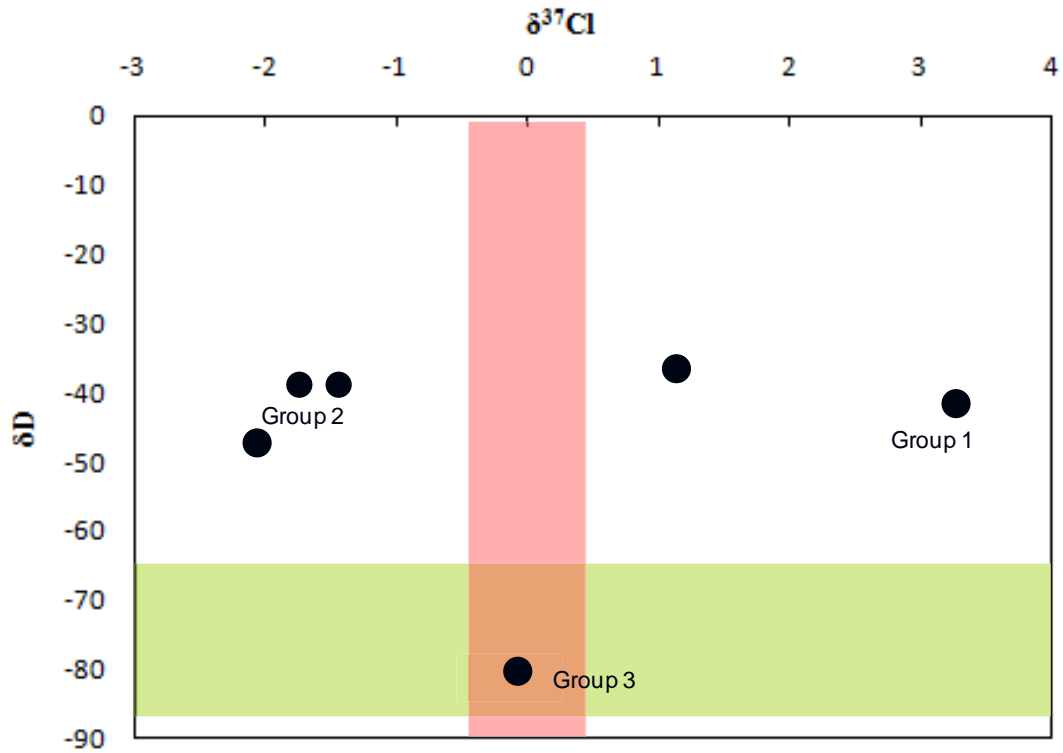


Figure 9. $\delta^{37}\text{Cl}$ vs. δD plot showing the different isotopic values for groups 1, 2 and 3. The green bar indicates δD values consistent with mantle values noted in Sharp (2007). The red bar indicated $\delta^{37}\text{Cl}$ value consistent with mantle values as described in Sharp et al. (2007).

CONCLUSIONS

The Finero samples for this study record the largest spread in $\delta^{37}\text{Cl}$ values yet reported for mantle-derived rocks. The combined $\delta^{37}\text{Cl}$ and δD values for the phlogopite peridotite and the amphibole cumulate body from the Finero Complex place the following constraints on the system:

- (1) Part of the metasomatic assemblage (phlogopite + amphibole) formed from hydrous fluids infiltrating the mantle wedge above ancient subduction system.

- (2) Chlorine and hydrogen isotopic values suggest that metasomatism responsible for phlogopite and amphibole formation occurred in multiple events from fluid sources with unique geochemical signatures.
- (3) Metasomatic minerals and isotopic values are heterogeneously distributed in the phlogopite peridotite, suggesting that chlorine isotopic ratios were preserved under mantle conditions. Fluid migration was limited, even where phlogopite + amphibole are pervasively developed. Variations in the $\delta^{37}\text{Cl}$ and the δD values indicate that distinct fluid infiltration events were channelized through the mantle wedge.
- (4) Serpentinite devolatilization may be the possible fluid source for amphibole + phlogopite segregations.
- (5) $\delta^{37}\text{Cl}$ and the δD values from the orthopyroxene + phlogopite segregation suggest that pristine mantle melts did play a role in the metasomatism observed at Finero.
- (6) The amphibole cumulate body has a relatively homogenous chlorine isotopic signature (based on three analyses), and consistent with expected chlorine isotopic ratios derived from one melt source.
- (7) This study demonstrates that chlorine isotopes provide a useful tracer of fluid-rock interaction and can be used to trace specific fluid sources through the sub-arc mantle. Further studies are needed to characterize additional chlorine isotopic inputs (metasedimentary rocks) and possible isotopic fractionation that might occur in subduction zones.

REFERENCES

- Banno, Y., Miyawaki, R., Kogure, T., Matsubara, S., Kamiya, T., and Yamada, S. (2005) Aspidolite, the Na analogue of phlogopite from Kasuga-mura, Gifu Prefecture, central Japan: description and structural data. *Mineralogy Magazine*, v.69, 1047-1057.
- Barnes, J. and Sharp, S. (2006) A chlorine isotope study of DSDP/ODP serpentinized ultramafic rocks; insights into the serpentinization process. *Chemical Geology*, v. 228, 246-265.
- Bebout, G. E., and Barton, M. D. (1993) Metasomatism during subduction: Products and possible paths in the Catalina Schist, California. *Chemical Geology*, v. 108, 61-92.
- Bonifacie, M., Jendrzejewski, N., Agrinier, P., Coleman, M., Pineau, F., and Javoy, M. (2007) Pyrohydrolysis-IRMS determination of silicate chlorine stable isotope compositions. Application to oceanic crust and meteorite samples. *Chemical Geology*, v. 242, 187-201.
- Bonifacie, M., Monnin, C., Jendrzejewski, N., Agrinier, P., and Javoy, M. (2007) Chlorine stable isotopic composition of basement fluids of the eastern flank of the Juan de Fuca Ridge (ODP Leg 168). *Earth and Planetary Science Letters*, v. 260, p. 10–22.
- Bonifacie, M., Jendrzejewski, N., Agrinier, P., Humler, E., Coleman, M., and Javoy, M. (2008a) The chlorine isotope composition of the Earth's mantle. *Science*, v. 319, 1518-1520.
- Bonifacie, M., Busigny, V., Mével, C., Philippot, P., Agrinier, P., Jendrzejewski, N., Scambelluri, M., and Javoy, M. (2008b) Chlorine isotopic composition in seafloor

- serpentinites and high-pressure metaperidotites. Insights into oceanic serpentinization and subduction processes. *Geochimica et Cosmochimica Acta*, v. 72, 126–139.
- Cawthorn, R. G. (1975) The amphibole peridotite-metagabbro complex Finero, northern Italy. *Journal of Geology*, v. 83, 437-454.
- Connolly, J. A. D. (2009) The geodynamic equation of state: what and how. *Geochemistry, Geophysics, Geosystems* 10. DOI:10.1029/2009GC002540.
- Coltori, M. and Siena, F. (1984) Mantle tectonite and fractionate peridotite at Finero (Italian Western Alps). *Neues Jahrbuch für Mineralogie, Abhandlungen*, v. 149, 225-244.
- Costa, F., Dungan, M., and Singer, B (2001) Magmatic Na-rich phlogopite in a suite of gabbroic crustal xenoliths from Volcán San Pedro, Chilean Andes: Evidence for a solvus relation between phlogopite and aspidolite. *American Mineralogist*, v. 86, 29-35.
- Cumming, G.L., Koppel, V., and Ferrario, A. (1987) A lead isotope study of the northeastern Ivrea Zone and the adjoining Ceneri Zone (N Italy): Evidence for a contaminated subcontinental mantle. *Contributions to Mineralogy and Petrology*, v. 97, 19-30.
- Dienier J.F.A, Powell R., White R.W., and Holland T.J.B. (2007) A new thermodynamic model for clino- and orthoamphiboles in the system $\text{Na}_2\text{O}-\text{CaO}-\text{FeO}-\text{MgO}-\text{Al}_2\text{O}_3-\text{SiO}_2-\text{H}_2\text{O}-\text{O}$. *Journal of Metamorphic Geology*, v.25, 631-656.
- Ernst, W. G. (1978) Petrochemical study of some lherzolitic rocks from the Western Alps. *Journal of Petrology*, v. 19, 341-392.

- Eggenkamp, H.G.M., (1994) The geochemistry of chlorine isotopes. Ph.D. Thesis, Universiteit Utrecht.
- Eggenkamp, H.G.M., Kreulen, R., and Koster van Groos, A.F. (1995) Chloride stable isotope fractionation in evaporites. *Geochemica et Cosmochimica Acta* v. 59, 5169–5175.
- Exley, R.A., Sills, J.D., and Smith J.V. (1982) Geochemistry of micas from the Finero spinel-lherzolite, Italian Alps. *Contributions to Mineralogy and Petrology*, v. 81, 59–63.
- Ferrario, A. and Garuti, G. (1990) Platinum-group mineral inclusions in chromitites of the Finero mafic–ultramafic complex (Ivrea-Zone, Italy). *Mineralogy and Petrology* v. 41, 124–143.
- Früh-Green, G.L., Scambelluri, M. and Vallis F. (2001) O-H isotope ratios of high pressure ultramafic rocks: implications for fluid sources and mobility in the subducted hydrous mantle. *Contributions to Mineralogy and Petrology*, v.141, 145–159.
- Garuti, G., Bea, F., Zaccarini, F., and Montero, P. (2001) Age, geochemistry and petrogenesis of the ultramafic pipes in the Ivrea Zone, NW Italy. *Journal of Petrology*, v. 42, 433–457.
- Grieco, G., Ferrario, A., Von Quadt, A., Koeppel, V., and Mathez, E.A. (2001) The zircon-bearing chromitites of the phlogopite peridotite of Finero (Ivrea Zone, Southern Alps): evidence and geochronology of a metasomatized mantle slab. *Journal of Petrology*, v. 42, 89–101.

- Grieco, G., Ferrario, A., and Mathez, E.A. (2004) The effect of metasomatism on the Cr-PGE mineralization in the Finero Complex, Ivrea Zone, Southern Alps. *Ore Geology Reviews*, v. 24, 299-314.
- Hartmann, G. and Wedepohl, K.H. (1993) The composition of peridotite tectonites from the Ivrea Complex, northern Italy: residues from melt extraction. *Geochimica et Cosmochimica Acta*, v. 57, 1761-1782.
- Hirth, G. (2002) Laboratory constraints on the rheology of the upper mantle. *Reviews in Mineralogy and Geochemistry*, v. 51, 97-120.
- Holland T. and Powell R (1996) Thermodynamics of order-disorder in minerals, Symmetric formalism applied to solid solutions. *American Mineralogist* v. 81, 1425-1437.
- Holland T.J.B. and Powell R (1998) An internally consistent thermodynamic data set for phases of petrological interest. *Journal of Metamorphic Geology*, v. 16, 309-343.
- Hunziker, J. (1974) Rb–Sr and K–Ar age determination and the Alpine tectonic history of the western Alps. *Mem. Ist. Geol. Mineral.* v. 31, 1–54.
- Hunziker, J. C. and Zingg, A. (1982) Zur Genese der ultrabasischen Gesteine der Ivrea-Zone. *Schweizerische Mineralogische und Petrographische Mitteilungen*, v.62, 483-486.
- Jung, H. and Karato, S. (2001) Water-induced fabric transitions in olivine. *Science*, v. 293, 1460-1463.
- Klemme, S., Ivanic, T. J., Connolly, J. A. D., and Harte, B. (2009) Thermodynamic modeling of Cr-bearing garnets with implications for diamond inclusions and peridotite xenoliths. *Lithos*, DOI:10.1016/j.lithos.2009.05.007.

- Kullerud, K., Flaatt, K. and Davidsen, B. (2001) High-pressure fluid-rock reactions involving Cl-bearing fluids in lower-crustal ductile shear zones of the Flakstadoy basic complex, Lofoten, Norway. *Journal of Petrology*, v. 42, 1349-1372.
- Layne, G.D., Kent, A. J., Bach, W. (2009) $\delta^{37}\text{Cl}$ systematics of a backarc spreading system: The Lau Basin. *Geology*, May 2009.
- Lensch, G. (1968) Die Ultramafite der Zone von Ivrea und ihre Geologische Interpretation. *Schweizerische Mineralogische und Petrographische Mitteilungen*, v.48,91-102.
- Lu, M., Hofmann, A.W., Mazzucchelli, M., and Rivalenti, G. (1997) The mafic-ultramafic complex near Finero (Ivrea-Verbano Zone), II. Geochronology and isotope geochemistry. *Chemical Geology*, v. 140, 223-235.
- Magenheim, A.J., Spivack, A.J., Volpe, C., and Ransom, B. (1994) Precise determination of stable chlorine isotopic ratios in low-concentration natural samples. *Geochimica et Cosmochimica Acta* v. 58, 3117– 3121.
- Magenheim A. J., Spivack A. J., Michael P. J., and Gieskes J. M. (1995) Chlorine stable isotope composition of the oceanic crust: Implications for Earth's distribution of chlorine. *Earth and Planetary Science Letters*, v. 131, 417–432.
- Manning, C.E. (2004) The chemistry of subduction-zone fluids. *Earth and Planetary Science Letters*, v. 223, 1-16.
- Matsumoto, T., Morishita, T., Masuda, J., Fujioka, T., Takebe, M., Yamamoto, K., and Arai, S. (2005) Noble gases in the Finero Phlogopite–Peridotites, Italian Western Alps. *Earth and Planetary Science Letters*, v. 238, 130–145.

- Mayer, A., Mezger, K., and Sinigoi, S. (2000) New Sm-Nd ages for the Ivrea-Verbano Zone, Sesia and Sessera Valleys (Northern Italy). *Journal of Geodynamics*, v. 30, 147-166.
- Mehnert, K. R. (1975) The Ivrea Zone; a model of the deep crust: *Neues Jahrbuch für Mineralogie Abhandlungen*, v. 125, 156–199.
- Morishita, T., Hattori, K. H., Terada, K., Matsumoto, T., Yamamoto, K., Takebe, M., Ishida, Y., Tamura, A., and Arai, S. (2008) Geochemistry of apatite-rich layers in the Finero phlogopite-peridotite massif (Italian Western Alps) and ion microprobe dating of apatite. *Chemical Geology*, v.251, 99-111.
- Newton, R.C., Charlu, T.V., and Kleppa, O.J. (1980) Thermochemistry of the high structural state plagioclases. *Geochemica Cosmochimica Acta*, v. 44, 933-941.
- Passchier, C.W. and Trouw, R.A. (2005) *Microtectonics*, 2nd edition, Springer Berlin Heidelberg, New York.
- Peressini, G., Quick, J.E., Sinigoi, S., Hofmann, A.W., and Fanning, M. (2007) Duration of a large mafic intrusion and heat transfer in the lower crust: a SHRIMP U–Pb zircon study in the Ivrea–Verbano Zone (Western Alps, Italy). *Journal of Petrology*, v. 48, 1185–1218.
- Philippot, P. (1993) Fluid-melt-rock interaction in mafic eclogites and coesite-bearing metasediments: constraints on volatile re-cycling during subduction. *Chemical Geology* v. 108, 93-112.
- Philippot, P., Agrinier, P. and Scambelluri, M. (1998) Chlorine cycling during subduction of altered oceanic crust. *Earth and Planetary Science Letters*, v. 161, 33-44.

- Powell, R. and Holland, T. (1999) Relating formulations of the thermodynamics of mineral solid solutions: Activity modeling of pyroxenes, amphiboles, and micas. *American Mineralogist*, v. 84, 1-14.
- Quick, J., Sinigoi, S., and Mayer, A. (1995) Emplacement of mantle peridotite in the lower continental crust, Ivrea-Verbano zone, northwest Italy. *Geology*, v.23, 739-742.
- Quick, J. E., Sinigoi, S., Snoke, A. W., Kalakay, T. J., Mayer, A. and Peressini, G. (2003) Geologic map of the Southern Ivrea-Verbano Zone, Northwestern Italy. U.S. Geological Survey I-Map 2776.
- Raffone, N., Le Fevre, B., Ottolini, L., Vannucci, R., and Zanetti, A. (2006) Light-lithophile element metasomatism of Finero peridotite (W Alps): A secondary-ion mass spectrometry study. *Microchimica Acta*, v. 155, 251-255.
- Ransom, B., Spivack, A.J., and Kastner, M. (1995) Stable Cl isotopes in subduction-zone pore waters: Implications for fluid-rock reactions and the cycling of chlorine. *Geology*, v. 23, 715–718.
- Rivalenti, G., Garuti, G., Rossi, A., Siena, F., and Sinigoi, S. (1981) Existence of different peridotite types and of a layered igneous complex in the Ivrea Zone of the Western Alps. *Journal of Petrology*, v. 22, 127–153.
- Scambelluri, M., and Philippot, P. (2001) Deep fluids in subduction zones. *Lithos*, v. 55, 213-227.
- Schauble, E.A., Rossman, G.R., and Taylor, H.P. (2003) Theoretical estimates of equilibrium chlorine-isotope fractionations. *Geochemica et Cosmochimica Acta*, v. 67, 3267– 3281.

- Selverstone, J., Franz, G., Thomas, S., and Getty, S. (1992) Fluid variability in 2 GPa eclogites as an indicator of fluid behavior during subduction. *Contributions to Mineralogy and Petrology*, v.112, 341-357.
- Sharp, Z. D., V. Atudorei, and T. Durakiewicz (2001) A rapid method for determination of hydrogen and oxygen isotope ratios from water and solid hydrous substances. *Chemical Geology*, v. 178, 197–210.
- Sharp, Z. and Barnes, J. (2004) Water-soluble chlorides in massive seafloor serpentinites: a source of chloride in subduction zones. *Earth and Planetary Science Letters*, v. 226, 243-254.
- Sharp, Z.D., Barnes, J.D., Brearley, A.J., Fischer, T.P., Chaussidon, M., and Kamenetsky, V.S. (2007) Chlorine isotope homogeneity of the mantle, crust and carbonaceous chondrites. *Nature*, v. 446, 1062–1065.
- Sharp, Z.D. (2007) *Stable Isotope Geochemistry*. Pearson Education, Inc. pp.252-254.
- Shervais, J. W. and Mukasa, S. B. (1991) The Balmuccia orogenic lherzolite massif, Italy. *Orogenic Lherzolites and Mantle Processes: Journal of Petrology, Special Lherzolite Issue*, 155-174.
- Siena, F. and Coltorti, M. (1989) The petrogenesis of a hydrated mafic–ultramafic complex and the role of amphibole fractionation at Finero (Italian Western Alps). *Neues Jahrbuch für Mineralogie, Abhandlungen*, v. 6, 255–274.
- Stähle, V., Frenzel, G., Kober, B., Michard, A., Puchelt, H., and Schneider, W. (1990) Zircon syenite pegmatites in the Finero peridotite (Ivrea zone): evidence for a syenite from a mantle source. *Earth and Planetary Science Letters*, v. 101, 196–205.

- Von Quadt, A., Ferrario, A., Diella, V., Hansmann, W., Vavra, G., and Köppel, V. (1993) U–Pb ages of zircons from chromitites of the phlogopite peridotite of Finero, Ivrea zone, N-Italy. *Schweizerische Mineralogische und Petrographische Mitteilungen*, v. 73, 137–138.
- Voshage, H., Hunziker, J.C., Hofmann, A.W., and Zingg, A. (1987) A Nd and Sr isotopic study of the Ivrea zone, Southern Alps, N-Italy. *Contributions to Mineralogy and Petrology*, v. 97, 31-42.
- Vosage, H., Hofmann, A.W., Mazzucchelli, M., Rivalenti, G., Sinigoi, S., Raczek, I., and Demarchi, G. (1990) Isotopic evidence from the Ivrea Zone for a hybrid lower crust formed by magmatic underplating. *Nature*, v. 347, 731-736.
- Zanetti, A., Mazzucchelli, M., Rivalenti, G., and Vannucci, R. (1999) The Finero phlogopite-peridotite massif: an example of subduction-related metasomatism. *Contributions to Mineralogy and Petrology*, v. 134, 107-122.
- Zaccarini, F., Stumpfl, E.F., and Garuti, G. (2004) Zirconolite and Zr–Th–U minerals in chromitites of the Finero complex, Western Alps, Italy: evidence for carbonatite-type metasomatism in a subcontinental mantle plume. *Canadian Mineralogist*, v. 42, 1825–1845.

APPENDICES

Perplex modeling

Minimum stability fields for the respective mineralogy for each sample are as follows:

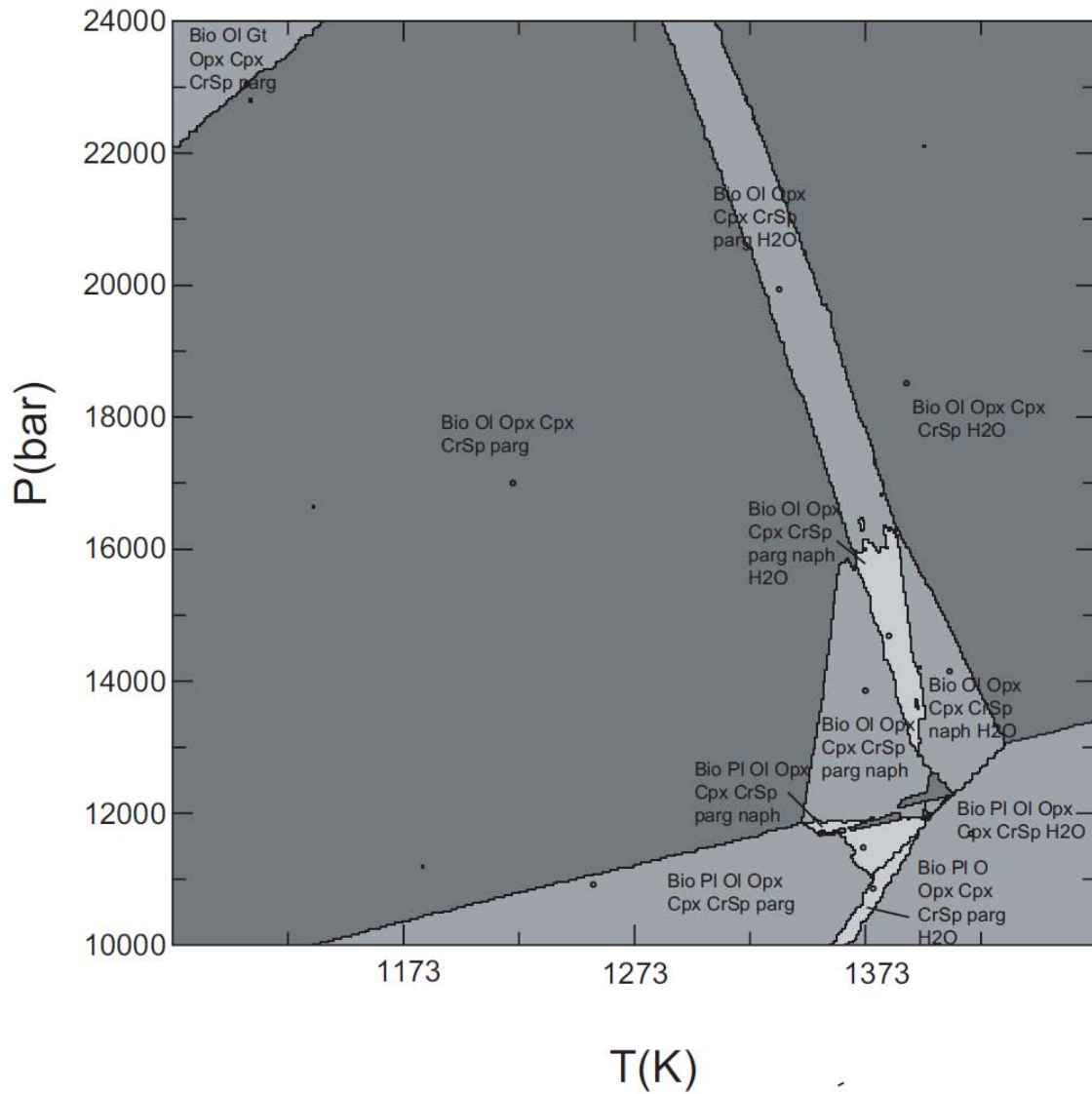
FIN-21C-RUN3

cr_hp02ver.dat

O(HP), Cpx(HP), Opx(HP), CrSp, Bio(HP), Gt(HP), Pl(h)

Amphibole was approximated as pure pargasite

0.03 wt% H₂O; minimum stability



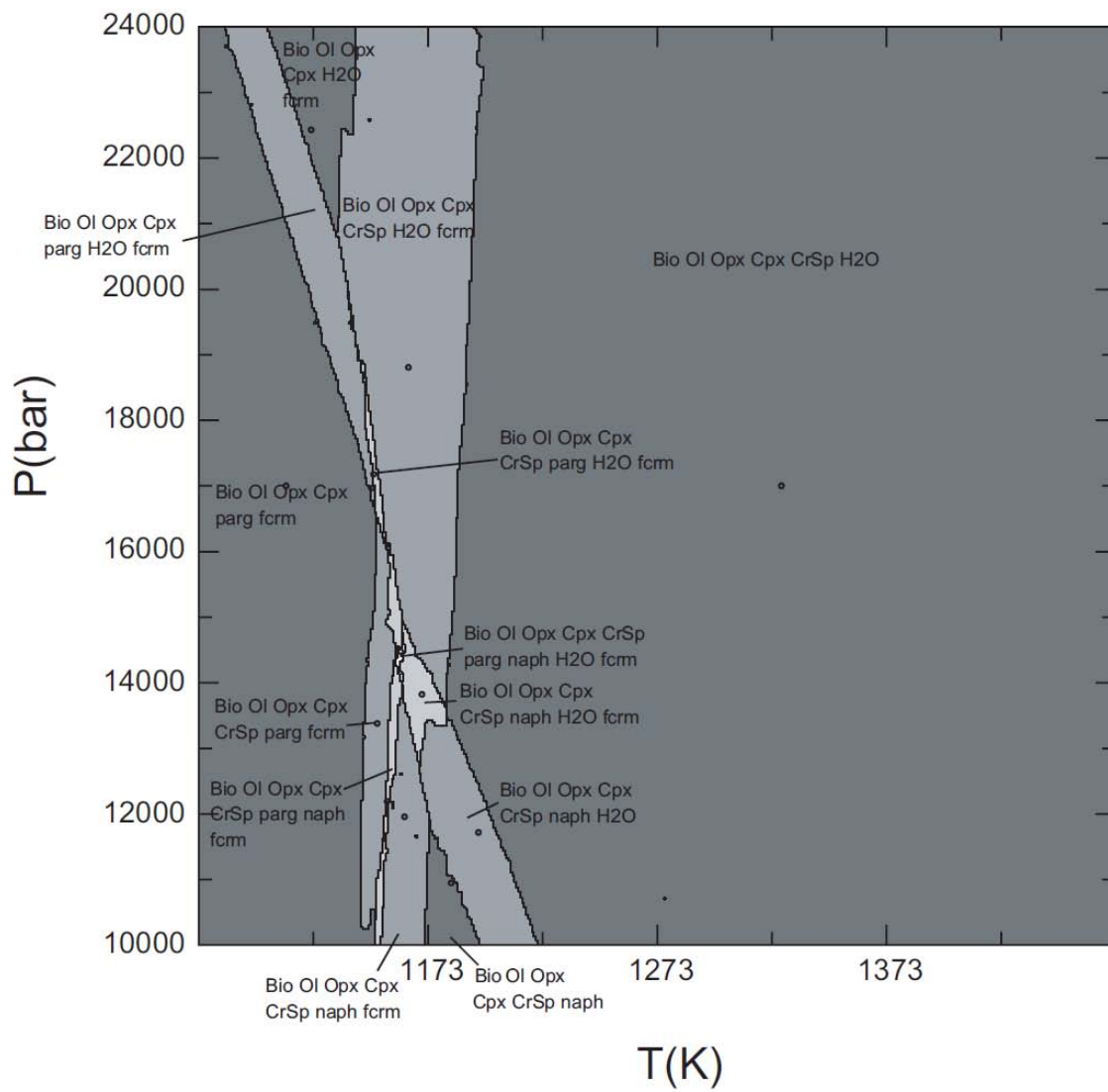
FIN-21D-RUN3

cr_hp02ver.dat

O(HP), Cpx(HP), Opx(HP), CrSp, Bio(HP), Gt(HP), Pl(h)

Amphibole was approximated as pure pargasite

0.05 wt% H₂O; minimum stability



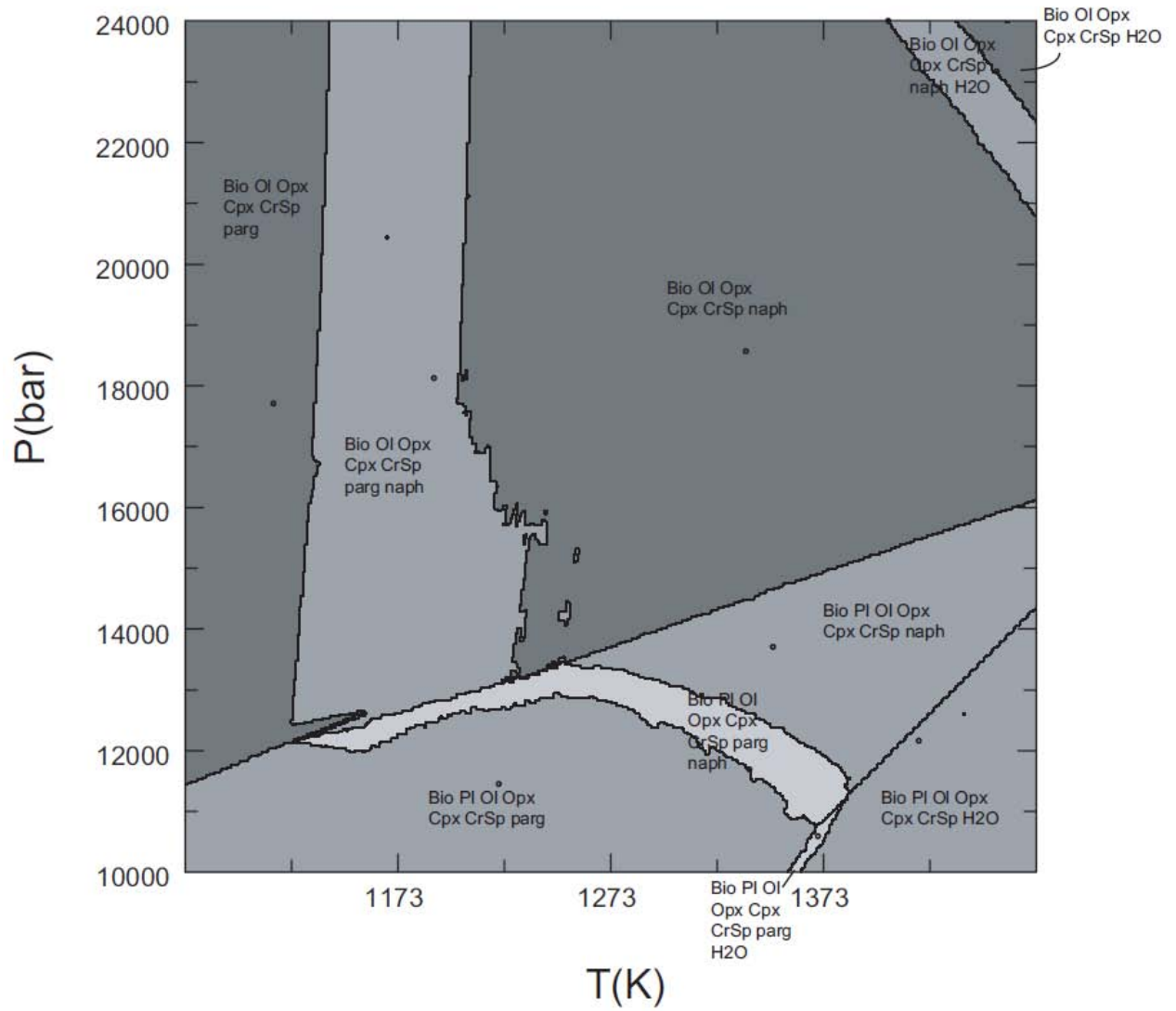
FIN-24B-RUN3

cr_hp02ver.dat

O(HP), Cpx(HP), Opx(HP), CrSp, Bio(HP), Gt(HP), Pl(h)

Amphibole was approximated as pure pargasite

0.01 wt% H₂O; minimum stability



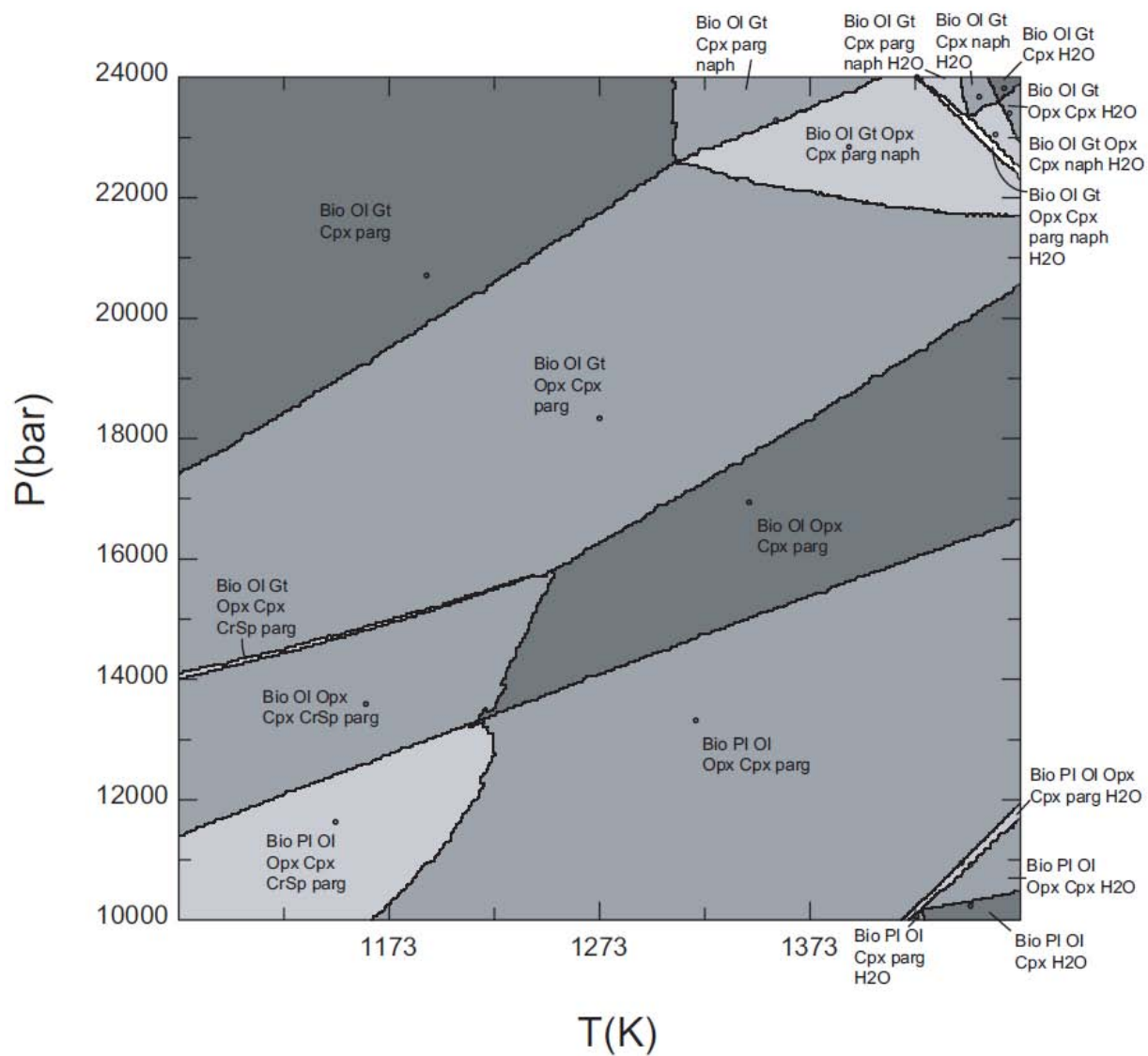
FIN-25B-RUN4

cr_hp02ver.dat

O(HP), Cpx(HP), Opx(HP), CrSp, Bio(HP), Gt(HP), Pl(h)

Amphibole was approximated as pure pargasite

1.5 wt% H₂O; maximum stability



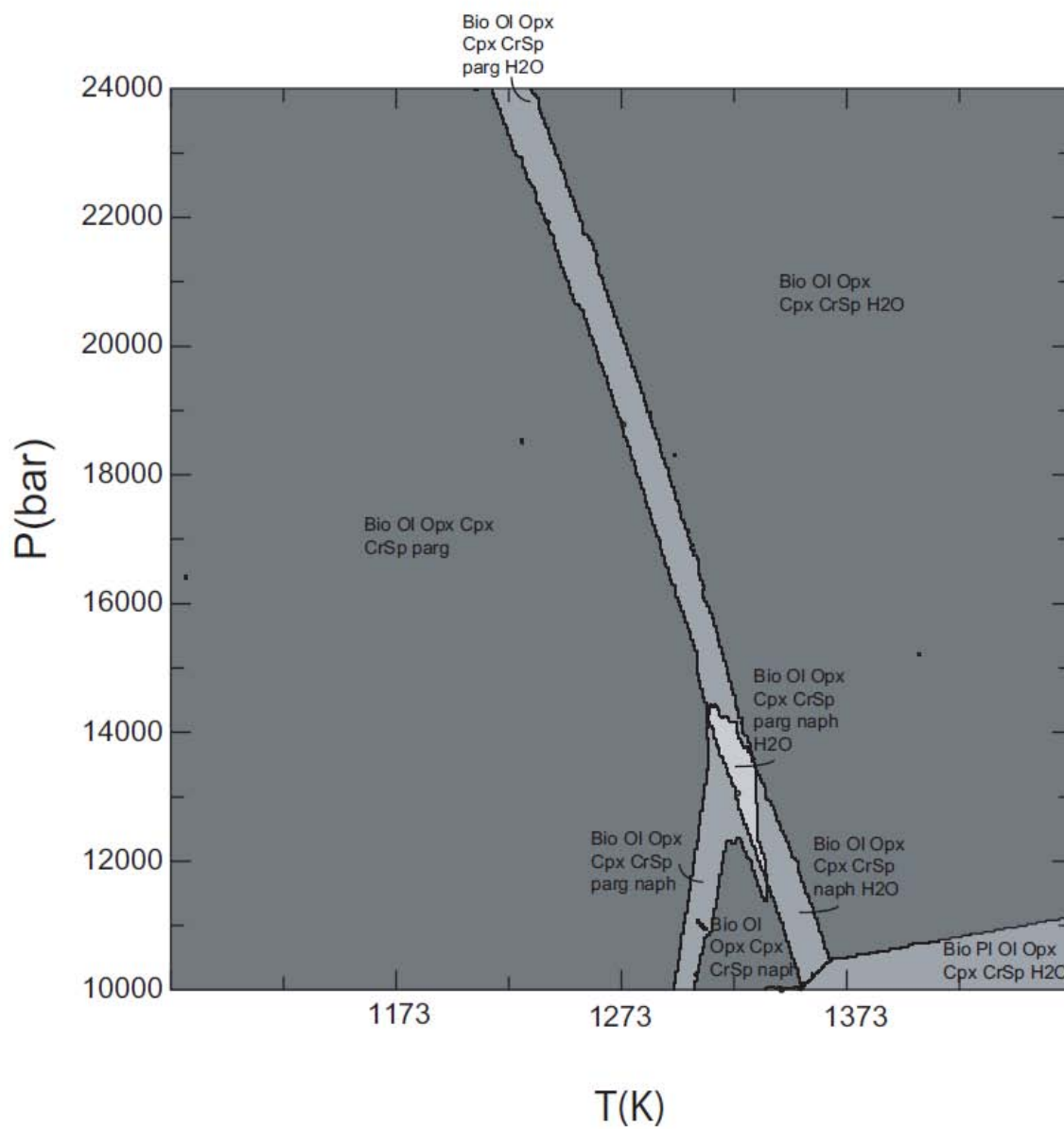
FIN-25C-RUN5

cr_hp02ver.dat

O(HP), Cpx(HP), Opx(HP), CrSp, Bio(HP), Gt(HP), Pl(h)

Amphibole was approximated as pure pargasite

0.02 wt% H₂O; minimum stability



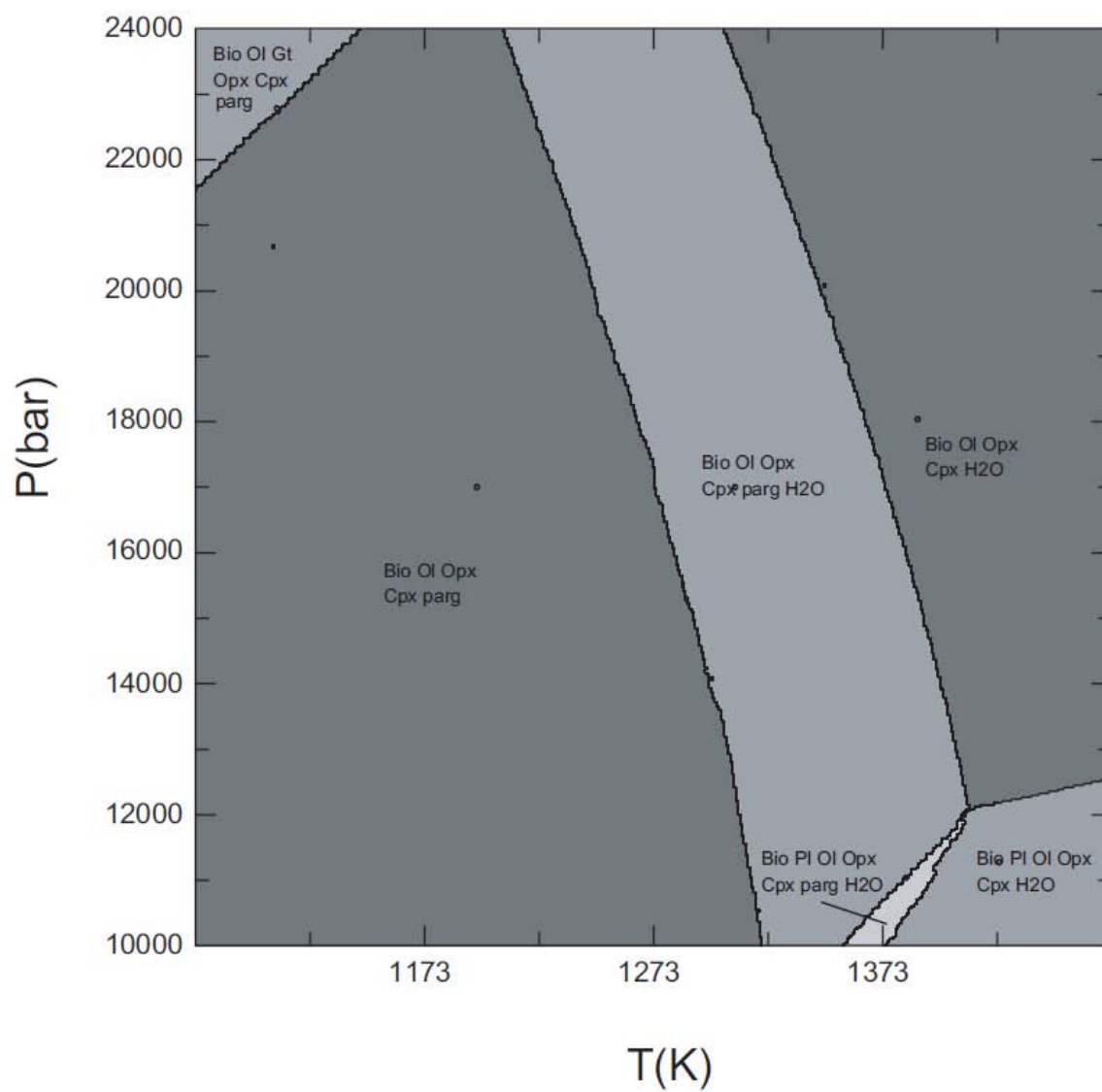
FIN-25D-RUN2

cr_hp02ver.dat

O(HP), Cpx(HP), Opx(HP), CrSp, Bio(HP), Gt(HP), Pl(h)

Amphibole was approximated as pure pargasite

0.2 wt% H₂O; minimum and maximum stability



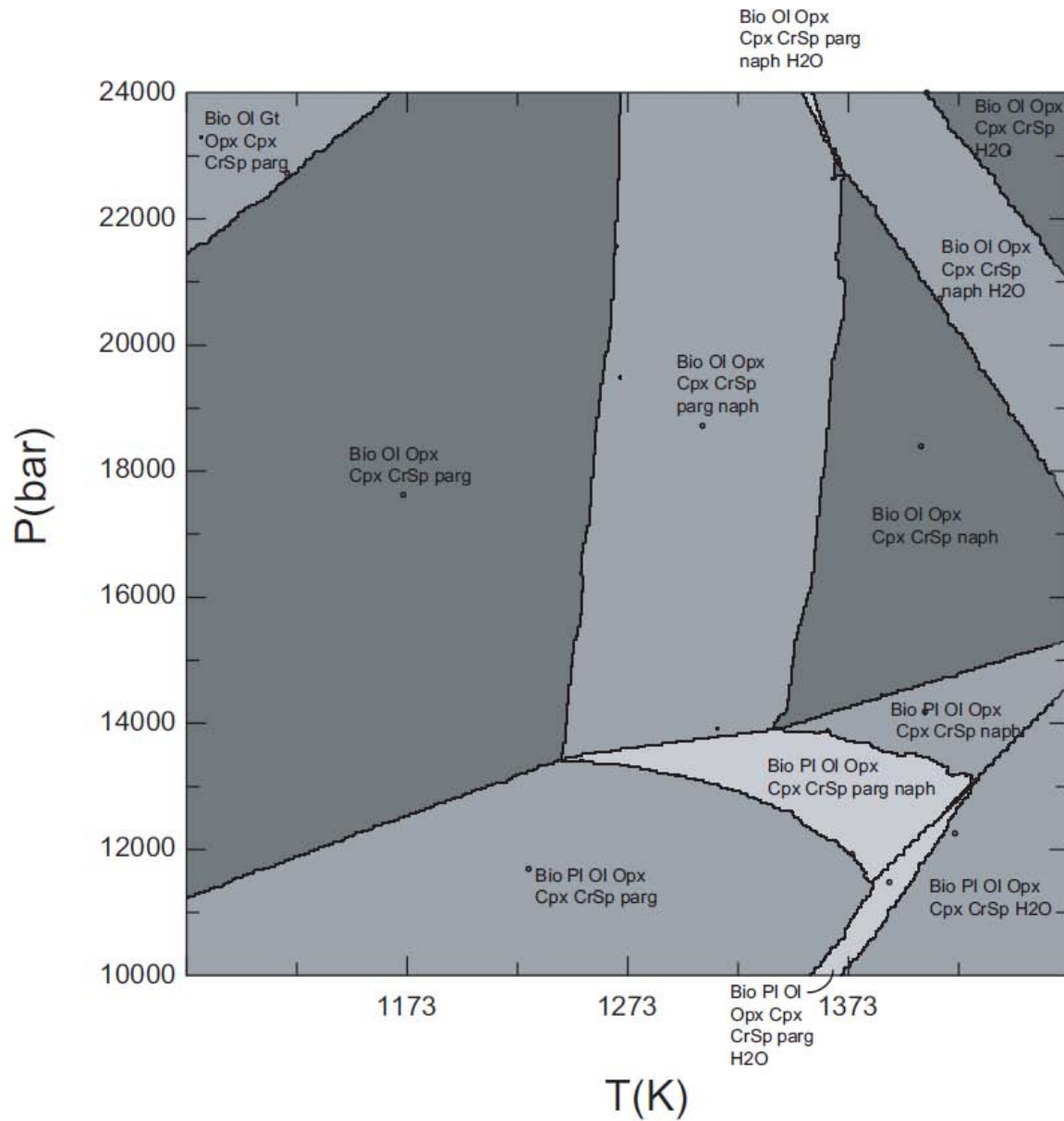
FIN-25Ji-RUN2

cr_hp02ver.dat

O(HP), Cpx(HP), Opx(HP), CrSp, Bio(HP), Gt(HP), Pl(h)

Amphibole was approximated as pure pargasite

0.4 wt% H₂O; minimum stability



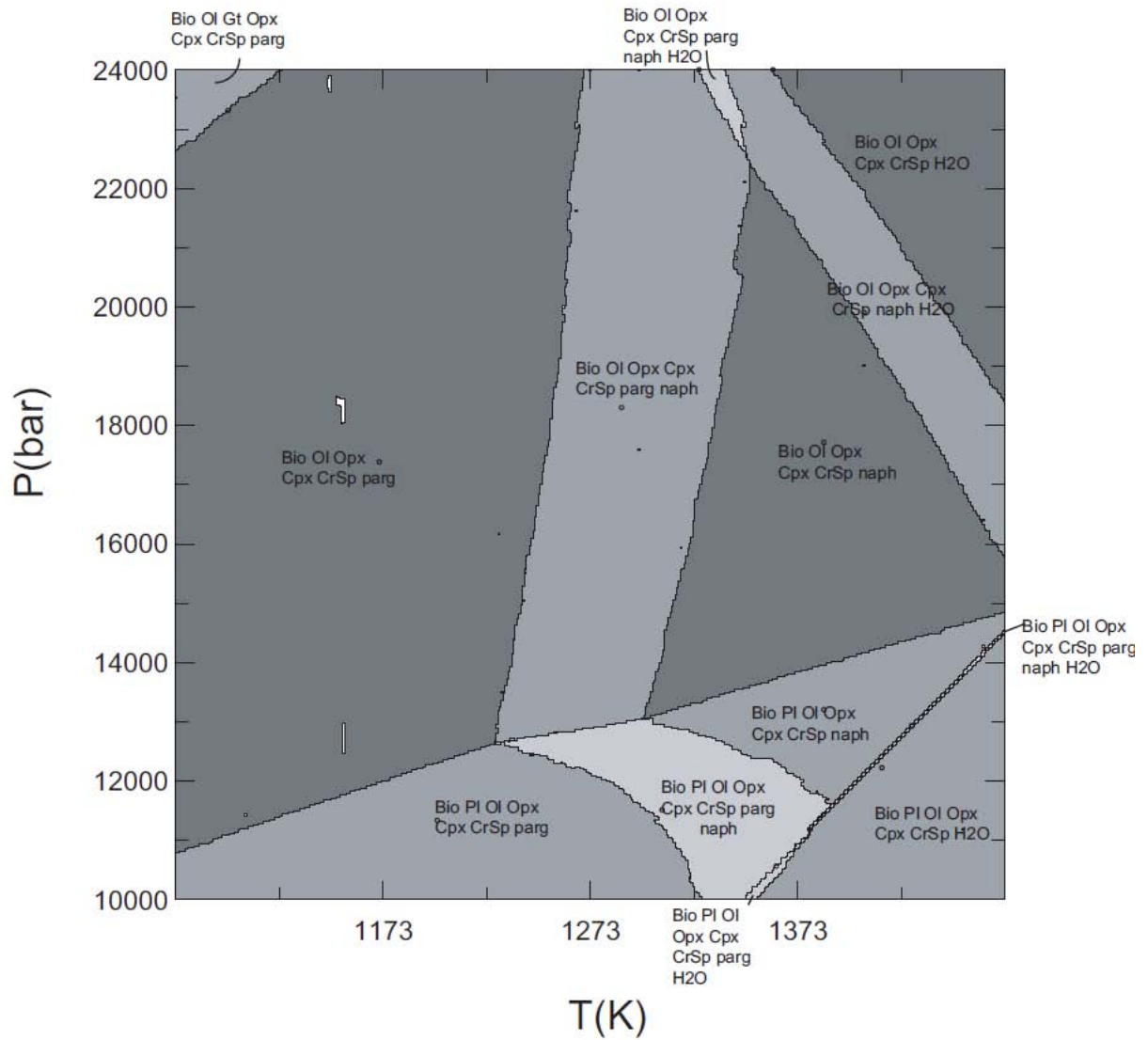
FIN-25Jii-RUN2

cr_hp02ver.dat

O(HP), Cpx(HP), Opx(HP), CrSp, Bio(HP), Gt(HP), Pl(h)

Amphibole was approximated as pure pargasite

2.0 wt% H₂O; minimum stability



Maximum stability fields for the respective mineralogy for each sample are as follows:

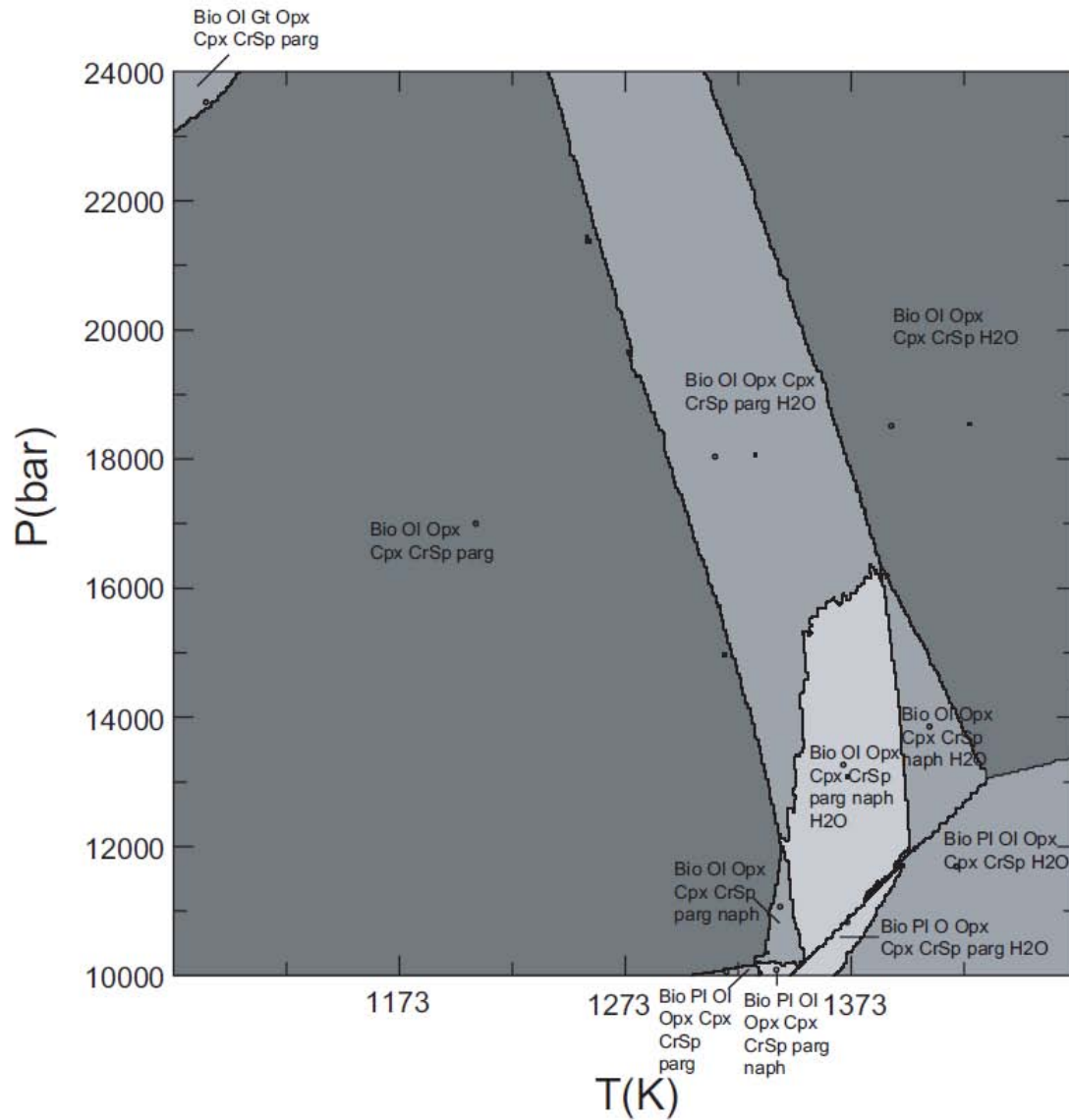
FIN-21C-RUN1

cr_hp02ver.dat

O(HP), Cpx(HP), Opx(HP), CrSp, Bio(HP), Gt(HP), Pl(h)

Amphibole was approximated as pure pargasite

0.05 wt% H₂O; maximum stability



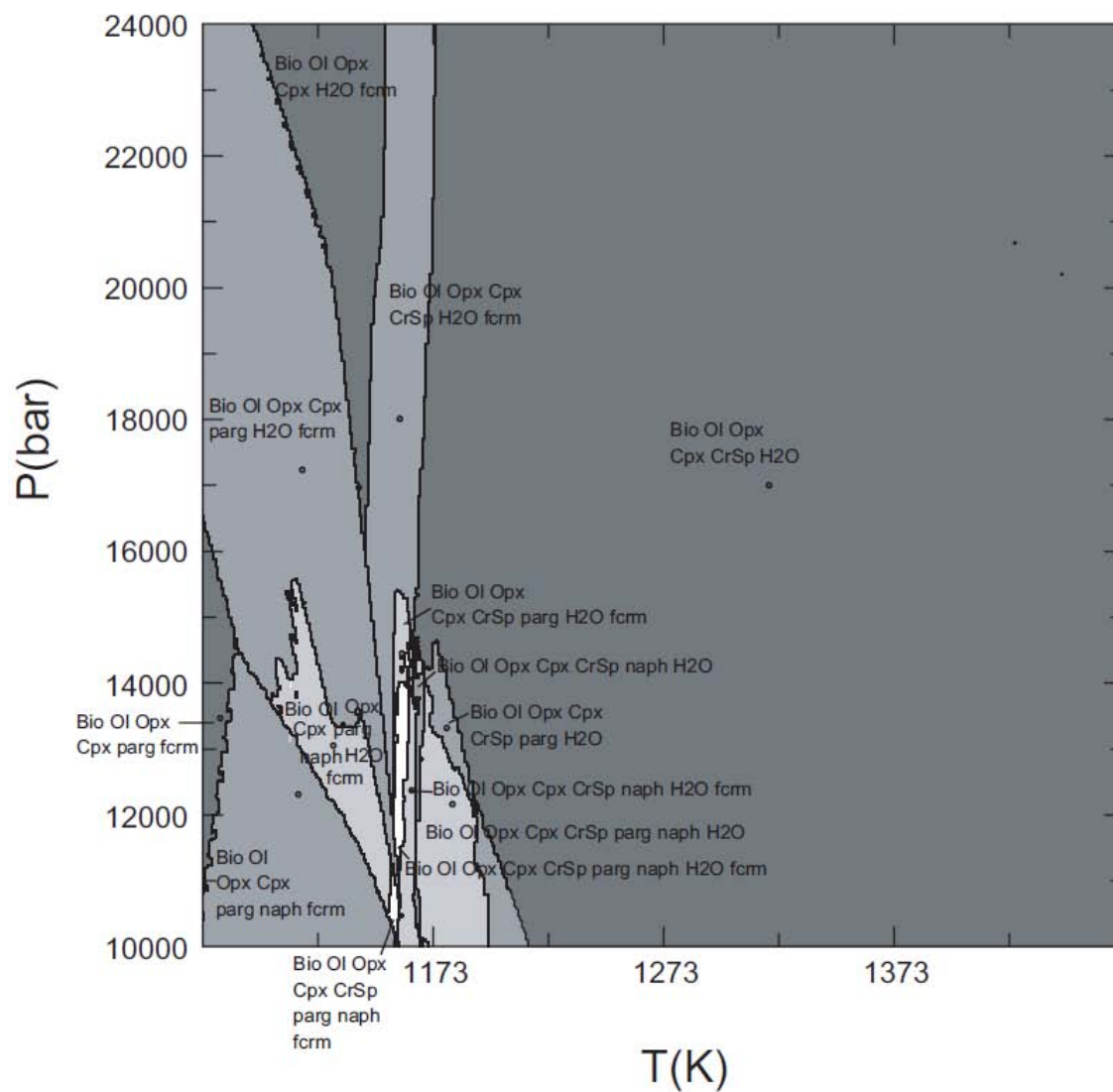
FIN-21D-RUN2

cr_hp02ver.dat

O(HP), Cpx(HP), Opx(HP), CrSp, Bio(HP), Gt(HP), Pl(h)

Amphibole was approximated as pure pargasite

0.1 wt% H₂O; maximum stability



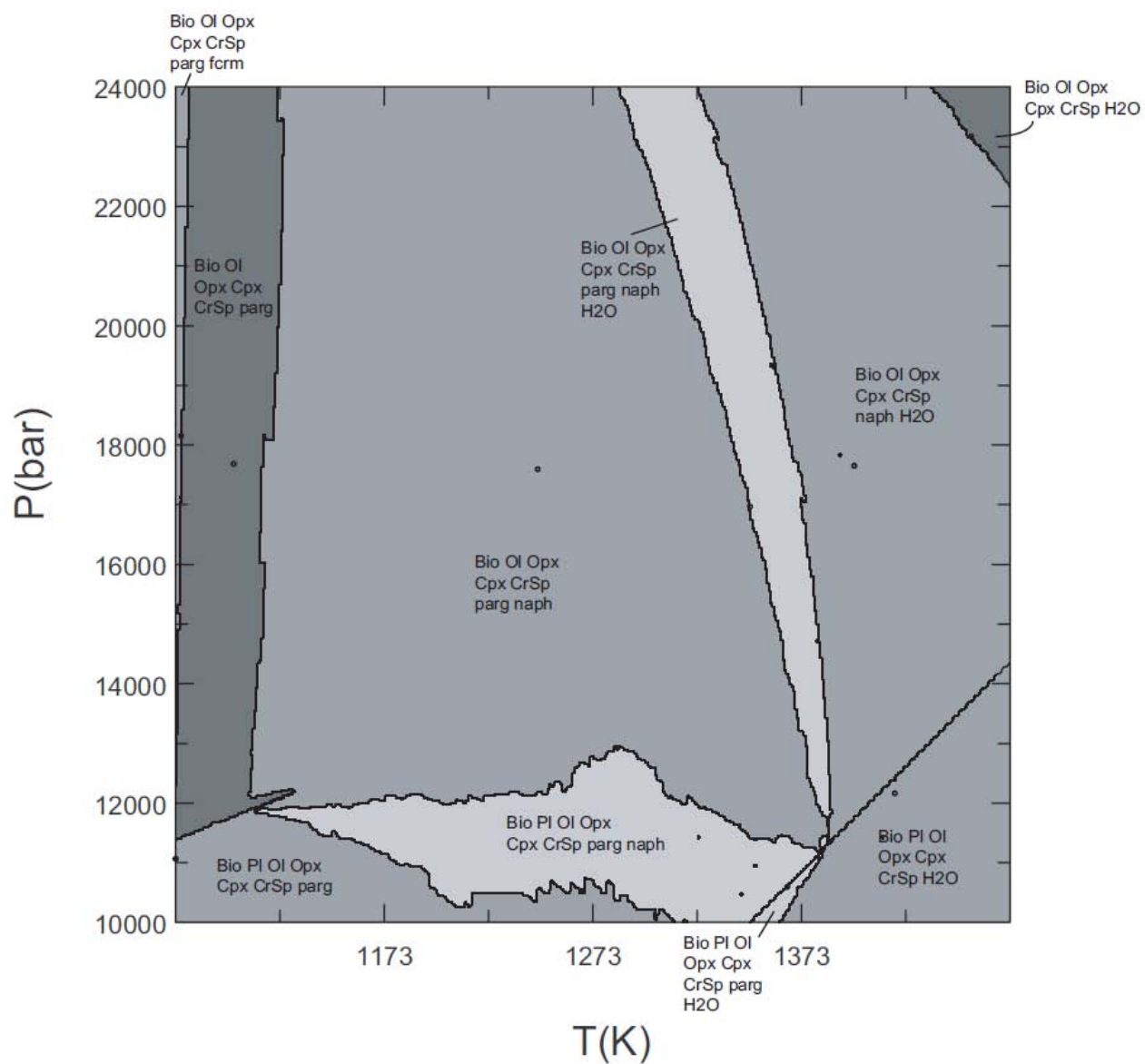
FIN-24B-RUN7

cr_hp02ver.dat

O(HP), Cpx(HP), Opx(HP), CrSp, Bio(HP), Gt(HP), Pl(h)

Amphibole was approximated as pure pargasite

0.02 wt% H₂O; maximum stability

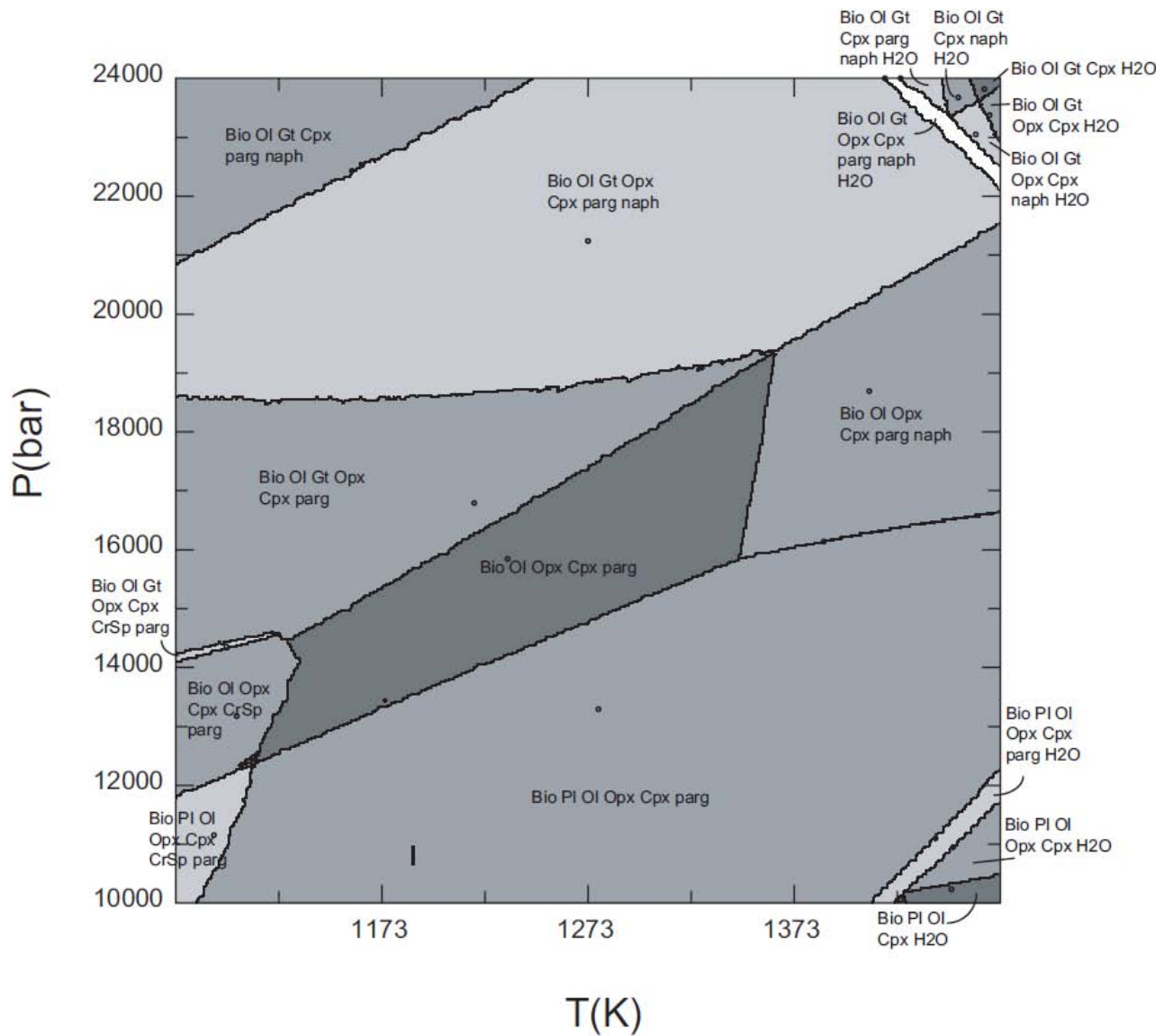


cr_hp02ver.dat

O($\bar{H}\dot{P}$), Cpx(HP), Opx(HP), CrSp, Bio(HP), Gt(HP), Pl(h)

Amphibole was approximated as pure pargasite

1.6 wt% H₂O; maximum stability



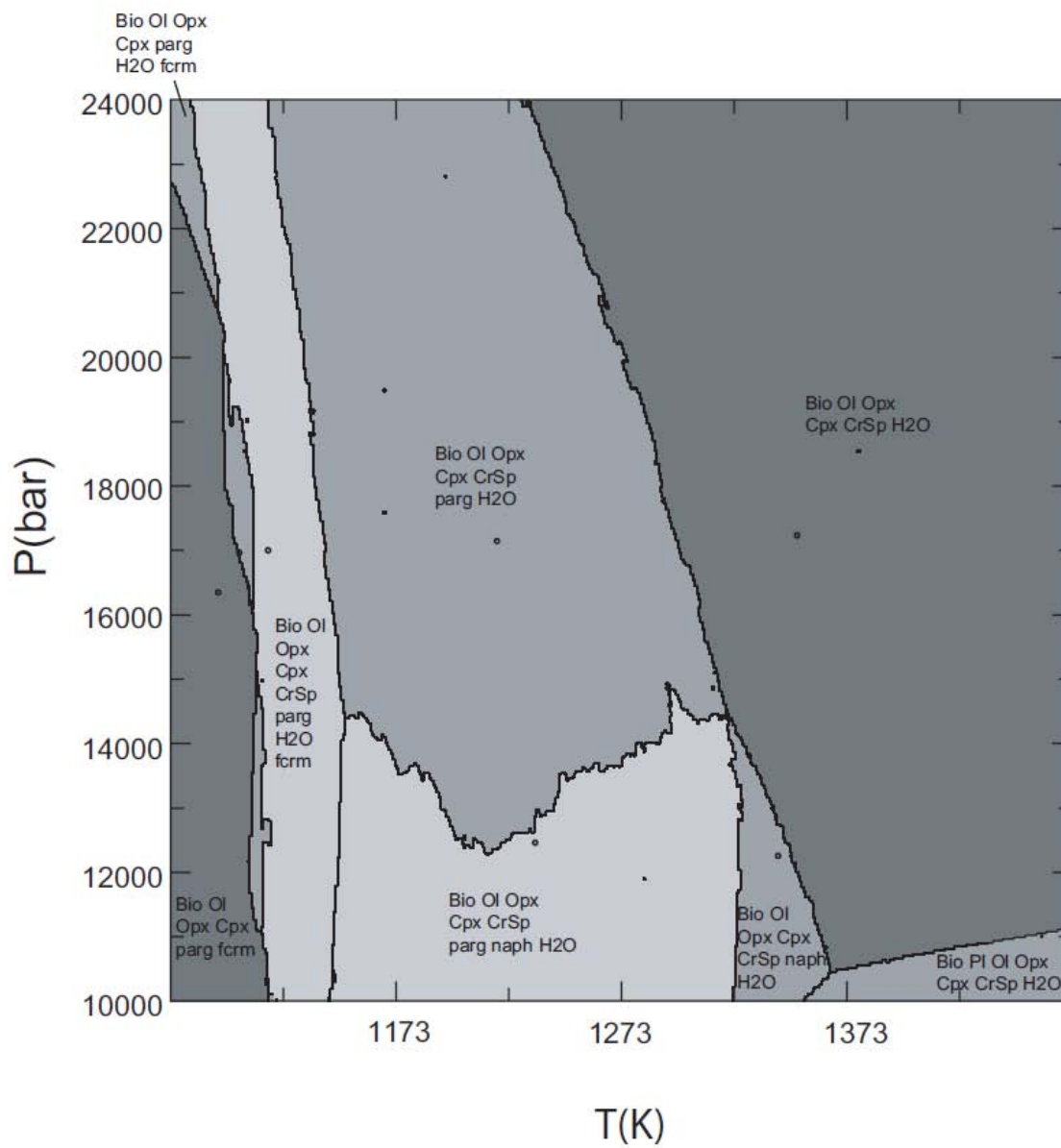
FIN-25C-RUN8

cr_hp02ver.dat

O(HP), Cpx(HP), Opx(HP), CrSp, Bio(HP), Gt(HP), Pl(h)

Amphibole was approximated as pure pargasite

0.7 wt% H₂O; maximum stability



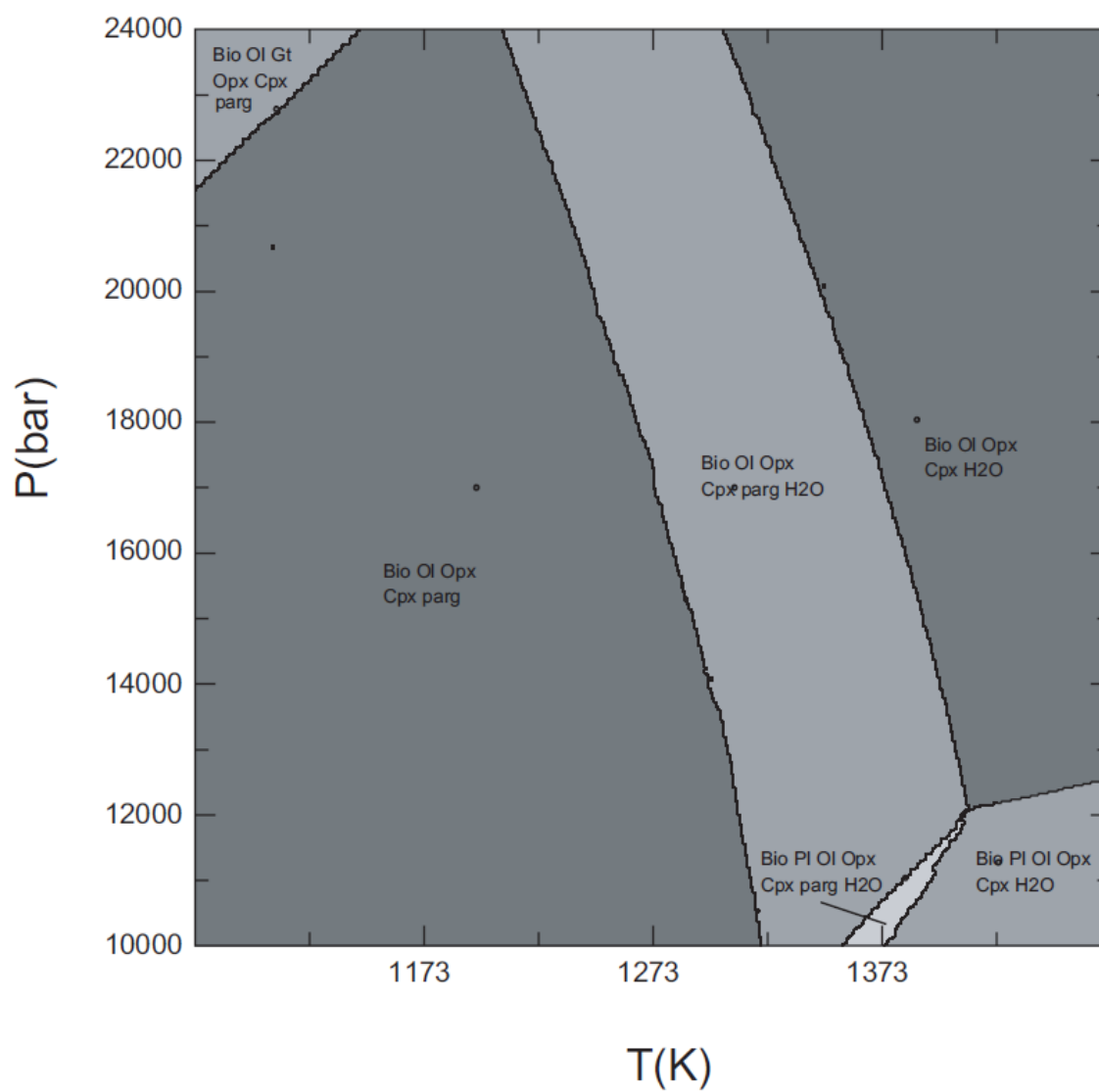
FIN-25D-RUN2

cr_hp02ver.dat

O(HP), Cpx(HP), Opx(HP), CrSp, Bio(HP), Gt(HP), Pl(h)

Amphibole was approximated as pure pargasite

0.2 wt% H₂O; minimum and maximum stability



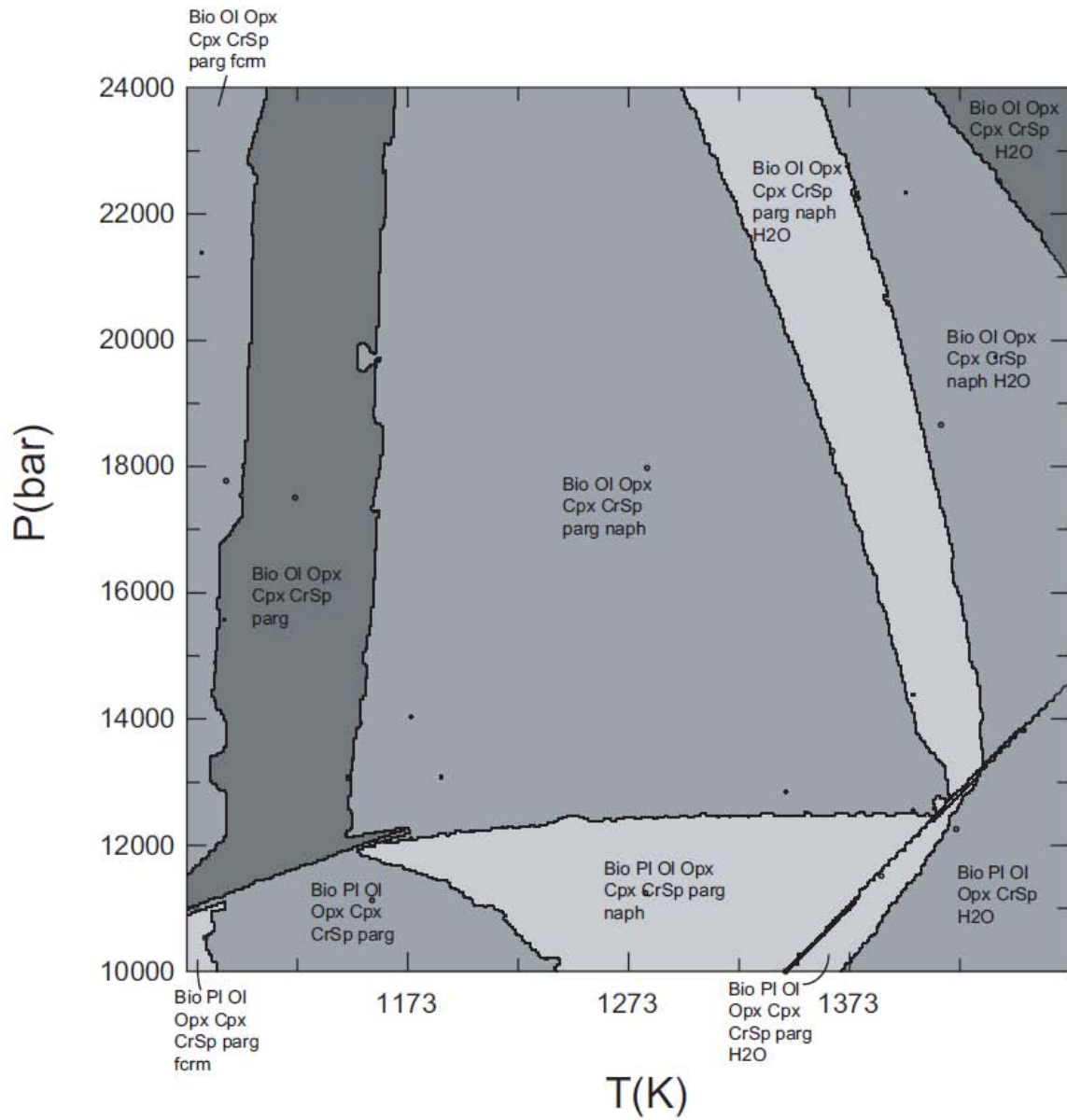
FIN-25Ji-RUN1

cr_hp02ver.dat

O(HP), Cpx(HP), Opx(HP), CrSp, Bio(HP), Gt(HP), Pl(h)

Amphibole was approximated as pure pargasite

0.5 wt% H₂O; maximum stability



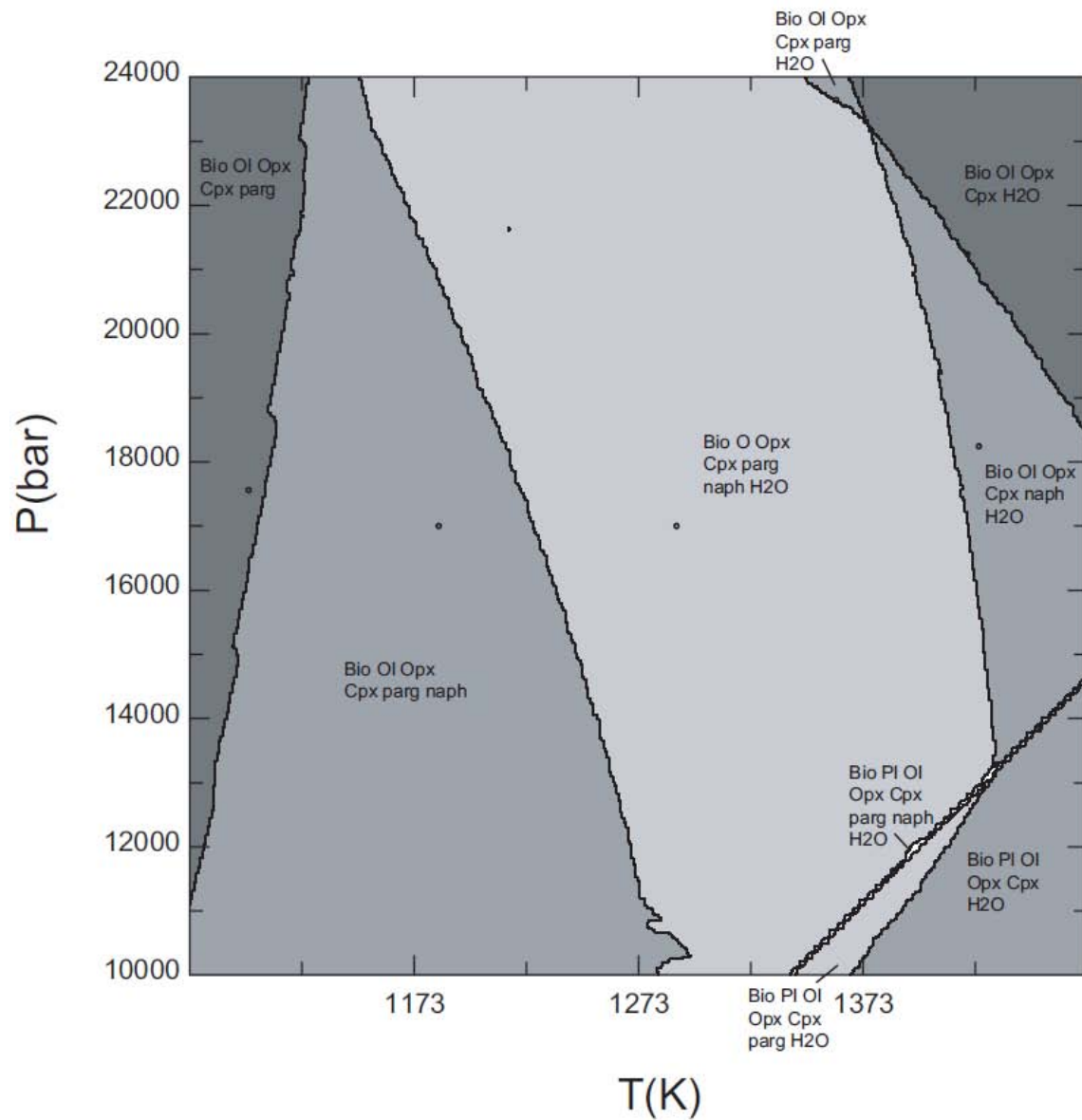
FIN-25Jii-RUN6

cr_hp02ver.dat

O(HP), Cpx(HP), Opx(HP), CrSp, Bio(HP), Gt(HP), Pl(h)

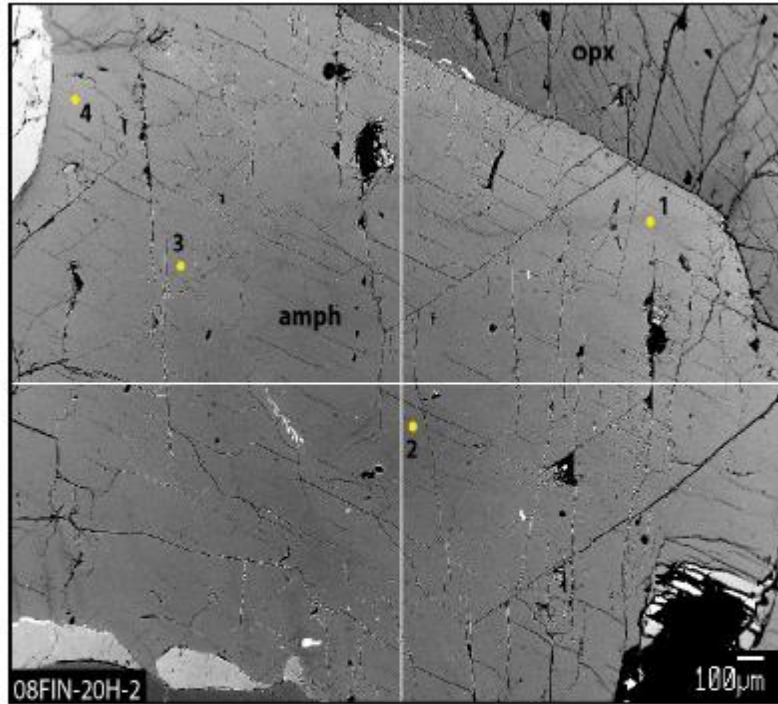
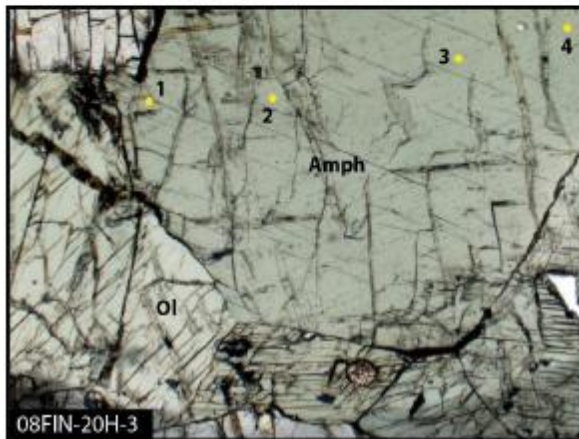
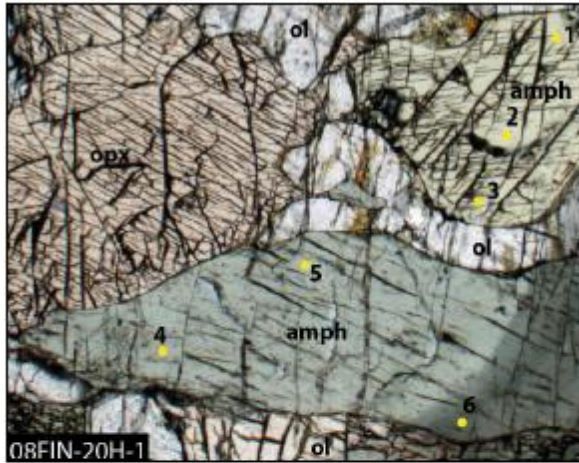
Amphibole was approximated as pure pargasite

2.3 wt% H₂O; maximum stability



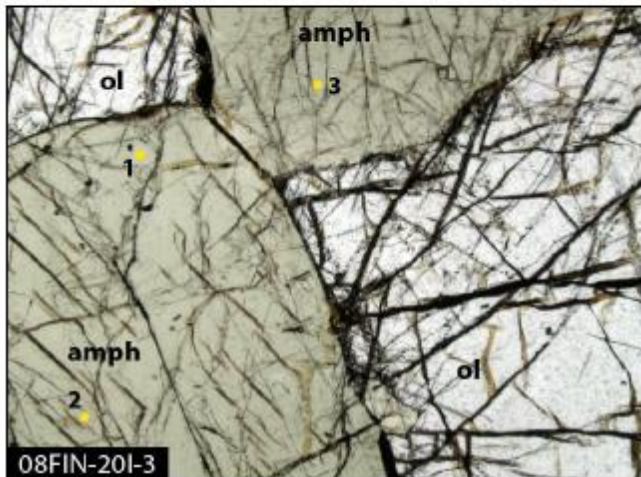
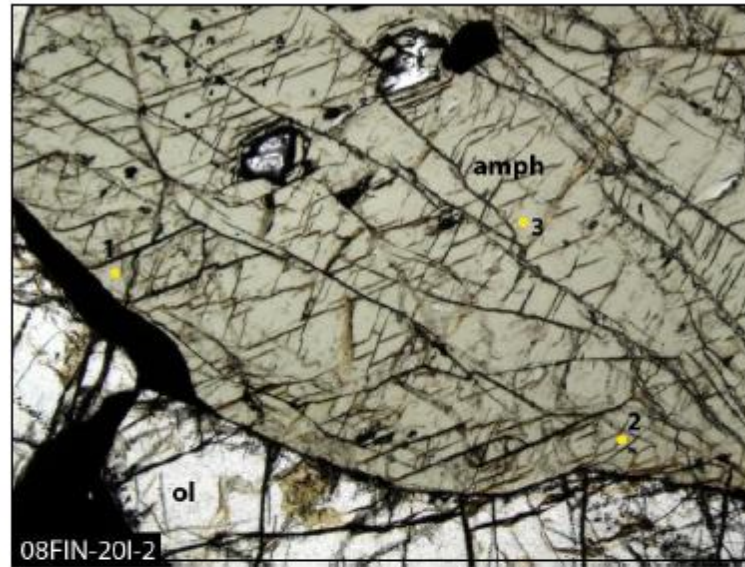
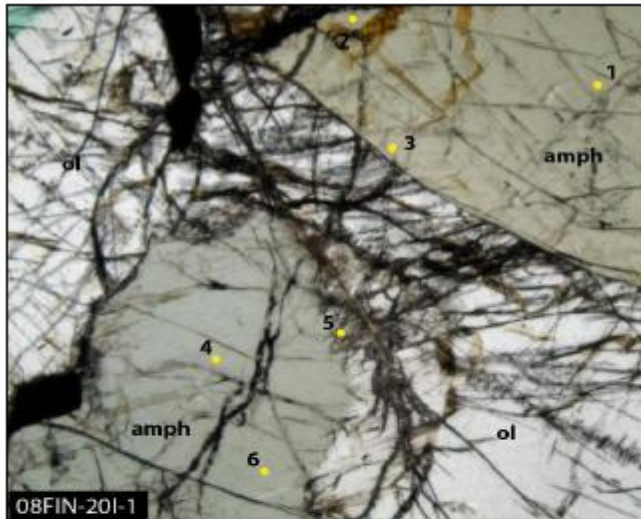
Microprobe Sections

08FIN-20H: Amphibole Peridotite



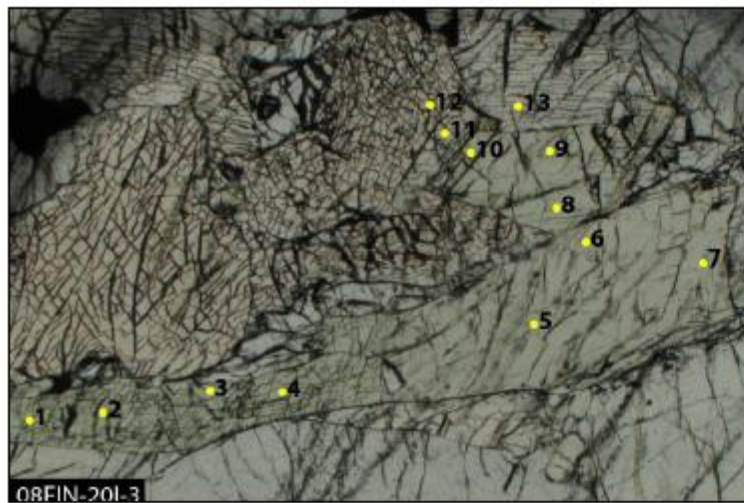
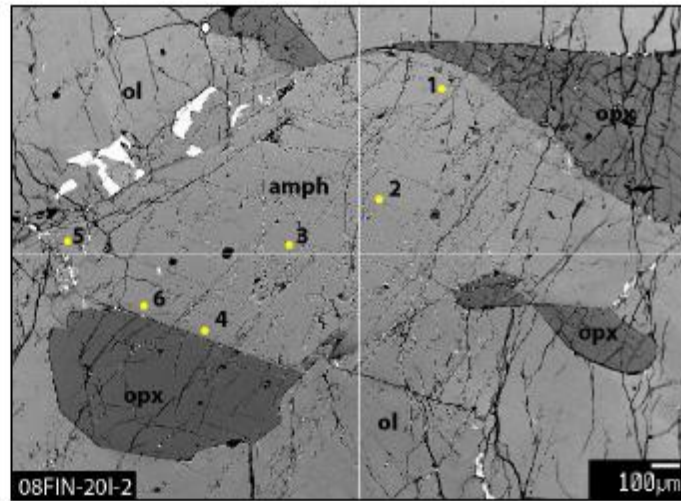
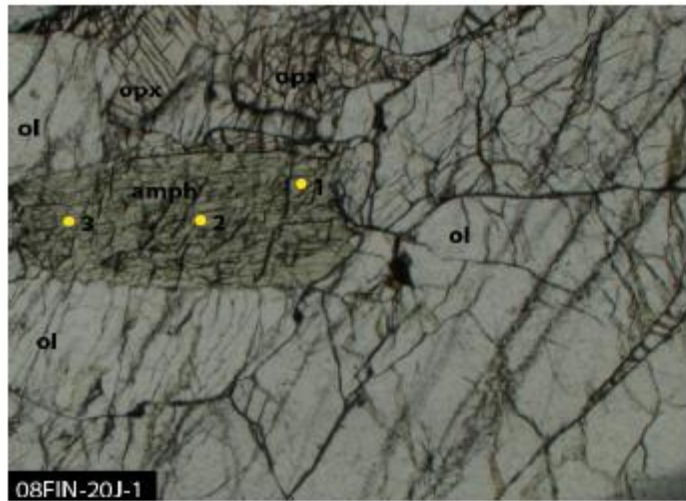
ANALYSIS	08FIN-20H 1	08FIN-20H 1	08FIN-20H 1	08FIN-20H 1	08FIN-20H 1	08FIN-20H 1	08FIN-20H 1	08FIN-20H 2	08FIN-20H 2	08FIN-20H 2	08FIN-20H 2	08FIN-20H 3	08FIN-20H 3	08FIN-20H 3
	1	2	3	4	5	6	1	2	3	4	1	2	3	4
Mass %														
SiO2	42.98	43.35	43.48	42.77	43.23	42.87	43.25	43.55	43.32	42.98	42.06	41.83	42.62	42.62
Al2O3	14.47	14.33	14.19	14.45	14.10	14.45	14.81	14.42	14.52	14.31	14.74	14.74	15.09	14.71
TiO2	0.45	0.45	0.45	0.41	0.39	0.42	0.37	0.37	0.39	0.38	0.46	0.42	0.42	0.38
MgO	17.21	17.09	17.26	17.02	17.26	16.97	17.06	17.24	17.14	17.25	17.02	17.00	17.01	17.01
FeO	7.37	7.20	7.30	7.32	7.14	6.91	7.40	7.21	7.47	7.47	7.43	7.69	7.69	7.70
MnO	0.10	0.07	0.06	0.05	0.09	0.08	0.09	0.08	0.10	0.07	0.10	0.10	0.10	0.11
Cr2O3	0.20	0.22	0.20	0.26	0.19	0.24	0.33	0.29	0.32	0.27	0.25	0.25	0.28	0.28
CaO	11.92	12.01	11.95	11.75	11.80	11.75	11.68	11.79	11.83	11.61	11.94	12.03	11.98	11.96
Na2O	2.73	2.77	2.70	2.71	2.58	2.65	2.68	2.62	2.71	2.77	2.80	2.80	2.79	2.81
K2O	0.20	0.21	0.22	0.20	0.21	0.21	0.20	0.19	0.20	0.20	0.23	0.22	0.21	0.21
F	0.00	0.00	0.00	0.00	0.01	0.00	0.00	0.00	0.00	0.01	0.02	0.02	0.02	0.00
Cl	0.008	0.012	0.002	0.008	0.007	0.000	0.003	0.025	0.000	0.031	0.000	0.000	0.000	0.025
Total	97.63	97.70	97.79	96.95	97.00	96.55	97.88	97.77	98.01	97.33	97.05	97.08	98.20	97.79
Cation Total														
Si	6.182	6.223	6.235	6.191	6.243	6.216	6.195	6.238	6.204	6.201	6.104	6.081	6.110	6.138
Ti	0.048	0.049	0.048	0.044	0.042	0.046	0.040	0.040	0.042	0.041	0.050	0.046	0.045	0.041
Al	2.453	2.426	2.398	2.466	2.401	2.469	2.501	2.435	2.451	2.434	2.522	2.525	2.550	2.497
Mg	3.691	3.656	3.689	3.671	3.716	3.669	3.642	3.680	3.658	3.711	3.680	3.683	3.635	3.651
Fe	0.886	0.864	0.875	0.887	0.863	0.838	0.886	0.863	0.895	0.901	0.902	0.934	0.922	0.927
Mn	0.012	0.008	0.007	0.006	0.011	0.009	0.011	0.010	0.012	0.009	0.013	0.012	0.013	0.014
Cr	0.023	0.025	0.023	0.029	0.022	0.028	0.038	0.033	0.037	0.031	0.028	0.029	0.032	0.032
Ca	1.837	1.847	1.836	1.823	1.825	1.826	1.793	1.809	1.816	1.794	1.856	1.873	1.840	1.846
Na	0.760	0.770	0.750	0.761	0.722	0.744	0.744	0.726	0.751	0.774	0.789	0.789	0.776	0.783
K	0.037	0.039	0.040	0.036	0.038	0.039	0.036	0.035	0.036	0.036	0.043	0.041	0.039	0.038
F	0.001	0.000	0.000	0.000	0.002	0.000	0.000	0.000	0.001	0.001	0.003	0.005	0.005	0.000
Cl	0.001	0.001	0.000	0.001	0.001	0.000	0.000	0.003	0.000	0.004	0.000	0.000	0.000	0.003
Total	15.934	15.910	15.901	15.917	15.889	15.883	15.887	15.875	15.905	15.941	15.994	16.021	15.971	15.974
Comment	amph	amph	amph	amph	amph	amph	amph	amph	amph	amph	amph	amph	amph	amph

08FIN-20I: Amphibole Peridotite



ANALYSIS	08FIN-20I 1-	08FIN-20I 1-	08FIN-20I 1-	08FIN-20I 1-	08FIN-20I 1-	08FIN-20I 1-	08FIN-20I 2-	08FIN-20I 2-	08FIN-20I 2-	08FIN-20I 3-	08FIN-20I 3-	08FIN-20I 3-
	1	2	3	4	5	6	1	2	3	1	2	3
Mass %												
SiO2	43.92	44.41	45.02	44.60	44.09	56.41	44.48	43.41	43.94	44.48	44.40	44.05
Al2O3	13.71	13.22	13.41	13.70	13.60	2.11	13.97	14.26	13.92	13.48	13.93	13.58
TiO2	0.73	0.65	0.71	0.68	0.67	0.06	0.76	0.73	0.72	0.67	0.72	0.69
MgO	17.11	17.65	17.40	17.06	17.17	31.64	17.12	17.06	17.22	17.33	17.04	17.13
FeO	7.47	7.13	7.04	7.35	7.51	11.82	7.43	7.73	7.53	7.27	7.44	7.26
MnO	0.08	0.10	0.09	0.09	0.08	0.29	0.09	0.10	0.09	0.11	0.09	0.07
Cr2O3	0.59	0.50	0.48	0.55	0.55	0.12	0.62	0.50	0.59	0.50	0.58	0.61
CaO	12.14	12.04	12.40	12.07	12.15	0.31	12.11	12.18	12.33	12.24	12.20	12.22
Na2O	2.61	2.47	2.54	2.60	2.58	0.01	2.61	2.67	2.69	2.62	2.59	2.45
K2O	0.28	0.27	0.27	0.29	0.27	0.02	0.28	0.31	0.28	0.27	0.29	0.27
F	0.00	0.00	0.00	0.00	0.00	0.00	0.00	0.00	0.00	0.00	0.00	0.01
Cl	0.000	0.013	0.013	0.014	0.004	0.016	0.011	0.013	0.000	0.000	0.001	0.005
Total	98.65	98.45	99.35	99.00	98.68	102.80	99.47	98.96	99.31	98.97	99.26	98.34
Cation Total												
Si	6.257	6.320	6.344	6.316	6.278	1.940	6.275	6.179	6.226	6.306	6.278	6.257
Al	2.303	2.217	2.227	2.287	2.282	0.086	2.323	2.393	2.325	2.253	2.322	2.306
Ti	0.079	0.069	0.075	0.072	0.072	0.002	0.080	0.078	0.077	0.071	0.077	0.075
Mg	3.635	3.745	3.655	3.602	3.644	1.622	3.601	3.620	3.638	3.663	3.591	3.681
Fe	0.890	0.849	0.829	0.870	0.894	0.340	0.877	0.921	0.892	0.862	0.880	0.851
Mn	0.010	0.012	0.010	0.011	0.010	0.008	0.011	0.012	0.011	0.013	0.011	0.010
Cr	0.067	0.056	0.053	0.061	0.062	0.003	0.069	0.056	0.066	0.056	0.064	0.057
Ca	1.853	1.836	1.872	1.832	1.854	0.012	1.831	1.858	1.872	1.859	1.848	1.870
Na	0.720	0.681	0.695	0.714	0.713	0.001	0.713	0.737	0.739	0.720	0.709	0.702
K	0.051	0.049	0.049	0.052	0.050	0.001	0.050	0.056	0.051	0.049	0.052	0.057
F	0.001	0.000	0.000	0.000	0.000	0.000	0.000	0.002	0.000	0.000	0.001	0.000
Cl	0.000	0.003	0.003	0.003	0.001	0.001	0.003	0.003	0.000	0.000	0.000	0.001
Total	15.865	15.839	15.813	15.822	15.859	4.015	15.831	15.915	15.897	15.852	15.833	15.866
Mineral	amph	amph	amph	amph	amph	opx	amph	amph	amph	amph	amph	amph

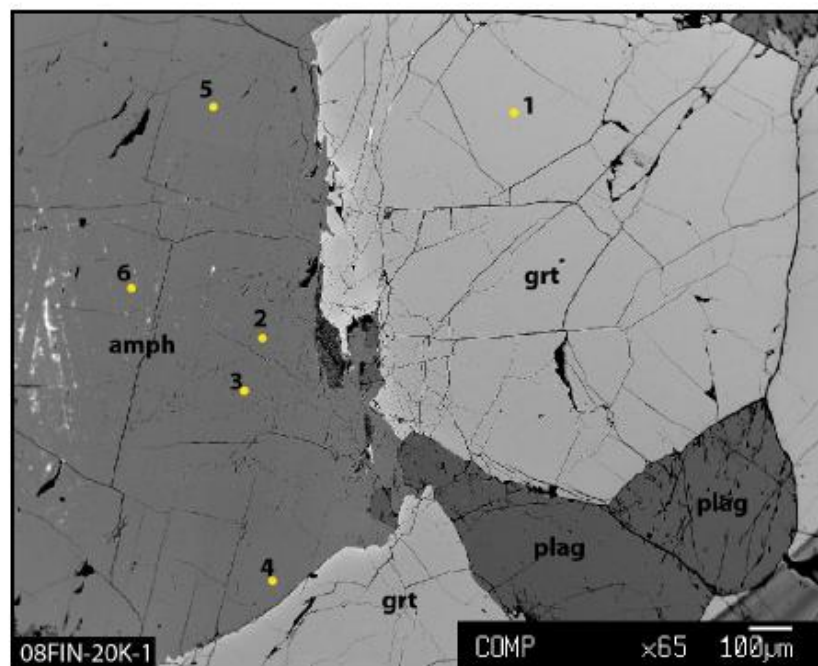
08FIN-20J: Amphibole Peridotite



ANALYSIS	08FIN-20J 1-1	08FIN-20J 2	08FIN-20J 1-3	08FIN-20J 1	08FIN-20J 2	08FIN-20J 2	08FIN-20J 2	08FIN-20J 2	08FIN-20J 2	08FIN-20J 2	08FIN-20J 3	08FIN-20J 3
	1-1	2	3	1	2	3	4	5	6	1	2	
Mass %												
SiO2	44.77	43.50	43.46	44.75	43.76	43.85	44.28	44.41	44.04	43.14	43.12	
Al2O3	13.63	13.97	13.79	13.33	14.00	13.98	13.85	13.55	13.78	13.52	13.77	
TiO2	0.46	0.43	0.52	0.46	0.47	0.46	0.43	0.45	0.45	0.47	0.48	
MgO	17.90	17.99	17.82	18.00	18.00	17.84	18.14	18.22	18.05	17.97	17.96	
FeO	5.89	6.06	6.33	5.91	6.11	6.15	5.93	6.07	6.05	5.87	5.97	
MnO	0.10	0.07	0.08	0.10	0.10	0.07	0.06	0.05	0.09	0.10	0.11	
Cr2O3	0.68	0.68	0.66	0.73	0.77	0.78	0.70	0.52	0.63	0.68	0.72	
CaO	12.36	12.42	12.44	12.06	12.10	12.24	12.15	12.43	12.15	12.07	12.10	
Na2O	2.36	2.50	2.61	2.35	2.48	2.47	2.41	2.43	2.35	2.40	2.52	
K2O	0.18	0.19	0.20	0.16	0.17	0.16	0.15	0.15	0.14	0.15	0.14	
F	0.00	0.00	0.01	0.01	0.00	0.00	0.00	0.00	0.00	0.00	0.00	
Cl	0.008	0.003	0.024	0.033	0.011	0.006	0.003	0.007	0.006	0.000	0.008	
Total	98.33	97.83	97.92	97.89	97.96	98.00	98.10	98.29	97.75	96.35	96.89	
Cation Total												
Si	6.338	6.216	6.218	6.362	6.237	6.248	6.286	6.301	6.280	6.248	6.218	
Al	2.274	2.354	2.326	2.234	2.352	2.347	2.317	2.265	2.316	2.307	2.340	
Ti	0.049	0.047	0.056	0.049	0.050	0.049	0.046	0.048	0.048	0.051	0.052	
Mg	3.778	3.831	3.800	3.814	3.823	3.789	3.839	3.854	3.836	3.879	3.860	
Fe	0.698	0.724	0.757	0.703	0.728	0.733	0.704	0.720	0.721	0.711	0.719	
Mn	0.012	0.009	0.009	0.012	0.012	0.009	0.008	0.006	0.011	0.012	0.013	
Cr	0.076	0.077	0.074	0.082	0.087	0.087	0.079	0.059	0.071	0.078	0.082	
Ca	1.874	1.902	1.907	1.837	1.847	1.868	1.847	1.889	1.857	1.874	1.870	
Na	0.649	0.694	0.724	0.648	0.686	0.684	0.662	0.669	0.650	0.673	0.706	
K	0.032	0.035	0.036	0.029	0.032	0.029	0.026	0.027	0.025	0.027	0.026	
F	0.000	0.000	0.001	0.002	0.001	0.000	0.000	0.000	0.000	0.000	0.000	
Cl	0.001	0.000	0.003	0.004	0.001	0.001	0.000	0.001	0.001	0.000	0.001	
Total	15.782	15.888	15.914	15.782	15.857	15.844	15.815	15.839	15.817	15.859	15.887	
Mineral	amph	amph	amph	amph	amph	amph	amph	amph	amph	amph	amph	

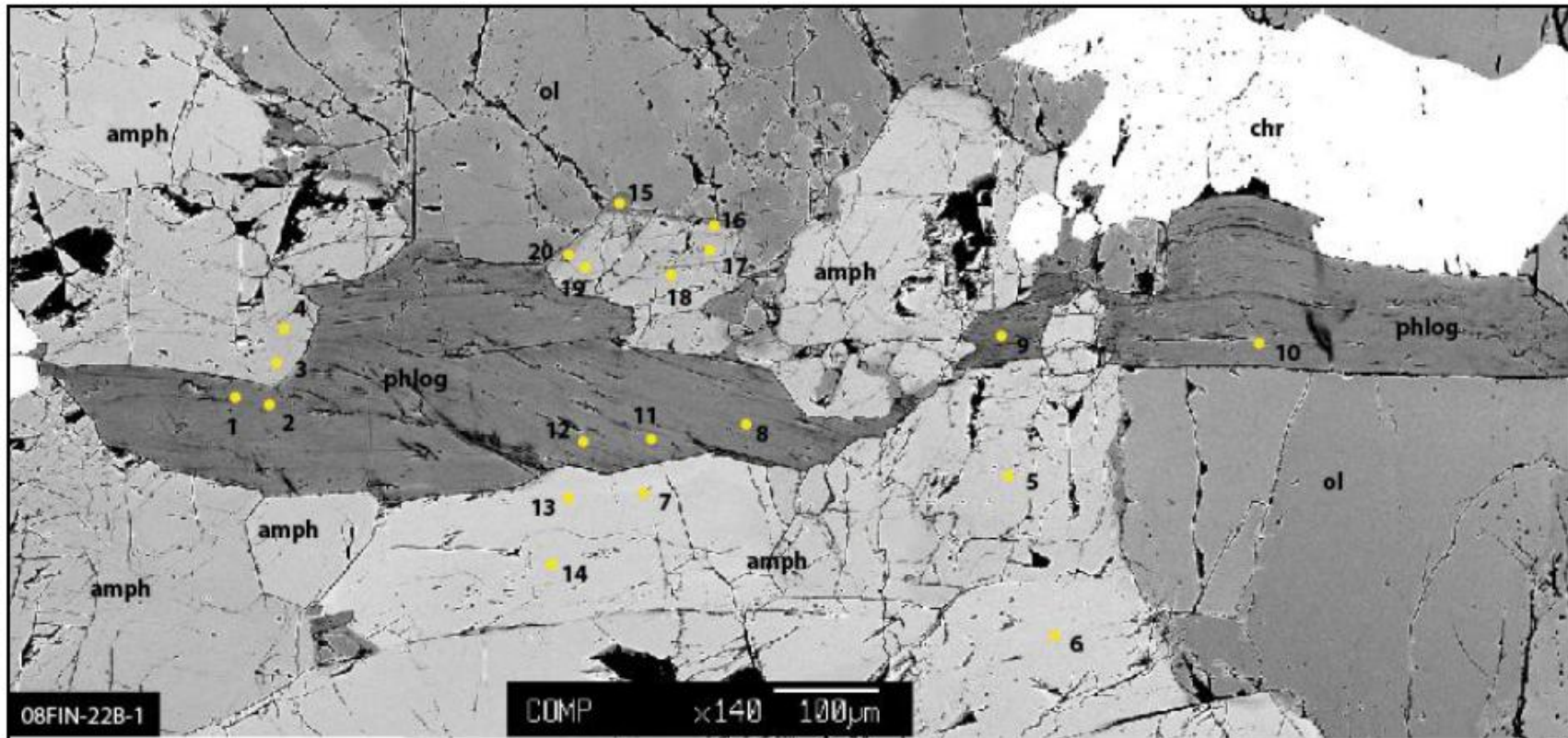
ANALYSIS	08FIN-20J 3-	08FIN-20J 3-	08FIN-20J 3-	08FIN-20J 3-	08FIN-20J 3-7	08FIN-20J 3-	08FIN-20J 3-	08FIN-20J 3-	08FIN-20J 3-	08FIN-20J 3-	08FIN-20J 3-
	3	4	5	6	3-7	8	9	10	11	12	13
Mass %											
SiO2	43.41	43.63	42.96	45.33	43.98	40.73	43.63	43.76	44.47	54.41	54.48
Al2O3	13.79	13.05	13.44	12.56	13.33	12.33	13.61	13.08	12.66	2.99	2.98
TiO2	0.44	0.43	0.45	0.40	0.44	0.42	0.47	0.44	0.42	0.06	0.06
MgO	17.91	18.12	17.94	18.61	17.91	16.93	17.78	17.94	18.47	32.82	32.81
FeO	5.64	5.76	5.88	5.17	5.70	5.64	5.88	6.00	5.68	8.96	8.99
MnO	0.08	0.09	0.09	0.09	0.11	0.12	0.08	0.10	0.09	0.17	0.19
Cr2O3	0.75	0.74	0.67	0.30	0.59	0.72	0.71	0.46	0.52	0.18	0.19
CaO	11.85	12.06	11.79	12.07	12.00	11.33	11.79	11.69	11.97	0.35	0.23
Na2O	2.39	2.52	2.39	2.13	2.46	2.27	2.52	2.50	2.43	0.01	0.01
K2O	0.16	0.15	0.16	0.13	0.14	0.13	0.14	0.13	0.13	0.00	0.00
F	0.02	0.02	0.03	0.00	0.01	0.02	0.00	0.00	0.00	0.00	0.00
Cl	0.011	0.000	0.006	0.000	0.000	0.051	0.004	0.002	0.000	0.000	0.000
Total	96.43	96.55	95.80	96.80	96.65	90.67	96.61	96.10	96.82	99.95	99.93
Cation Total											
Si	6.266	6.303	6.255	6.473	6.331	6.278	6.291	6.341	6.385	1.905	1.907
Al	2.346	2.222	2.308	2.114	2.262	2.240	2.312	2.234	2.142	0.124	0.123
Ti	0.048	0.047	0.049	0.043	0.047	0.049	0.051	0.048	0.045	0.002	0.001
Mg	3.853	3.902	3.895	3.962	3.843	3.891	3.822	3.874	3.953	1.713	1.713
Fe	0.681	0.696	0.716	0.618	0.686	0.727	0.709	0.727	0.682	0.262	0.263
Mn	0.010	0.011	0.011	0.010	0.013	0.015	0.009	0.012	0.011	0.005	0.006
Cr	0.085	0.084	0.077	0.034	0.066	0.088	0.081	0.053	0.058	0.005	0.005
Ca	1.833	1.867	1.840	1.848	1.852	1.871	1.821	1.815	1.841	0.013	0.009
Na	0.670	0.705	0.676	0.590	0.685	0.677	0.703	0.703	0.676	0.001	0.001
K	0.029	0.027	0.031	0.024	0.027	0.026	0.027	0.023	0.023	0.000	0.000
F	0.005	0.004	0.006	0.000	0.002	0.003	0.000	0.000	0.000	0.000	0.000
Cl	0.001	0.000	0.001	0.000	0.000	0.006	0.001	0.000	0.000	0.000	0.000
Total	15.833	15.871	15.870	15.717	15.816	15.882	15.828	15.831	15.818	4.030	4.028
Mineral	amph	amph	amph	amph	amph	amph	amph	amph	amph	opx	opx

08FIN-20K: Internal Mafic Unit



ANALYSIS	08FIN-20K 1	08FIN-20K 1	08FIN-20K 1	08FIN-20K 1	08FIN-20K 1	08FIN-20K 1
	1	2	3	4	5	6
Mass %						
Si	41.05	42.15	42.00	41.53	41.35	41.31
Ti	0.00	0.60	0.60	0.67	0.63	0.61
Al	23.98	16.10	16.08	16.48	16.52	16.48
Mg	14.62	16.23	16.32	16.05	16.27	16.00
Fe	14.84	7.45	7.48	7.59	7.41	7.48
Mn	0.64	0.08	0.07	0.10	0.09	0.13
Cr	0.00	0.01	0.01	0.07	0.04	0.05
Ca	6.52	11.21	11.35	11.32	11.43	11.22
Na	0.00	3.04	3.00	3.09	2.98	3.04
K	0.00	0.18	0.18	0.20	0.19	0.19
F	0.00	0.00	0.00	0.00	0.01	0.01
Cl	0.000	0.026	0.021	0.055	0.030	0.021
Total	101.64	97.06	97.08	97.13	96.95	96.52
Cation Total						
Si	2.963	6.086	6.068	6.008	5.993	6.012
Ti	0.000	0.065	0.065	0.073	0.068	0.067
Al	2.040	2.741	2.738	2.810	2.822	2.827
Mg	1.573	3.493	3.515	3.462	3.515	3.472
Fe	0.896	0.900	0.904	0.918	0.898	0.910
Mn	0.039	0.010	0.008	0.013	0.011	0.016
Cr	0.000	0.001	0.001	0.008	0.005	0.006
Ca	0.504	1.735	1.757	1.755	1.775	1.750
Na	0.000	0.852	0.839	0.867	0.838	0.858
K	0.000	0.033	0.033	0.037	0.036	0.036
F	0.000	0.000	0.000	0.000	0.003	0.003
Cl	0.000	0.006	0.005	0.014	0.007	0.005
Total	8.016	15.921	15.934	15.963	15.972	15.960
Mineral	garnet	amph	amph	amph	amph	amph

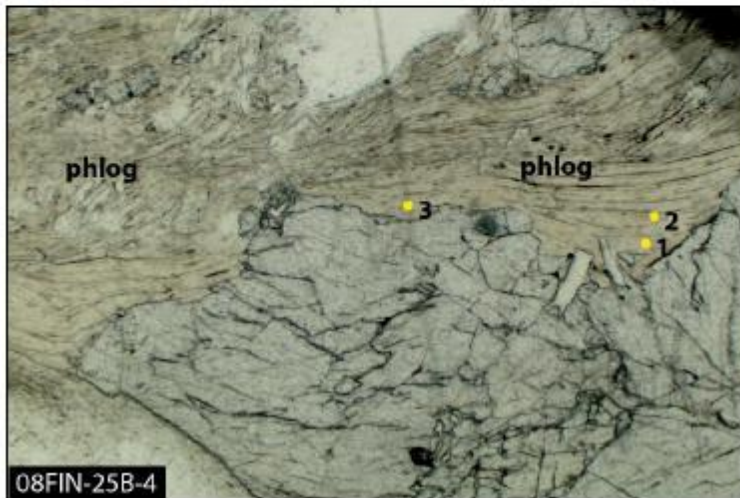
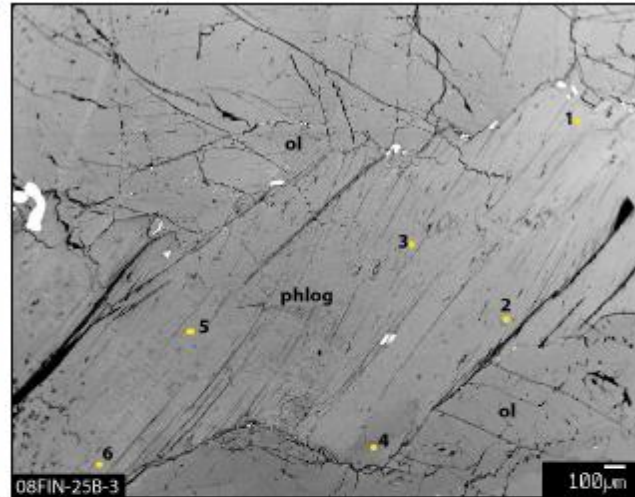
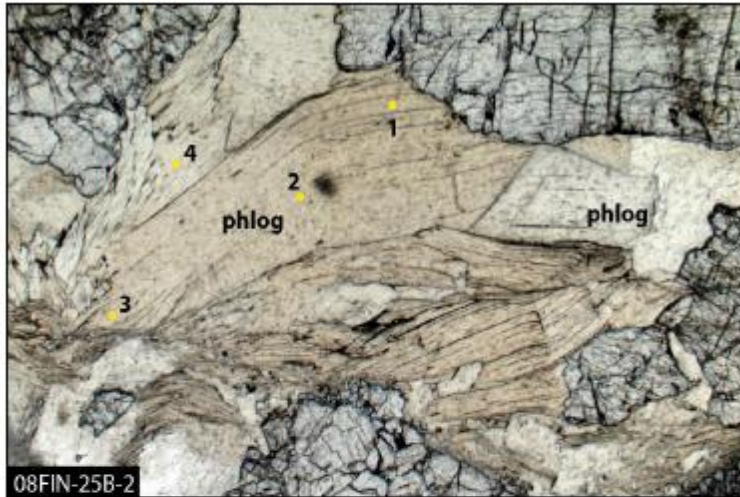
08FIN-22B: Phlogopite-Amphibole Peridotite



ANALYSIS	08FIN-22B 1-1	08FIN-22B 1-2	08FIN-22B 1-3	08FIN-22B 1-4	08FIN-22B 1-5	08FIN-22B 1-6	08FIN-22B 1-7	08FIN-22B 1-8	08FIN-22B 1-9	08FIN-22B 1-10
Mass %										
SiO ₂	41.28	41.06	47.88	48.37	49.43	49.22	49.14	41.73	41.58	41.29
TiO ₂	0.51	0.52	0.35	0.33	0.33	0.34	0.32	0.51	0.44	0.49
Al ₂ O ₃	14.34	14.05	7.93	7.41	7.39	7.36	7.32	13.63	13.22	13.52
MgO	26.68	26.88	20.50	20.72	21.04	20.78	20.84	26.91	27.51	26.99
FeO	2.25	2.48	3.27	3.22	3.22	3.30	3.26	2.60	2.58	2.73
MnO	0.01	0.03	0.04	0.06	0.07	0.06	0.07	0.00	0.00	0.01
Cr ₂ O ₃	1.31	1.26	1.78	1.84	2.01	2.01	1.91	1.28	0.97	1.26
CaO	0.03	0.04	11.09	10.89	10.85	10.68	10.75	0.02	0.01	0.00
Na ₂ O	1.61	1.80	3.79	3.84	3.93	3.84	3.83	1.84	1.43	1.29
K ₂ O	7.88	7.67	0.36	0.40	0.51	0.50	0.48	7.91	7.99	8.65
F	0.00	0.00	0.00	0.02	0.00	0.00	0.00	0.00	0.00	0.00
Cl	0.011	0.026	0.048	0.049	0.06	0.049	0.087	0.048	0.02	0.015
Total	95.90	95.81	97.03	97.10	98.81	98.12	97.98	96.47	95.74	96.24
Cation Total										
Si	2.865	2.857	6.817	6.877	6.904	6.919	6.919	2.887	2.895	2.874
Ti	0.026	0.027	0.038	0.036	0.034	0.035	0.034	0.026	0.023	0.026
Al	1.173	1.152	1.330	1.241	1.216	1.220	1.214	1.112	1.085	1.109
Mg	2.760	2.788	4.352	4.390	4.381	4.354	4.375	2.776	2.855	2.801
Fe	0.131	0.144	0.389	0.383	0.376	0.388	0.384	0.150	0.150	0.159
Mn	0.001	0.002	0.005	0.007	0.008	0.007	0.008	0.000	0.000	0.000
Cr	0.072	0.070	0.201	0.207	0.222	0.223	0.213	0.070	0.053	0.070
Ca	0.003	0.003	1.692	1.659	1.624	1.609	1.622	0.002	0.001	0.000
Na	0.217	0.243	1.045	1.058	1.063	1.047	1.045	0.247	0.193	0.175
K	0.698	0.681	0.065	0.072	0.090	0.089	0.086	0.698	0.710	0.768
F	0.000	0.000	0.000	0.007	0.000	0.000	0.000	0.000	0.000	0.000
Cl	0.001	0.003	0.012	0.012	0.014	0.012	0.021	0.006	0.002	0.002
Total	7.945	7.970	15.946	15.947	15.933	15.903	15.920	7.974	7.967	7.984
Mineral	phlog	phlog	amph	amph	amph	amph	amph	phlog	phlog	phlog

ANALYSIS	08FIN-22B 1-11	08FIN-22B 1-12	08FIN-22B 1-13	08FIN-22B 1-14
Mass %				
SiO ₂	41.55	41.18	48.31	49.09
TiO ₂	0.50	0.50	0.37	0.31
Al ₂ O ₃	13.68	13.91	7.70	7.27
MgO	26.99	26.92	20.83	20.86
FeO	2.53	2.48	3.15	3.23
MnO	0.02	0.01	0.07	0.05
Cr ₂ O ₃	1.33	1.33	1.99	1.98
CaO	0.03	0.04	11.22	10.58
Na ₂ O	1.63	1.73	3.80	3.87
K ₂ O	8.13	8.00	0.33	0.50
F	0.00	0.01	0.01	0.01
Cl	0.059	0.035	0.053	0.057
Total	96.42	96.12	97.80	97.79
Cation Total				
Si	2.879	2.861	6.825	6.922
Ti	0.026	0.026	0.039	0.033
Al	1.117	1.139	1.282	1.209
Mg	2.787	2.788	4.386	4.386
Fe	0.147	0.144	0.372	0.380
Mn	0.001	0.001	0.008	0.006
Cr	0.073	0.073	0.223	0.221
Ca	0.002	0.003	1.698	1.598
Na	0.220	0.233	1.042	1.059
K	0.719	0.710	0.059	0.090
F	0.000	0.002	0.005	0.002
Cl	0.007	0.004	0.013	0.014
Total	7.977	7.985	15.951	15.920
Mineral	phlog	phlog	amph	amph

08FIN-25B: Phlogopite-Amphibole Peridotite



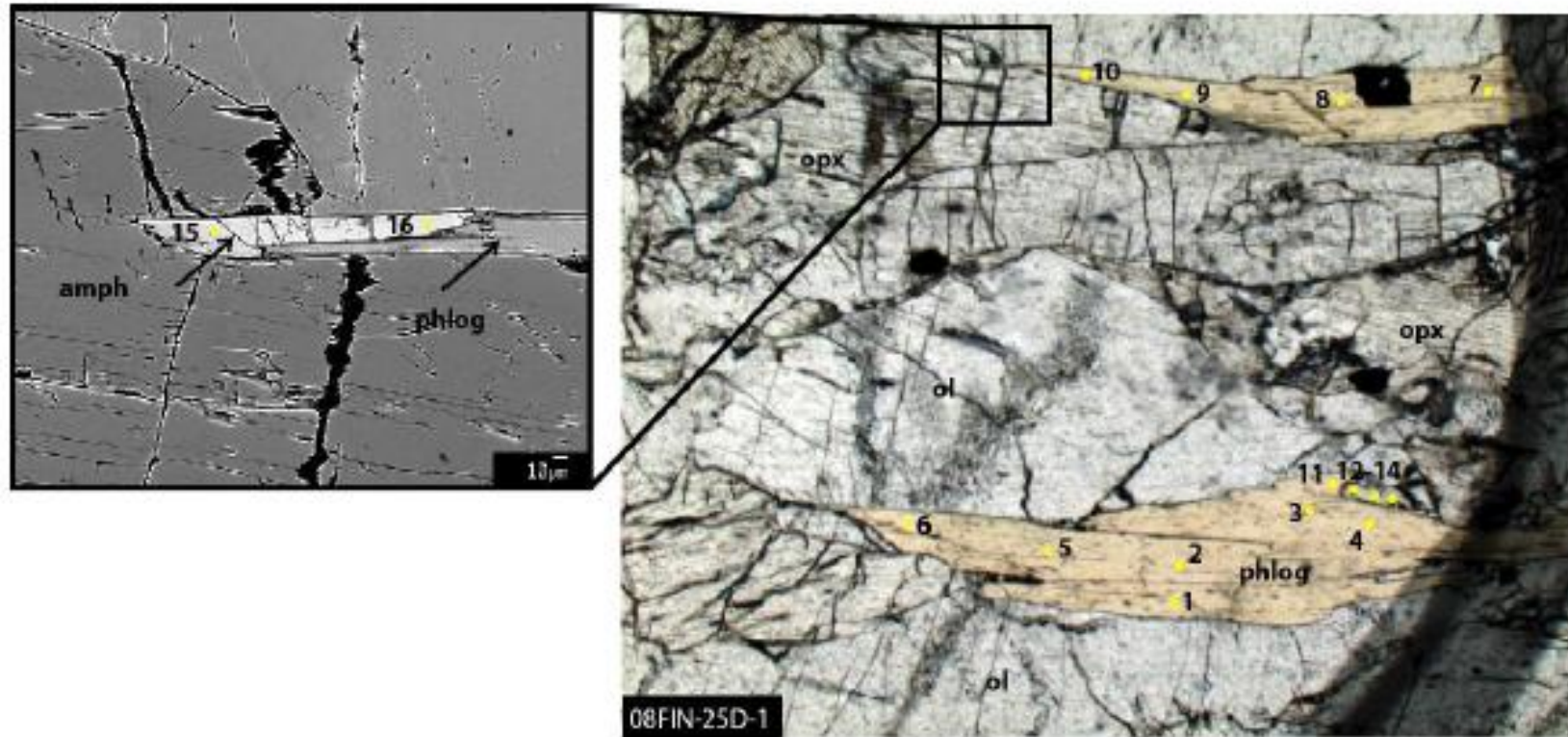
Mass %

SiO2	39.50	38.63	39.02	38.81	39.63	39.14	39.35	39.59	39.89	40.23	40.03	39.86	39.64
Al2O3	15.88	15.93	16.04	15.91	15.88	15.76	15.79	15.80	15.91	15.89	16.02	16.33	15.91
TiO2	0.89	0.85	0.83	0.88	0.90	0.93	0.88	0.88	0.90	0.91	0.89	0.89	0.91
MgO	25.23	25.38	25.82	25.28	25.23	24.96	25.13	24.79	25.47	25.43	25.33	25.03	25.20
FeO	2.74	2.82	2.68	2.66	2.70	2.77	2.83	2.72	2.78	2.67	2.54	2.75	2.61
MnO	0.01	0.03	0.02	0.00	0.02	0.00	0.00	0.00	0.03	0.02	0.00	0.02	0.02
Cr2O3	1.25	1.24	0.74	1.13	1.31	1.36	1.34	1.22	1.26	1.25	1.14	1.14	1.23
CaO	0.00	0.00	0.01	0.01	0.03	0.01	0.00	0.00	0.00	0.00	0.00	0.02	0.01
Na2O	0.44	0.54	0.38	0.56	0.54	0.65	0.59	0.54	0.51	0.60	0.51	0.44	0.68
K2O	8.98	8.96	9.18	9.22	9.09	9.02	9.00	8.99	8.80	8.73	9.33	9.23	9.27
F	0.02	0.01	0.00	0.00	0.00	0.01	0.00	0.00	0.00	0.00	0.00	0.01	0.00
Cl	0.039	0.051	0.026	0.041	0.048	0.025	0.023	0.02	0.014	0.013	0.017	0.029	0.016
Total	94.96	94.43	94.74	94.49	95.38	94.62	94.93	94.55	95.56	95.73	95.81	95.72	95.50

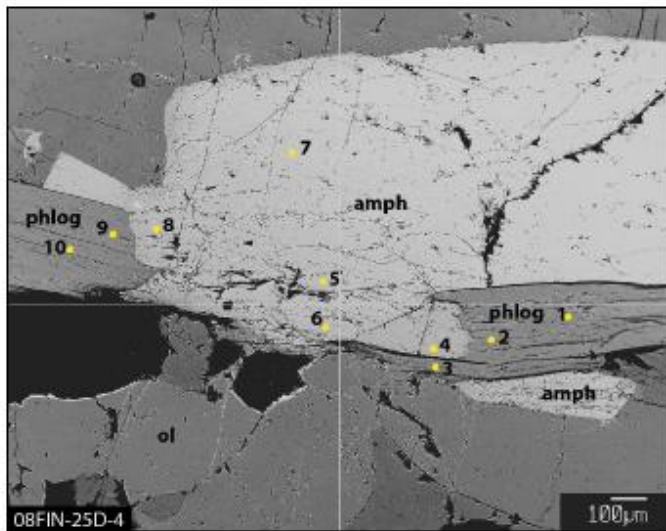
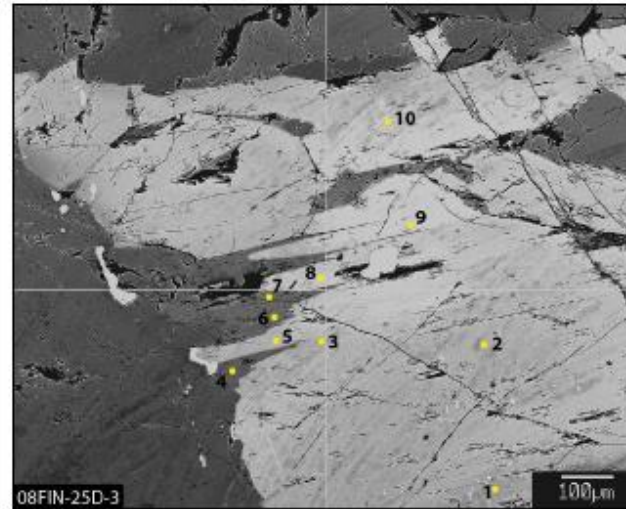
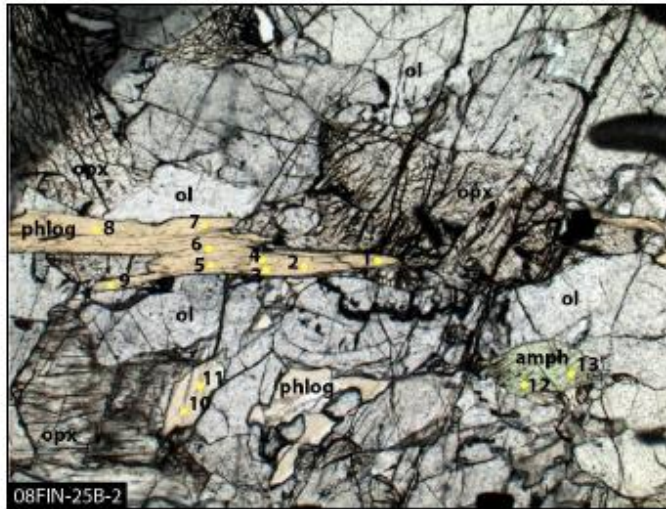
Cation Total

Si	2.786	2.748	2.760	2.759	2.785	2.777	2.780	2.803	2.792	2.806	2.798	2.788	2.784
Al	1.320	1.336	1.337	1.333	1.316	1.318	1.315	1.319	1.312	1.306	1.320	1.347	1.318
Ti	0.047	0.046	0.044	0.047	0.048	0.050	0.047	0.047	0.047	0.048	0.047	0.047	0.048
Mg	2.653	2.691	2.722	2.678	2.644	2.639	2.647	2.616	2.657	2.645	2.639	2.611	2.639
Fe	0.162	0.168	0.159	0.158	0.159	0.164	0.167	0.161	0.163	0.156	0.148	0.161	0.153
Mn	0.001	0.002	0.001	0.000	0.001	0.000	0.000	0.000	0.002	0.001	0.000	0.001	0.001
Cr	0.070	0.070	0.041	0.063	0.073	0.076	0.075	0.068	0.070	0.069	0.063	0.063	0.068
Ca	0.000	0.000	0.001	0.001	0.002	0.000	0.000	0.000	0.000	0.000	0.000	0.001	0.000
Na	0.060	0.074	0.053	0.077	0.073	0.089	0.081	0.074	0.069	0.081	0.069	0.060	0.093
K	0.808	0.813	0.828	0.837	0.815	0.816	0.812	0.812	0.786	0.777	0.832	0.823	0.831
F	0.004	0.003	0.000	0.000	0.000	0.001	0.000	0.000	0.000	0.000	0.000	0.001	0.000
Cl	0.005	0.006	0.003	0.005	0.006	0.003	0.003	0.002	0.002	0.002	0.002	0.003	0.002
Total	7.914	7.956	7.950	7.958	7.923	7.934	7.927	7.902	7.899	7.889	7.917	7.906	7.938
Mineral	phlog	phlog	phlog	phlog	phlog	phlog	phlog	phlog	phlog	phlog	phlog	phlog	phlog

08FIN-25D: Phlogopite-Amphibole Peridotite



08FIN-25D: Phlogopite-Amphibole Pyroxenite continued



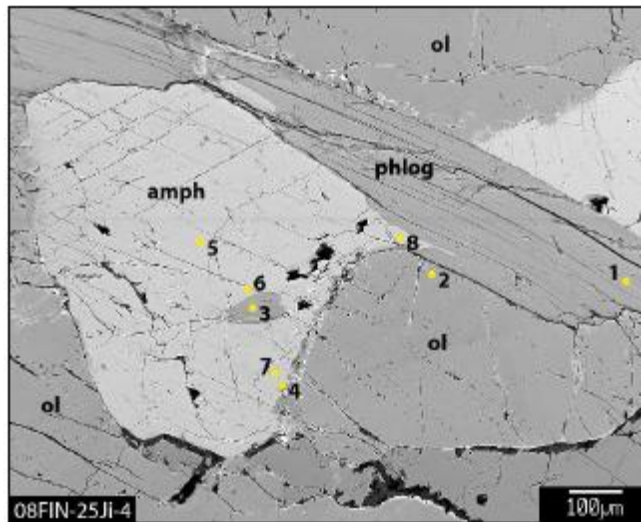
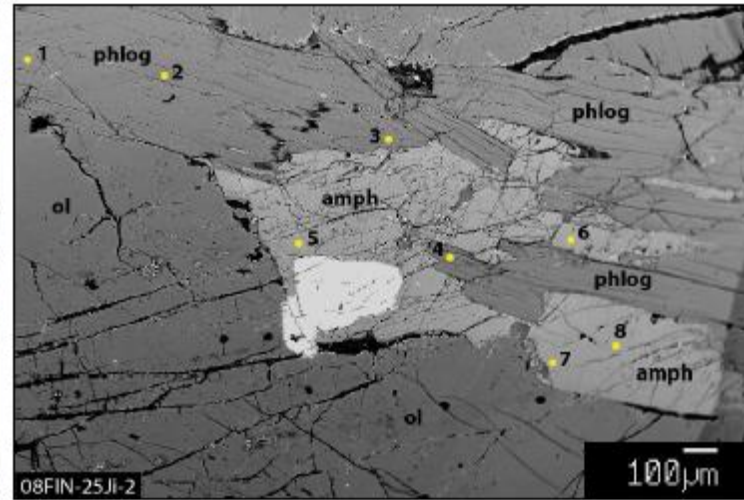
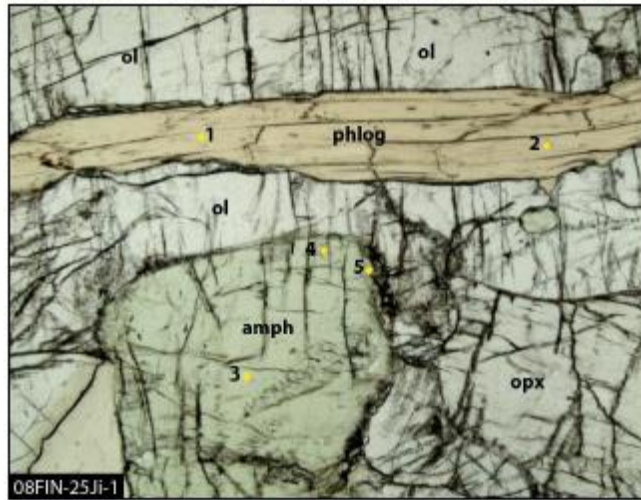
ANALYSIS	08FIN-25D 1	08FIN-25D 1	08FIN-25D 1	08FIN-25D 1	08FIN-25 1-	08FIN-25D 1	08FIN-25D 1	08FIN-25D 1	08FIN-25D 1	08FIN-25D 1	08FIN-25D
	1	2	3	4	5	6	7	8	9	10	11
Mass %											
SiO2	40.63	40.46	40.54	40.34	40.18	40.32	39.78	39.66	39.66	39.77	40.68
Al2O3	15.86	15.85	15.84	15.97	15.96	15.98	15.88	15.79	15.66	15.85	16.01
TiO2	0.75	0.70	0.76	0.76	0.74	0.70	0.70	0.72	0.73	0.73	0.74
MgO	25.60	25.47	25.65	25.56	25.44	25.95	25.81	25.60	25.69	25.99	25.72
FeO	2.67	2.63	2.61	2.54	2.69	2.68	2.56	2.51	2.70	2.70	2.43
MnO	0.03	0.02	0.00	0.01	0.03	0.00	0.00	0.02	0.03	0.02	0.02
Cr2O3	1.29	1.27	1.29	1.26	1.29	1.30	1.24	1.25	1.32	1.36	1.13
CaO	0.01	0.00	0.00	0.00	0.00	0.00	0.00	0.00	0.00	0.00	0.00
Na2O	0.53	0.58	0.55	0.59	0.57	0.50	0.60	0.58	0.57	0.52	0.53
K2O	9.00	9.27	9.18	9.22	9.18	9.02	8.99	9.11	9.03	8.89	9.20
F	0.02	0.02	0.01	0.01	0.01	0.00	0.01	0.01	0.00	0.00	0.00
Cl	0.02	0.027	0.04	0.02	0.025	0.025	0.038	0.035	0.053	0.057	0.034
Total	96.39	96.28	96.45	96.26	96.11	96.47	95.59	95.28	95.44	95.88	96.48
Cation Total											
Si	2.817	2.814	2.813	2.804	2.800	2.796	2.786	2.788	2.787	2.778	2.816
Al	1.296	1.299	1.295	1.308	1.311	1.306	1.311	1.309	1.297	1.305	1.306
Ti	0.039	0.037	0.039	0.040	0.039	0.037	0.037	0.038	0.039	0.039	0.039
Mg	2.647	2.641	2.653	2.649	2.643	2.682	2.694	2.683	2.691	2.707	2.654
Fe	0.155	0.153	0.152	0.148	0.157	0.156	0.150	0.148	0.159	0.158	0.141
Mn	0.002	0.001	0.000	0.001	0.002	0.000	0.000	0.001	0.002	0.001	0.001
Cr	0.071	0.070	0.071	0.069	0.071	0.071	0.069	0.070	0.073	0.075	0.062
Ca	0.001	0.000	0.000	0.000	0.000	0.000	0.000	0.000	0.000	0.000	0.000
Na	0.071	0.079	0.074	0.080	0.077	0.067	0.081	0.078	0.078	0.070	0.071
K	0.796	0.822	0.812	0.818	0.816	0.798	0.803	0.817	0.809	0.792	0.813
F	0.004	0.004	0.002	0.002	0.003	0.000	0.001	0.002	0.001	0.000	0.000
Cl	0.002	0.003	0.005	0.002	0.003	0.003	0.005	0.004	0.006	0.007	0.004
Total	7.900	7.922	7.915	7.920	7.923	7.915	7.936	7.939	7.940	7.932	7.907
Mineral	phlog	phlog	phlog	phlog	phlog	phlog	phlog	phlog	phlog	phlog	phlog

ANALYSIS	08FIN-25D 1	08FIN-25D 1	08FIN-25 1-	08FIN-25D 1	08FIN-25D 1	08FIN-25D 2	08FIN-25D 2	08FIN-25D 2	08FIN-25D 2	08FIN-25D 2	08FIN-25D 2
	12	13	14	15	16	1	2	3	4	5	6
Mass %											
SiO2	47.42	47.15	47.79	49.32	48.91	39.18	39.27	39.98	40.24	40.50	40.66
Al2O3	10.27	10.35	10.14	9.18	9.05	15.68	15.78	15.78	15.83	15.84	15.68
TiO2	0.44	0.38	0.37	0.38	0.36	0.76	0.74	0.75	0.73	0.76	0.72
MgO	20.05	20.19	20.24	20.85	20.64	25.70	25.48	25.32	25.68	25.39	25.57
FeO	3.32	3.38	3.28	3.06	2.97	2.61	2.72	2.68	2.73	2.54	2.63
MnO	0.05	0.06	0.05	0.05	0.06	0.03	0.04	0.02	0.04	0.04	0.02
Cr2O3	1.70	1.67	1.61	1.05	1.47	1.44	1.29	1.30	1.27	1.28	1.14
CaO	12.52	12.57	12.66	12.73	12.60	0.03	0.00	0.01	0.00	0.00	0.00
Na2O	2.23	2.29	2.23	2.08	2.04	0.43	0.59	0.57	0.56	0.60	0.65
K2O	0.71	0.69	0.61	0.47	0.44	8.86	9.02	9.01	9.07	9.15	9.15
F	0.02	0.00	0.01	0.01	0.01	0.01	0.02	0.02	0.00	0.01	0.00
Cl	0	0	0	0.04	0.027	0.023	0.021	0.025	0.039	0.052	0.036
Total	98.73	98.73	98.99	99.21	98.55	94.73	94.96	95.45	96.17	96.14	96.24
Cation Total											
Si	6.633	6.602	6.659	6.820	6.811	2.771	2.775	2.804	2.802	2.818	2.826
Al	1.694	1.708	1.666	1.497	1.485	1.307	1.314	1.305	1.299	1.299	1.285
Ti	0.046	0.040	0.039	0.040	0.038	0.040	0.039	0.040	0.038	0.040	0.038
Mg	4.182	4.214	4.204	4.298	4.284	2.710	2.684	2.647	2.665	2.634	2.649
Fe	0.388	0.396	0.382	0.354	0.346	0.154	0.161	0.158	0.159	0.148	0.153
Mn	0.006	0.007	0.006	0.006	0.007	0.002	0.003	0.001	0.002	0.002	0.001
Cr	0.188	0.185	0.178	0.114	0.161	0.081	0.072	0.072	0.070	0.071	0.063
Ca	1.877	1.886	1.890	1.886	1.881	0.002	0.000	0.001	0.000	0.000	0.000
Na	0.606	0.621	0.604	0.558	0.552	0.059	0.080	0.077	0.076	0.081	0.087
K	0.127	0.124	0.109	0.082	0.077	0.799	0.813	0.806	0.805	0.812	0.811
F	0.004	0.000	0.002	0.002	0.001	0.002	0.004	0.004	0.000	0.002	0.000
Cl	0.000	0.000	0.000	0.004	0.003	0.003	0.003	0.003	0.005	0.006	0.004
Total	15.755	15.784	15.740	15.668	15.652	7.929	7.947	7.916	7.921	7.912	7.916
Mineral	amph	amph	amph	amph	amph	phlog	phlog	phlog	phlog	phlog	phlog

ANALYSIS	08FIN-25D 2	08FIN-25D 2	08FIN-25D 2	08FIN-25D 2	08FIN-25D 2	08FIN-25D 2	08FIN-25D 2	08FIN-25D 2	08FIN-25D 3	08FIN-25D 3	08FIN-25D 3	08FIN-25D 3	08FIN-25D 3
	7	8	9	10	11	12	13	3-1	2	3	4	5	6
Mass %													
SiO2	40.24	40.36	40.31	40.39	39.69	47.15	46.93	46.39	44.68	45.44	39.85	45.87	39.56
Al2O3	15.73	15.53	15.78	15.81	15.75	10.46	10.57	9.55	11.14	11.52	16.33	11.42	16.26
TiO2	0.74	0.73	0.74	0.76	0.74	0.46	0.46	0.42	0.50	0.52	0.80	0.52	0.83
MgO	25.71	25.40	25.46	26.31	25.69	19.91	19.87	20.09	19.67	19.73	25.56	19.64	25.49
FeO	2.49	2.56	2.49	2.55	2.54	3.42	3.28	2.91	3.39	3.34	2.30	3.41	2.40
MnO	0.00	0.02	0.02	0.00	0.01	0.06	0.03	0.07	0.07	0.06	0.02	0.06	0.01
Cr2O3	1.32	1.29	1.28	1.34	1.22	1.83	1.83	1.47	1.97	1.93	1.10	1.86	1.11
CaO	0.00	0.00	0.01	0.02	0.00	12.45	12.45	12.28	12.39	12.62	0.03	12.63	0.01
Na2O	0.58	0.50	0.65	0.56	0.69	2.23	2.24	2.00	2.41	2.39	0.65	2.44	0.65
K2O	9.14	9.46	9.11	9.20	9.15	0.78	0.79	0.64	0.71	0.71	9.14	0.69	9.23
F	0.00	0.00	0.00	0.01	0.01	0.01	0.00	0.01	0.01	0.02	0.00	0.01	0.01
Cl	0.045	0.027	0.049	0.03	0.039	0.033	0.022	0.046	0.025	0.037	0	0	0
Total	95.99	95.87	95.88	96.97	95.51	98.78	98.47	95.86	96.97	98.29	95.78	98.54	95.54
Cation Total													
Si	2.805	2.822	2.813	2.790	2.786	6.603	6.589	6.670	6.405	6.417	2.781	6.456	2.772
Al	1.293	1.280	1.298	1.288	1.303	1.727	1.749	1.618	1.883	1.918	1.343	1.894	1.343
Ti	0.039	0.038	0.039	0.040	0.039	0.049	0.049	0.045	0.054	0.055	0.042	0.055	0.044
Mg	2.672	2.647	2.648	2.709	2.689	4.155	4.159	4.305	4.203	4.154	2.659	4.121	2.663
Fe	0.145	0.150	0.145	0.147	0.149	0.400	0.385	0.350	0.407	0.394	0.134	0.401	0.141
Mn	0.000	0.001	0.001	0.000	0.001	0.008	0.004	0.008	0.008	0.007	0.001	0.007	0.001
Cr	0.073	0.072	0.071	0.073	0.068	0.202	0.203	0.167	0.224	0.215	0.061	0.207	0.061
Ca	0.000	0.000	0.001	0.001	0.000	1.868	1.873	1.892	1.903	1.910	0.002	1.904	0.001
Na	0.079	0.068	0.088	0.075	0.094	0.605	0.610	0.559	0.671	0.654	0.087	0.666	0.088
K	0.813	0.844	0.811	0.811	0.820	0.139	0.142	0.117	0.129	0.127	0.814	0.123	0.825
F	0.000	0.000	0.000	0.003	0.003	0.002	0.000	0.002	0.003	0.004	0.001	0.005	0.002
Cl	0.005	0.003	0.006	0.004	0.005	0.004	0.003	0.005	0.003	0.004	0.000	0.000	0.000
Total	7.924	7.924	7.920	7.939	7.954	15.768	15.767	15.745	15.899	15.868	7.927	15.838	7.940
Mineral	phlog	phlog	phlog	phlog	phlog	amph	amph	amph	amph	amph	phlog	amph	phlog

ANALYSIS	08FIN-25D 3	08FIN-25D 3	08FIN-25D 3	08FIN-25D 3	08FIN-25D 4	08FIN-25D 4	08FIN-25D 4	08FIN-25D 4	08FIN-25D 4	08FIN-25D 4	08FIN-25D 4	08FIN-25D 4
	7	8	9	10	1	2	4	5	7	8	9	10
Mass %												
SiO2	40.18	45.43	46.07	45.88	39.74	39.73	46.83	46.92	45.47	46.90	40.28	40.25
Al2O3	16.19	11.02	10.75	10.38	15.88	15.69	10.41	10.45	10.37	10.50	15.71	15.76
TiO2	0.82	0.51	0.47	0.46	0.74	0.72	0.43	0.44	0.43	0.43	0.74	0.72
MgO	25.68	20.58	19.84	19.87	25.32	25.29	20.06	19.78	19.31	19.77	25.42	25.39
FeO	2.42	3.29	3.22	3.22	2.62	2.65	3.30	3.23	3.20	3.20	2.59	2.74
MnO	0.01	0.04	0.04	0.05	0.00	0.00	0.04	0.05	0.06	0.06	0.03	0.01
Cr2O3	1.12	1.71	1.93	1.83	1.25	1.28	1.86	1.95	1.92	1.89	1.28	1.30
CaO	0.00	12.50	12.68	12.52	0.02	0.01	12.47	12.42	12.64	12.56	0.00	0.01
Na2O	0.66	2.54	2.41	2.30	0.59	0.34	2.27	2.18	2.08	2.20	0.60	0.63
K2O	9.20	0.71	0.64	0.64	9.31	9.63	0.72	0.84	0.84	0.75	9.24	9.28
F	0.00	0.00	0.01	0.00	0.03	0.02	0.02	0.00	0.01	0.00	0.00	0.00
Cl	0.026	0.031	0.044	0.03	0.013	0	0	0.023	0.03	0.03	0.019	0
Total	96.30	98.36	98.10	97.17	95.49	95.34	98.39	98.28	96.34	98.28	95.90	96.08
Cation Total												
Si	2.791	6.414	6.509	6.538	2.791	2.798	6.582	6.602	6.544	6.597	2.813	2.808
Al	1.325	1.834	1.790	1.744	1.315	1.303	1.724	1.733	1.760	1.740	1.293	1.296
Ti	0.043	0.055	0.050	0.049	0.039	0.038	0.046	0.046	0.046	0.046	0.039	0.038
Mg	2.659	4.330	4.179	4.222	2.651	2.655	4.203	4.149	4.143	4.146	2.646	2.640
Fe	0.141	0.389	0.381	0.384	0.154	0.156	0.387	0.380	0.386	0.377	0.152	0.160
Mn	0.001	0.005	0.005	0.006	0.000	0.000	0.005	0.006	0.007	0.008	0.002	0.001
Cr	0.062	0.191	0.216	0.206	0.070	0.071	0.207	0.217	0.218	0.210	0.071	0.072
Ca	0.000	1.891	1.920	1.911	0.001	0.000	1.879	1.873	1.950	1.892	0.000	0.001
Na	0.088	0.696	0.660	0.636	0.080	0.047	0.619	0.594	0.580	0.599	0.081	0.085
K	0.815	0.127	0.116	0.117	0.834	0.866	0.128	0.150	0.153	0.134	0.823	0.826
F	0.000	0.000	0.001	0.000	0.006	0.004	0.004	0.000	0.001	0.001	0.000	0.000
Cl	0.003	0.004	0.005	0.004	0.002	0.000	0.000	0.003	0.004	0.004	0.002	0.000
Total	7.928	15.938	15.839	15.821	7.942	7.937	15.788	15.755	15.798	15.758	7.921	7.926
Mineral	phlog	amph	amph	amph	phlog	phlog	amph	amph	amph	amph	phlog	phlog

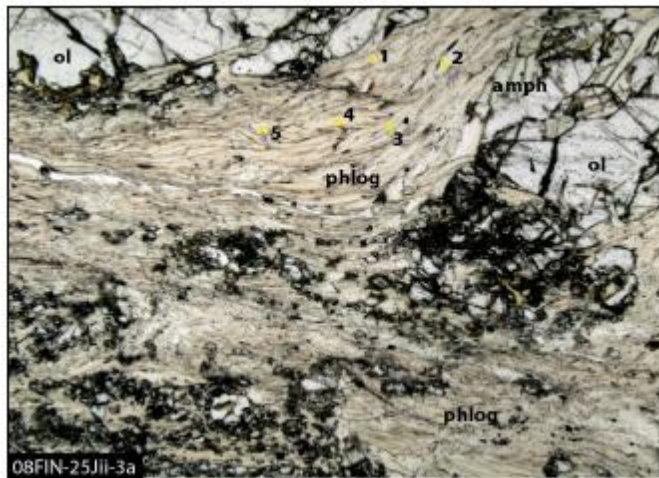
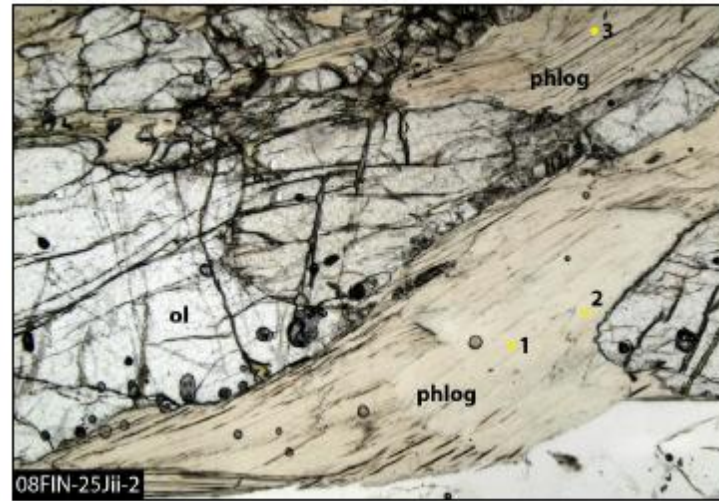
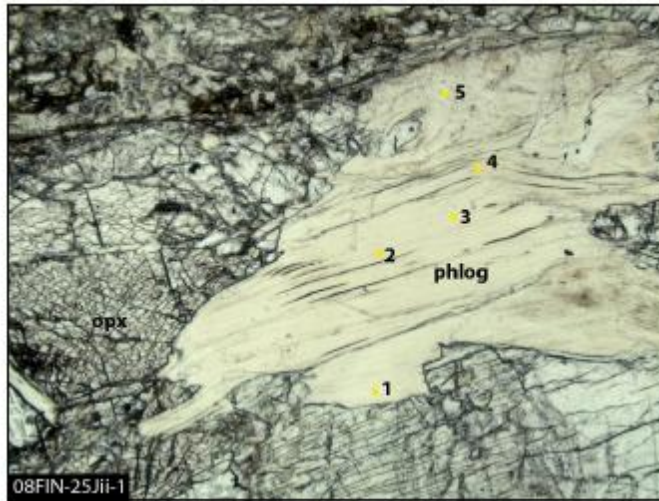
08FIN-25Ji: Phlogopite-Amphibole Peridotite



ANALYSIS	08FIN-25Ji 1-1	08FIN-25Ji 1-2	08FIN-25Ji 1-3	08FIN-25Ji 1-4	08FIN-25Ji 1-5	08FIN-25Ji 2-1	08FIN-25Ji 2-2	08FIN-25Ji 2-3	08FIN-25Ji 2-4	08FIN-25Ji 2-5	08FIN-25Ji 2-6
Mass %											
SiO2	41.11	40.92	47.65	47.51	46.96	40.28	40.98	40.61	40.81	47.24	47.43
Al2O3	15.31	15.25	10.00	9.95	10.05	15.26	15.37	15.29	14.98	9.66	9.83
TiO2	0.72	0.72	0.50	0.49	0.49	0.71	0.72	0.73	0.59	0.47	0.48
MgO	26.21	25.63	20.32	20.38	20.03	25.98	25.75	25.82	26.20	20.61	20.54
FeO	2.55	2.64	3.05	3.25	3.28	2.51	2.55	2.41	2.41	3.31	3.04
MnO	0.02	0.03	0.07	0.07	0.04	0.01	0.00	0.00	0.01	0.04	0.01
Cr2O3	1.47	1.51	2.15	2.19	2.23	1.57	1.51	1.43	1.56	2.24	2.13
CaO	0.01	0.00	11.90	11.83	11.82	0.00	0.00	0.00	0.02	12.24	12.17
Na2O	1.24	1.24	2.98	3.16	3.23	1.21	1.29	0.90	1.01	3.16	3.10
K2O	7.74	8.29	0.64	0.63	0.56	8.46	8.04	8.78	8.41	0.50	0.46
F	0.00	0.01	0.00	0.00	0.00	0.01	0.01	0.01	0.02	0.01	0.01
Cl	0.061	0.054	0.064	0.060	0.066	0.034	0.037	0.054	0.038	0.043	0.046
Total	96.41	96.27	99.30	99.49	98.74	96.01	96.24	96.03	96.05	99.49	99.21
Cation Total											
Si	2.836	2.838	6.629	6.609	6.587	2.807	2.837	2.827	2.836	6.584	6.608
Al	1.244	1.247	1.640	1.631	1.662	1.254	1.254	1.255	1.227	1.587	1.614
Ti	0.037	0.038	0.052	0.051	0.052	0.037	0.037	0.038	0.031	0.049	0.050
Mg	2.695	2.650	4.213	4.226	4.188	2.698	2.657	2.679	2.714	4.282	4.267
Fe	0.147	0.153	0.355	0.378	0.385	0.146	0.148	0.140	0.140	0.386	0.354
Mn	0.001	0.002	0.008	0.009	0.005	0.000	0.000	0.000	0.001	0.004	0.001
Cr	0.080	0.083	0.236	0.240	0.247	0.086	0.083	0.079	0.086	0.247	0.235
Ca	0.000	0.000	1.774	1.763	1.777	0.000	0.000	0.000	0.002	1.829	1.816
Na	0.166	0.166	0.803	0.853	0.878	0.164	0.174	0.122	0.137	0.854	0.836
K	0.681	0.734	0.113	0.112	0.101	0.752	0.710	0.780	0.745	0.088	0.081
F	0.000	0.003	0.000	0.000	0.000	0.002	0.001	0.002	0.004	0.002	0.004
Cl	0.007	0.006	0.015	0.014	0.016	0.004	0.004	0.006	0.005	0.010	0.011
Total	7.895	7.918	15.839	15.887	15.896	7.950	7.905	7.927	7.926	15.921	15.877
Comment	phlog	phlog	amph	amph	amph	phlog	phlog	phlog	phlog	amph	amph

ANALYSIS	08FIN-25Ji 2-7	08FIN-25Ji 2-8	08FIN-25Ji 4-1	08FIN-25Ji 4-2	08FIN-25Ji 4-3	08FIN-25Ji 4-4	08FIN-25Ji 4-5	08FIN-25J 4-6	08FIN-25Ji 4-7	08FIN-25Ji 4-8
Mass %										
SiO2	47.55	47.42	40.83	40.81	40.43	40.76	47.54	47.19	48.20	47.53
Al2O3	9.88	10.07	15.52	15.11	15.03	15.48	10.14	9.99	9.43	10.03
TiO2	0.43	0.46	0.71	0.75	0.81	0.66	0.49	0.48	0.47	0.46
MgO	20.50	20.35	26.00	25.97	26.16	26.90	20.20	20.41	20.58	20.31
FeO	3.17	3.07	2.63	2.56	2.57	2.63	3.25	3.22	3.19	3.11
MnO	0.04	0.04	0.01	0.02	0.00	0.02	0.07	0.06	0.07	0.06
Cr2O3	2.06	2.11	1.33	1.44	1.31	1.09	2.08	2.05	1.90	2.10
CaO	12.18	11.93	0.00	0.02	0.01	0.06	11.97	11.88	12.17	12.22
Na2O	3.12	3.09	1.22	1.21	0.97	0.74	3.04	3.06	3.07	3.11
K2O	0.53	0.58	8.21	8.53	8.30	7.59	0.64	0.62	0.41	0.45
F	0.00	0.00	0.00	0.01	0.01	0.00	0.00	0.00	0.00	0.01
Cl	0.034	0.035	0.018	0.039	0.016	0.035	0.018	0.028	0.004	0.038
Total	99.49	99.14	96.47	96.45	95.62	95.95	99.42	98.97	99.49	99.40
Cation Total										
Si	6.613	6.611	2.822	2.829	2.822	2.818	6.615	6.598	6.689	6.611
Al	1.620	1.655	1.265	1.235	1.236	1.261	1.663	1.647	1.543	1.644
Ti	0.045	0.049	0.037	0.039	0.043	0.034	0.051	0.050	0.049	0.048
Mg	4.250	4.228	2.679	2.683	2.722	2.773	4.190	4.253	4.259	4.211
Fe	0.368	0.358	0.152	0.148	0.150	0.152	0.378	0.377	0.371	0.361
Mn	0.005	0.005	0.000	0.001	0.000	0.001	0.009	0.007	0.008	0.007
Cr	0.226	0.232	0.073	0.079	0.072	0.059	0.228	0.227	0.208	0.230
Ca	1.815	1.782	0.000	0.002	0.001	0.004	1.784	1.779	1.810	1.822
Na	0.842	0.836	0.163	0.163	0.132	0.099	0.819	0.829	0.826	0.837
K	0.093	0.102	0.724	0.754	0.739	0.669	0.114	0.110	0.072	0.080
F	0.001	0.000	0.000	0.002	0.003	0.000	0.000	0.000	0.000	0.003
Cl	0.008	0.008	0.002	0.005	0.002	0.004	0.004	0.007	0.001	0.009
Total	15.887	15.866	7.918	7.940	7.921	7.876	15.855	15.885	15.836	15.863
Comment	amph	amph	phlog	phlog	phlog	phlog	amph	amph	amph	amph

08FIN-25Jii: Phlogopite-Amphibole Peridotite



Analysis	08FIN-25Jii 1	08FIN-25Jii 2	08FIN-25Jii 3	08FIN-25Jii 4	08FIN-25Jii 5	08FIN-25Jii 1	08FIN-25Jii 2	08FIN-25Jii 3	08FIN-25Jii 1	08FIN-25Jii 2	08FIN-25Jii 3	08FIN-25Jii 4	08FIN-25Jii 5
Mass %													
SiO2	41.22	40.59	40.85	40.83	41.49	41.21	41.06	41.15	41.58	41.57	40.79	41.24	41.29
Al2O3	14.85	14.99	14.55	15.02	14.62	15.15	14.44	14.64	14.30	14.86	14.73	14.51	14.53
TiO2	0.66	0.70	0.70	0.73	0.73	0.69	0.66	0.71	0.70	0.69	0.72	0.70	0.72
MgO	26.02	25.83	25.93	26.06	25.82	26.17	25.77	25.99	26.31	26.08	26.06	25.96	26.13
FeO	2.65	2.83	2.66	2.58	2.43	2.52	2.51	2.52	2.48	2.62	2.69	2.75	2.53
MnO	0.01	0.02	0.01	0.01	0.01	0.02	0.01	0.02	0.00	0.04	0.02	0.00	0.00
Cr2O3	1.43	1.58	1.50	1.48	1.35	1.46	1.46	1.39	1.11	1.28	1.27	1.28	1.25
CaO	0.03	0.00	0.00	0.00	0.00	0.01	0.02	0.01	0.00	0.01	0.00	0.00	0.00
Na2O	1.06	1.10	1.10	1.15	0.80	1.10	1.07	1.12	0.82	1.00	1.00	1.02	0.97
K2O	7.76	7.95	8.35	8.13	8.93	7.71	8.06	8.62	9.02	8.33	8.60	8.80	8.85
F	0.01	0.01	0.01	0.00	0.00	0.00	0.01	0.00	0.01	0.00	0.00	0.00	0.00
Cl	0.068	0.066	0.047	0.056	0.057	0.018	0.031	0.025	0.030	0.063	0.051	0.051	0.041
Total	95.74	95.65	95.69	96.04	96.23	96.06	95.08	96.19	96.34	96.53	95.91	96.31	96.29
Cation Total													
Si	2.846	2.815	2.837	2.821	2.864	2.835	2.861	2.844	2.868	2.854	2.828	2.849	2.851
Al	1.209	1.225	1.191	1.223	1.190	1.228	1.186	1.193	1.163	1.202	1.204	1.182	1.183
Ti	0.034	0.036	0.037	0.038	0.038	0.036	0.034	0.037	0.036	0.036	0.037	0.036	0.037
Mg	2.678	2.670	2.683	2.684	2.657	2.684	2.676	2.678	2.706	2.669	2.693	2.674	2.690
Fe	0.138	0.148	0.139	0.134	0.126	0.131	0.132	0.131	0.129	0.135	0.141	0.143	0.131
Mn	0.000	0.001	0.000	0.001	0.000	0.001	0.001	0.001	0.000	0.002	0.001	0.000	0.000
Cr	0.078	0.087	0.082	0.081	0.074	0.079	0.080	0.076	0.061	0.069	0.070	0.070	0.068
Ca	0.002	0.000	0.000	0.000	0.000	0.001	0.001	0.001	0.000	0.001	0.000	0.000	0.000
Na	0.141	0.148	0.148	0.154	0.108	0.147	0.145	0.150	0.110	0.133	0.134	0.137	0.129
K	0.684	0.703	0.740	0.717	0.786	0.677	0.716	0.760	0.793	0.730	0.760	0.776	0.780
F	0.002	0.003	0.003	0.000	0.001	0.000	0.002	0.001	0.002	0.000	0.000	0.000	0.000
Cl	0.008	0.008	0.006	0.007	0.007	0.002	0.004	0.003	0.003	0.007	0.006	0.006	0.005
Total	7.820	7.844	7.865	7.858	7.850	7.821	7.837	7.875	7.871	7.838	7.875	7.873	7.875
Mineral	phlog	phlog	phlog	phlog	phlog	phlog	phlog	phlog	phlog	phlog	phlog	phlog	phlog

Analysis	08FIN-25Jii 3 6	08FIN-25Jii 3 7	08FIN-25Jii 3 8
Mass %			
SiO ₂	41.44	42.12	42.74
Al ₂ O ₃	14.35	2.80	2.96
TiO ₂	0.65	0.12	0.11
MgO	26.79	37.93	37.99
FeO	2.52	2.51	3.01
MnO	0.04	0.06	0.03
Cr ₂ O ₃	1.21	0.19	0.20
CaO	0.02	0.00	0.00
Na ₂ O	0.86	0.11	0.12
K ₂ O	8.50	1.36	1.35
F	0.01	0.00	0.00
Cl	0.058	0.020	0.025
Total	96.41	87.20	88.53

Cation Total			
Si	2.851	3.089	3.089
Al	1.164	0.242	0.252
Ti	0.033	0.006	0.006
Mg	2.748	4.146	4.092
Fe	0.130	0.139	0.164
Mn	0.002	0.004	0.002
Cr	0.066	0.011	0.011
Ca	0.001	0.000	0.000
Na	0.114	0.015	0.017
K	0.746	0.127	0.125
F	0.003	0.000	0.001
Cl	0.007	0.002	0.003
Total	7.866	7.780	7.762
Mineral	phlog	altered phlog	altered phlog

